Role played by Atg16L1 in maintaining macrophage homeostasis

Aleksandra Ivanova Zhekova

A Thesis submitted for the degree of Doctor of Philosophy.

Norwich Medical School

University of East Anglia

2017

University of East Anglia

Abstract

Autophagy is a membrane trafficking pathway that delivers portions of the cytoplasm to lysosomes for degradation. Degradation of damaged organelles and proteins allows autophagy to play key roles in maintaining cell and tissue homeostasis and reducing inflammation. Autophagy can also degrade intracellular pathogens and expose pathogen components to innate and adaptive immune systems. Recent work has identified LC3-associated phagocytosis (LAP) as a pathway related to autophagy that is activated during the phagocytosis of pathogens and may also facilitate delivery to lysosomes. Autophagy protein Atg16L1 is required for both autophagy and LAP, and also for the suppression of secretion of the pro-inflammatory cytokine IL-1beta from macrophages. The N-terminal region of Atg16L1 contains a short atg5-binding and coiled coil domain (CCD) that binds WIPI2b and is required for autophagy. The large C-terminal domain is made from seven tryptophan-aspartic acid (WD) repeats folded into a □-propeller thought to provide a platform for protein interactions important for autophagy. This study has used mice lacking the WD domain of Atg16L1 to investigate the role played by these domains in determining the inflammatory status of macrophages. Mice carrying a stop codon at the end of the CCD were unable to express the WD domain. The inflammatory status of macrophages isolated from these mice was compared with macrophages carrying an additional deletion that removed a glutamate residue at position 230 in the CCD required for WIPI2b binding and autophagy. Bone marrow-derived macrophages from mice lacking both the WD domain and glutamate 230 were unable to induce autophagy. They were also unable to suppress IL-1beta

secretion in response to LPS or differentiate into anti-inflammatory M2 macrophages. Mice that lacked the WD domain of Atg16L1, but retained glutamate 230 could activate autophagy, suppress inflammation and differentiate into anti-inflammatory macrophages. These results suggested that the inflammatory status of macrophages is maintained independently of the WD domain, and relies on the short N-terminal coiled coil domain of Atg16L1, which is able to activate autophagy. Parallel studies following the uptake of polystyrene beads by macrophages showed that the WD domain of Atg16L1 was required for LAP. LAP is therefore activated during phagocytosis, but since the inflammatory status of macrophages is independent of the WD domain, LAP does not appear to play a role in suppressing inflammatory responses of macrophages.

Table of Contents

List of Figures

List of Tables

Abbreviations

2-DG: 2-deoxyglucose 3MA: 3-methyladenine aa: Amino acid

AIM2: Absent in melanoma 2

ANOVA: ANalysis Of VAriance

Arg1: Arginase 1

ASC: Apoptosis-associated speck-like *protein*

Atg16L1: Autophagy-related 16-like 1

ATP: Adenosine triphosphate

BIR: Baculovirus inhibitory repeat

BMDMs: Bone marrow-derived macrophages

bp: Base pair

BSA: Bovine serum albumin

BzATP: 2'-3'-O-4-benzoylbenzoyl-adenosine-5'-triphosphate

CARD: Caspase-recruitment domain

CCD: Coiled-coil domain

CD: Crohn's disease

Chil3: Chinase 3

CpG oligodeoxynucleotide: Cysteine triphosphate deoxynucleotide-Guanine triphosphate deoxynucleotide

DAMPs: Danger-associated molecular pattern

DAPI: 4', 6-Diamidino-2-Phenylindole

DMSO: Dimethyl supfoxide

DNA: Deoxyribonucleic acid DTT: Dithiothreitol dNTP:

Deoxyribonucleotide triphosphate

ECAR: Extracellular acidification rate

E. coli: Escherichia coli

EDTA: Ethylene-Diamine-Tetra-Acetic acid

ELISA: Enzyme linked immunosorbent assay

ER: Endoplasmic reticulum

FACS: Fluorescence-activated cell sorting

FCCP: Carbonyl cyanide 4-(trifluoromethoxy)phenylhydrazone

FCS: Fetal calf serum

FGF: Fibroblast growth factor

FIP200: Focal adhesion kinase family interacting protein of 200 kDa

GFP: Green fluorescent protein

GWAS: Genome-wide association studies

HBSS: Hank's balanced salt solution

HCl: Hydrochloride

HEK293A: Human embryonic kidney cells 293

IBD: Inflammatory bowel disease

IFN-gamma: Interferon-gamma

IL: Interleukin

IkB: NF-kB inhibitor

IKK: IkB kinase

IRAK: IL-1 receptor associated kinase

LB agar: Luria-Bertani agar

LC3: Microtubule-associated protein 1 light chain 3

LPS: Lipopolysaccharide

LRR: Leucin-rich repeat

MD2: Myeloid differentiation factor 2

M-CSF: Macrophage colony-stimulating

MDP: Muramyl dipeptide

MeOH: Methanol

MHC-II: Major histocompatibility complex class II mRNA: Messenger

ribonucleic acid mTOR: Mechanistic target of rapamycin

MyD88: Myeloid differentiation protein 88

NaCl: Sodium chloride

NACHT: Nucleotide-binding oligomerization domain

NF-kB: Nuclear factor-kappa B

NLR family: NOD-like receptor

OCR: Oxygen consumption rate

OXPHOS: Oxidative phosphorylation

PAMPs: Pathogen-associated molecular pattern

PBS: Phosphate buffered saline

PCR: Polymerase chain reaction

PE: Phosphatidylethanolamine

PI3K: PhosphoInositide-3 Kinase

PRR: Pathogen recognition receptor

PtdIns(3)P: Phosphatidylinositol 3-phosphate

Ptgs2: Prostaglandin-endoperoxide synthase 2 PYD: Pyrin domain qRT-

PCR: Quantitative real-time PCR RFP: Red fluorescent protein

RIPK: Receptor interacting protein kinase

RNA: Ribonucleic acid

ROS: Reactive oxygen species

RPMI-1640: Roswell Park Memorial Institute medium

SOC medium: Super optimal broth with catabolite repression

SDS: Sodium dodecyl sulfate

TAE: Tris-acetate-EDTA

TBST: Tris-buffered saline (TBS) and Tween 20

Th-cells: Helper T-cells

TLR: Toll-like receptor

TMB solution: 3', 3', 5, 5'-Tetramethylbenzidine

TMEM protein: Transmembrane protein

TNF: Tumor necrosis factor

TRAF6: TNF receptor–associated factor 6

TRIM protein: Tripartite motif protein

ULK: Unc-51 like kinase

UVRAG: UV radiation resistance-associated gene protein

V-ATP: Vacuolar-type H^+-ATPase

Vps: Vacuolar protein sorting

WIPI: WD repeat domain phosphoinositide-interacting protein

WT: Wild type

Z-WEHD: Z-Trp-Glu(OMe)-His-Asp(OMe)

Acknowledgements

I would like to express my sincere gratitude to my primary supervisor Prof Tom Wileman for all his help, guidance and support throughout my PhD, and for giving me the opportunity to develop myself as a scientist by doing a PhD at the University of East Anglia. Deserving of special mention is my secondary supervisor Dr Norihito Kawasaki. I am thankful I had the opportunity to work with such a devoted scientist who is also a great and caring person.

A very special gratitude goes to my family for supporting me morally and emotionally throughout my PhD and in life in general. They have taught me the value of being disciplined and organized and brought me up as an independent individual who fights for their dreams. Although I will not be the first PhD holder in the family, I know I have made them proud.

I am grateful to my fellow lab mates: Tim, for his help and support during my hardest moments in the lab and during the writing of this thesis, as well as for appreciating me and putting a smile on my face every day; Shashank for always being there for me and sharing his delicious Indian delicacies with me; Sophia for being such a funny and amusing person and for being my lab buddy at 1am at night, I will always remember us sneaking out of the lab late in the afternoon and share chocolates and sweets; Matt for his continuous jokes and high spirit even when things do not look particularly great; Angela for her encouragements, delicious sweets, and great surprise presents; Oskar for his ability to always put a smile on my face; and last but by no means least Weijiao for always cheering me up.

Dedication

I would like to dedicate this work to my family – the people who have always wished the best for me. I know how hard it has been for them not to be able to see me regularly. It has been hard for me too. However, I hope I have made them proud.

Chapter 1

Introduction

1.1 Autophagy

Autophagy is a general term for the transfer of material from the cytoplasm to lysosomes for degradation. There are several different pathways including chaperone-mediated autophagy and microautophagy. The pathway studied in this thesis is called macro-autophagy, but as is conventional for studies of macro-autophagy, the pathway will be referred to as autophagy from now on. During autophagy, new membranes called autophagosomes are generated in cells and these engulf portions of the cytoplasm and fuse with lysosomes and their content is degraded. Autophagy plays an important role in maintaining tissue homeostasis by removing damaged organelles, protein aggregates and intracellular pathogens. Cargoes for autophagy are engulfed by a flattened membranous sac-like structure, called a phagophore, that elongates and seals to become the double-membraned autophagosome (Levine *et al*, 2011; Shibutani *et al*, 2015; Zavodsky *et al*, 2013). The mature autophagosomes use the microtubule motor protein dynein to move along microtubule tracts to perinuclear sites where lysosomes are clustered. The outer membrane of the autophagosomes fuses with the lysosomes to form autolysosomes which degrade the cargoes together with the inner autophagosome membrane (Zavodsky *et al*, 2013). The degradation products, such as amino acids, are recycled and used for metabolic processes and maintaining cellular homeostasis. Autophagy of damaged organelles, protein aggregates as well as pathogens involves the tagging of the potential cargo with poly-ubiquitin which binds an adaptor protein called p62 which in turn binds LC3 in the autophagosome membrane (Figure 1.1). Autophagy directed against pathogens, is termed

xenophagy, and plays a crucial role in suppressing excessive inflammatory responses. Capture of pathogens inside autophagosomes and subsequent killing in lysosomes can prevent dispersal of microbes to other cells and supress the inflammatory stimulus generated during pathogen replication (Shibutani *et al*, 2015; Randow&Munz, 2012).
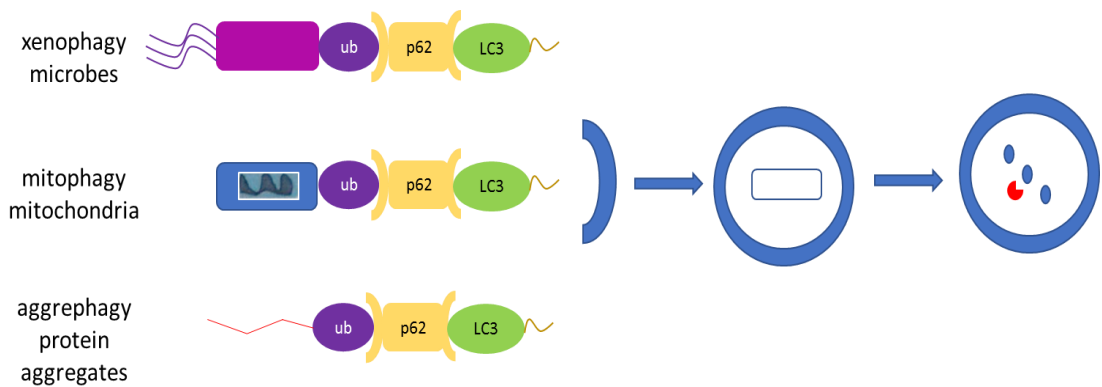
Figure 1.1 Different subsets of autophagy pathways. Three different autophagy subsets have been described depending on the cargo that is degraded. Damaged organelles, protein aggregates as well as pathogens get tagged with poly-ubiquitin (Ub) which binds an adaptor protein, p62, which in turn binds LC3 in the autophagosome membrane. Xenophagy is involved in the clearance of pathogens and has an essential role in suppressing inflammatory responses. Mitophagy leads to degradation of damaged mitochondria while aggrephagy results in degradation of protein aggregates.

1.1.i Mechanism of autophagosome formation

Autophagosomes were reported in electron microscopy studies in the 1950s, however the molecular mechanism of autophagy remained unknown until the discovery of yeast autophagy-related genes in the 1990s. More than 40 autophagy-related (Atg) proteins have been reported so far, of which 15 core proteins in yeasts are conserved in mammals, indicating that autophagy is an evolutionarily conserved process (Shibutani *et al*, 2015). In mammals, the initiation of phagophore formation is regulated by the mTOR kinase that senses the levels of amino acids in cells (Zavodsky *et al*, 2013) (Figure 1.2i). Under nutrient-rich conditions mTOR is active and promotes protein synthesis. During this process mTOR phosphorylates and inactivates the ULK1 kinase and Atg13. When amino acid levels fall, mTOR is inactivated and the inhibition of ULK1 and Atg13 is reversed (Kim *et al*, 2011). The next stage involves a complex containing the class III phosphatidylinositol 3-kinase (PI3K) Vps34, Beclin 1, Vps15 complex, and Atg2-WIPI2b complex. ULK1 activates the complex by phosphorylating Beclin, the main regulatory subunit of the Vps34 complex. The main function of the Vps34 complex is to phosphorylate lipids in cellular membranes, most commonly the endoplasmic reticulum, to generate binding sites for phospholipid-binding proteins such as WIPI2b which recruit the proteins required autophagosome expansion (Dooley *et al*, 2014).

The expansion, elongation and closure of the phagophore depends on two ubiquitin-like systems: the Atg12-Atg5 conjugation system which functions as a dimeric complex together with Atg16L1, and the microtubule-associated protein 1 light chain 3 (LC3) conjugation system (Levine *et al*, 2011; Zavodsky *et al*, 2013) (Figure 1.2ii). The ubiquitin-like

protein Atg12 is covalently linked to Atg5 by an E1-like enzyme, Atg7, and an E2-like enzyme, Atg10 (Shibutani *et al*, 2015). The N-terminal domain of Atg16L1 binds WIPI2b and at the same time is non-covalently bound to the Atg12-Atg5 complex, inducing its multimerization and the formation of 2:2:2 complex (Mizushima *et al*, 2003).

Atg12-Atg5-Atg16L1 is localised on the outer surface of the phagophore and dissociates after the mature autophagosome has been formed (Zavodsky *et al*, 2013). The Atg16L1 complex functions as an E3-like enzyme for the LC3 conjugation system. LC3 is a ubiquitin-like protein which, after synthesis, is processed by the Atg4 protease. The processing involves the removal of the C-terminal 22 residues of the precursor protein to generate the LC3-I form. The C-terminus of LC3-I is conjugated to phosphatidylethanolamine (PE) by a series of reactions involving Atg7, Atg3, as well as the Atg12-Atg5-Atg16L1 complex, thus resulting in the production of the lipidated form of LC3, LC3-II (Fujita *et al*, 2008). Prior to the fusion of the autophagosome with a lysosome, the LC3-II linked to the outer autophagosomal membrane dissociates by the deconjugation of PE from LC3, a process catalysed by the Atg4 protease. The LC3-II which is located on the inner autophagosomal membrane is retained but eventually degraded by the lysosomal hydrolases (Lai&Devenish, 2012) (Figure 1.2iii). GFP-LC3 is a widely used as a fluorescent marker for the detection of phagophores and autophagosomes by microscopy. Moreover, LC3-I and LC3-II can easily be detected by immunoblot (Figure 1.2iv) and the levels of LC3-II relative to LC3-I can provide an assay for autophagy activation (Shibutani *et al*, 2015).

1.2 Autophagy and inflammation: a link between Atg16L1 and Crohn's disease

The first evidence for a link between autophagy and inflammation was made by Saitoh and colleagues (2008) who showed that peritoneal and bone marrow-derived macrophages cultured from mice lacking Atg16L1, generated very high levels of IL-1beta in response to LPS. This suggested that autophagy may supress secretion of IL-1beta in response to TLR4 signalling. During the same period genome-wide association studies (GWAS) identified a T300A risk allele for Crohn's disease (CD) in the linker region of Atg16L1 (Hampe *et al*, 2007) suggesting that a malfunctioning Atg16L1 may in some way inhibit autophagy and predispose to inflammatory disease. The connection was further supported by work from Murthy *et al* (2014) who showed that the T300A mutation generated a caspase-3 cleavage site that could lead to degradation of Atg16L1, and by implication loss of autophagy, during environmental challenges that would activate caspase-3. The study went on to show that pathogen infection accelerated Atg16L1 cleavage which in turn impaired autophagy and resulted in increased cytokine production. Similarly, Lassen *et al* (2014), as well as Gao *et al* (2017), have demonstrated both *in vitro* and *in vivo* that Atg16L1 T300A mice exhibit autophagy defects and increased IL-1beta generation which is attributed to Atg16L1 inactivation.
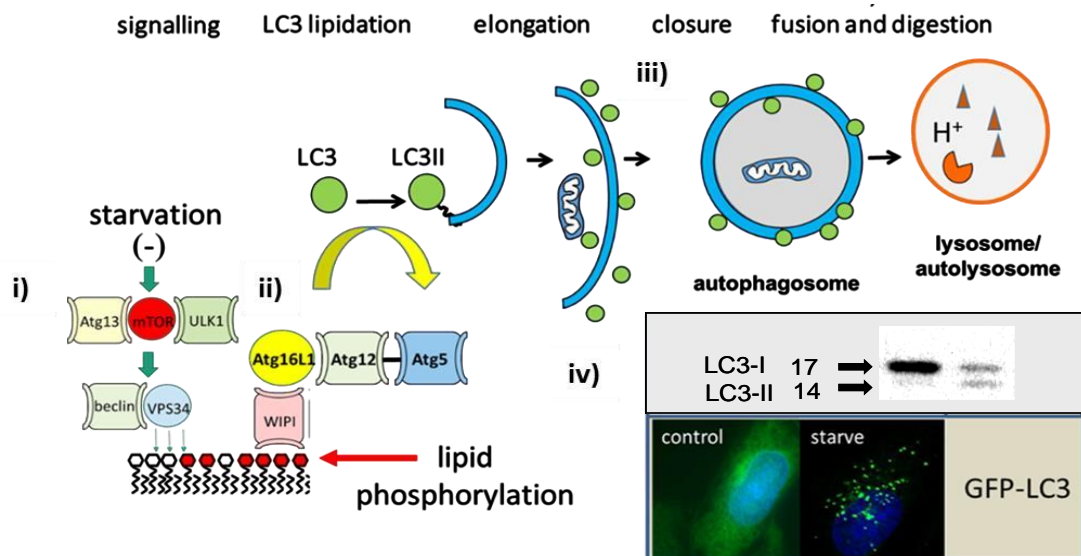
Figure 1.2 Regulation of autophagy and autophagosome formation in mammals. Autophagy is a complex catabolic process that involves the following key steps: **i)** mTOR kinase which senses the amino acid levels in the cell and promotes protein synthesis under nutrient-rich conditions. Under starvation, mTOR is inactivated which activates ULK1 and Atg13. ULK1 activates Beclin 1, the main regulatory subunit of the Vps34 complex. Vps34 is required for cellular membrane lipid phosphorylation, thus generating binding sites for WIPI2b which recruits the proteins involved in autophagosome expansion; **ii)** Atg12-Atg5-Atg16L1 conjugation system which is involved in the expansion, elongation and closure of the phagophore. The complex functions as an E3-like enzyme for the LC3 conjugation system. LC3-I get lapidated by a series of reactions, thus resulting in the generation of LC3II which is linked to the autophagosomal membrane; **iii)** The autophagosome fuses with a lysosome which leads to the degradation of the engulfed cargo by the lysosomal hydrolases; **iv)** LC3 can easily be detected by immunoblot or immunofluorescence. Moreover, the levels of LC3-II relative to LC3-I can be used for determining autophagy activation. [Figure provided by Tom Wileman].

Parallel work from Cadwell *et al* (2008), using hypomorphic mice expressing low levels of Atg16L1 (Atg16L1[HM]) showed that the mice developed gut inflammation and Paneth cell defects similar to that seen in CD. The inflammation was not seen in pathogen free mice but was induced by persistent strains of norovirus. The study suggested that inflammation results from dysregulated immune responses to gut microbes. The following sections summarise the evidence that loss of autophagy may be pro-inflammatory.

1.2.i Loss of autophagy from myeloid cells is pro-inflammatory

Myeloid cells are widely distributed throughout the body and are key regulators of both innate and adaptive immunity (Murray&Wynn, 2011; Ohashi *et al*, 2015). They play a vital part in the host defence system because they constantly survey their surroundings for invading pathogens and have the capacity to contain pathogens in the early phase of infection (Murray&Wynn, 2011; Wang *et al*, 2013). Inflammation resulting from tissue damage or invasive pathogens stimulates macrophages to secrete proinflammatory cytokines and chemokines, as well as other inflammatory mediators, thus activating lymphocytes and other immune cells (Ohashi *et al*, 2015; Murray&Wynn, 2011). On the other hand, macrophages can play antiinflammatory roles in wound healing and tissue repair because of their role in inflammation resolution and the ability to produce anti-inflammatory cytokines and to ingest pathogens due to their phagocytic activity (Ohashi *et al*, 2015). Inflammatory homeostasis therefore requires inflammatory responses by macrophages to be carefully regulated.

A complete knock-out of autophagy in mice through inactivation of genes essential for autophagy such as Atg5, Atg4, Atg7, Atg12 and Atg16 results in postnatal death (Komatsu *et al*, 2005; Sou *et al*, 2008; Saitoh *et al*, 2008; Malhotra *et al*, 2015; Yoshii *et al*, 2016). This has meant that most studies on the role played by autophagy genes *in vivo* rely on tissue-specific knock-out. The lysozyme-M-cre system (LysMcre) has been used to knock out autophagy genes from myeloid cells (macrophage, neutrophils, dendritic cells, eosinophils). Mice expressing cre recombinase from a lysozyme promoter are crossed with mice carrying autophagy genes flanked by floxp sites. The resulting offspring survive but lack autophagy in myeloid cells.

Studies using mice lacking Atg14, Fip200, Atg5 or Atg7 in myeloid cells show increased lung inflammation and increased resistance to influenza infection (Lu *et al*, 2016). The mice are resistant to infection because the lung is proinflammatory at the time of infection and innate and acquired immune responses are accelerated. Investigators (Park *et al*, 2016) have also studied infection of these mice with murine gamma herpesvirus 68. The autophagy deficient mice show raised systemic inflammation following infection and sustained production of IFN-gamma by T-cells. Taken together, the results suggest that the autophagy genes in macrophages supress virus-induced inflammation *in vivo*.

Tissue macrophages originate from self-renewing multipotent haematopoietic stem cells which multiply in the bone marrow and give rise to blood monocytes. These cells do not divide but enter the blood stream and colonise various tissues where they differentiate into mature tissue-specific macrophages which have distinct morphological and

functional features. The differentiation is triggered by the cytokine environment (Gordon&Taylor, 2005; Mosser&Edwards, 2008; Lawrence&Natoli, 2011; Fejer *et al*, 2015). It has been shown that certain macrophage subsets do not originate from a single lineage. For example, brain macrophages (microglia) and epidermal macrophages (Langerhans cells) have dual origin (embryonic and adult bone marrow). Interestingly, Langerhans cells and lung macrophages (alveolar) come from the foetal liver. Tissue-specific macrophages also include osteoblasts (bone), histiocytes (intestinal connective tissue), marginal zone macrophages (spleen), subcapsular sinus macrophages of lymph nodes (Murray&Wynn, 2011).

1.2.ii Effect of autophagy on M1 and M2 macrophages

The tissue environment provides a source of signals which shape macrophage activation and the subsequent gene and protein expression (Roszer, 2015). Two major macrophage subtypes with distinct functions have been described termed classically activated M1 and alternatively activated M2 macrophages (Murray&Wynn, 2011; Ohashi *et al*, 2015). Macrophages exposed to pathogen components and IFN-gamma become M1 macrophages which produce proinflammatory cytokines and chemokines and play a role in inflammation, tissue damage and killing of the phagocytosed microbes (Figure 1.3). They are characterized by the expression of markers, such as IL-6, which is a pleiotropic, hormone-like molecule whose deficiency is associated with impaired innate and adaptive immunity to viral, parasitic and bacterial infection; and Ptgs2 (prostaglandin-endoperoxide synthase 2), an enzyme which converts arachidonic acid to prostaglandins which are dramatically increased during inflammation (Ohashi *et al*, 2015; Hunter&Jones, 2015;

Morita, 2002). Conversely, M2 macrophages are a result of the activity of IL-4 and IL-13 which are produced by Th-2 cells, basophils and mast cells (Figure 1.3). M2 polarized macrophages are characterized by the production of anti-inflammatory cytokines and by the expression of certain markers, such as arginase-1 and chinase-3 which are involved in tissue remodelling and healing (Ohashi *et al*, 2015; Varin&Gordon, 2009). Arginase-1 is an enzyme which uses L-arginine to produce L-ornithine and urea. Its increased activity is associated with enhanced L-arginine metabolism which has been demonstrated to play a role in T-cell proliferation (Roszer, 2015; Gabrilovich&Nagaraj, 2009). Chinase-3 is a lectin which binds to heparin and heparin sulfate during pathogen infection. It displays chemotactic activity for T lymphocytes and is involved in inflammatory responses (Morita, 2002).

Autophagy appears to play a role in regulating M1/M2 polarisation *in vivo*. When Atg5 [LysMcre] mice, which lack autophagy in myeloid cells, are raised on a high fat diet containing low levels of LPS, they develop systemic inflammation and liver damage. Bone marrow-derived macrophages and Kupffer cells isolated form the mice show increased M1 phenotype compared to litter mate controls. The results suggest that in control mice Atg5 favours differentiation of macrophages into an anti-inflammatory M2 phenotype (Liu *et al*, 2015). The mechanism is unknown but may be related to the ability of autophagy to provide metabolites. M1 and M2 polarized macrophages differ in their metabolic profile. Classically activated M1 macrophages rely on glycolysis which is a process of quick energy supply needed during microbicidal activity. In contrast, alternatively activated M2 macrophages obtain much of their energy from fatty acid oxidation

which provides sustained energy for tissue repair and remodelling (Galvan-Pena&O'Neill, 2014; Mantovani *et al*, 2002).
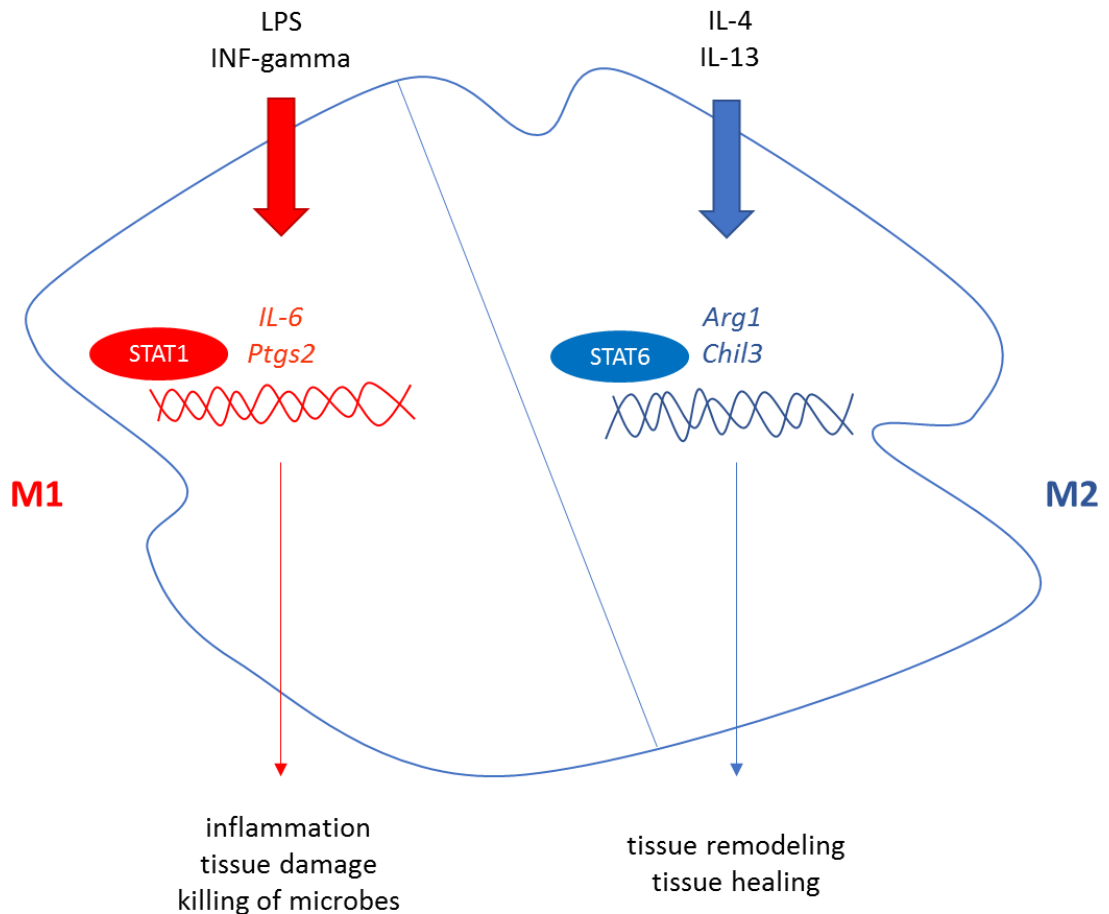
Figure 1.3 M1 vs M2 macrophages. LPS and IFN-gamma induce proinflammatory M1 macrophage polarization, whereas exposure to IL-4 and IL13 results in anti-inflammatory M2 phenotype. Upon ligand binding, latent cytoplasmic STAT transcription factors get activated which results in their homo- or heterodimerization and translocation to the nucleus, where they bind to DNA and regulate gene expression. The M1 macrophages are involved in inflammation, tissue damage and killing of invasive pathogens and are therefore characterized by the production of IL-6 and Ptgs2, whereas the M2 macrophages have anti-inflammatory properties and are involved in tissue remodeling and healing. Their marker expression profile is characterized by arginase-1 and chinase-3.

1.2.iii Autophagy and Toll-like receptors

In addition to being activated by starvation, autophagy can be activated by Toll-like receptor (TLR) signalling during infection. TLRs are transmembrane glycoproteins composed of an extracellular portion, containing leucine-rich repeat motifs (LRR) which are involved in the recognition of pathogenassociated molecular patterns (PAMPs); a transmembrane domain and a cytoplasmic domain which induces signal-transduction pathways (Akira *et al*, 2006; Vural&Kehrl, 2014) (Figure 1.4). TLRs are expressed predominantly on immune cells, such as macrophages, dendritic cells, B cells, T cells but can also be expressed on non-immune cells, such as fibroblasts and epithelial cells (Akira *et al*, 2006). Furthermore, they are positioned either on the cell surface or in intracellular compartments, such as endosomes, and lysosomes. The TLRs which are expressed in intracellular vesicles recognise ligands, mainly nucleic acids, which require internalization before signalling is possible. TLR1, TLR2, TLR4, TLR5, TLR6, and TLR10 are localised on the plasma membrane and recognise proteins, lipids and lipoproteins, whereas TLR3, TLR7, TLR8, and TLR9 are positioned in intracellular compartments and recognise pathogen nucleic acids. Interestingly, some TLRs bind to structurally unrelated ligands. One example is TLR4 which recognises viral proteins, fibronectin, heat-shock proteins as well as lipopolysaccharide (LPS), a signature component found on the membrane of Gram-negative bacteria (Akira *et al*, 2006; Vural&Kehrl, 2014).
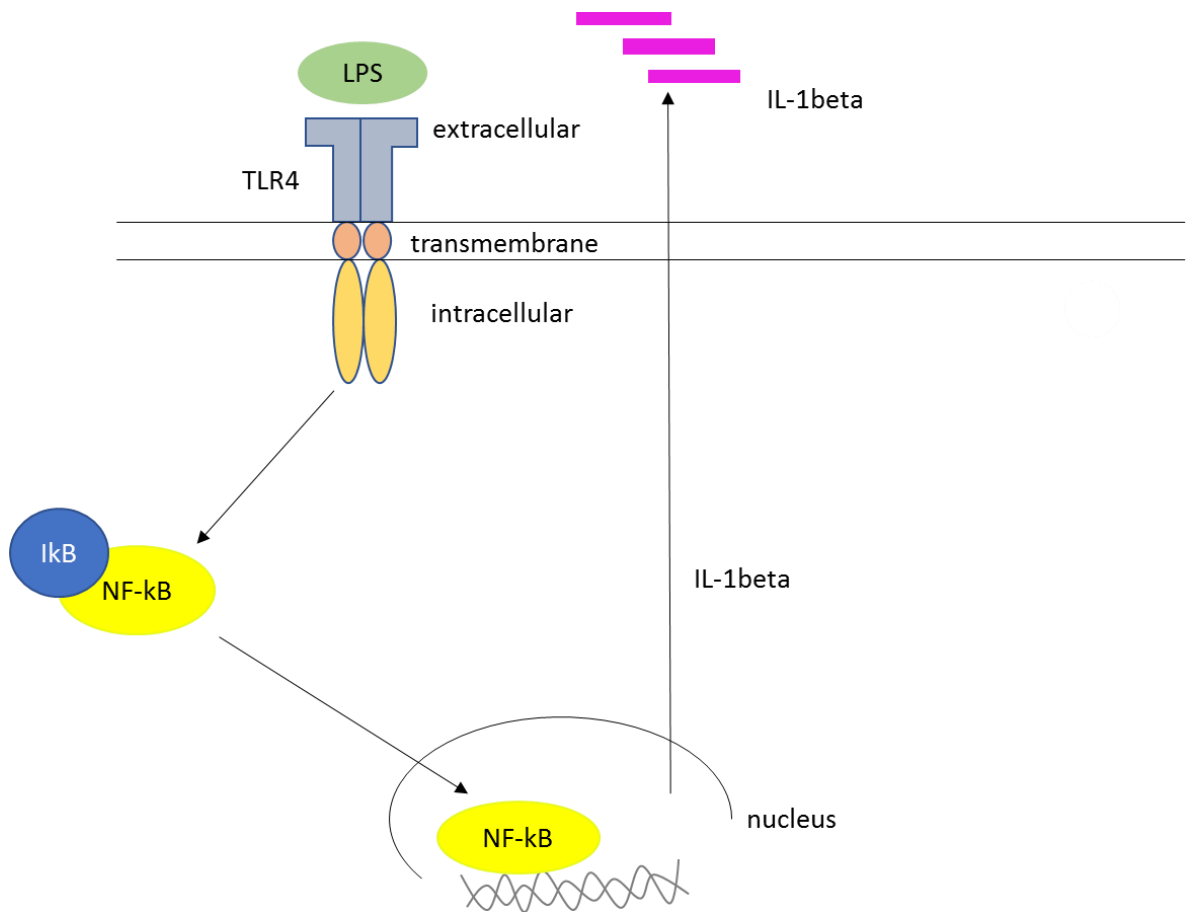
Figure 1.4 Mechanism of TLR4 stimulation and NF-kB activation. The extracellular domain of TLR4 recognizes LPS and transduces the signal with the help of the intracellular domain. IkB gets phosphorylated and ubiquitinated which results in its proteolytic degradation. NF-kB in turn translocates into the nucleus and activates *IL-1beta* transcription.

1.2.iv TLR4 and lipopolysaccharide

TLR expression is not a static but a dynamic process which corresponds to the pathogen, a variety of cytokines, as well as environmental stresses (Akira *et al*, 2006). The binding of PAMPs to TLRs initiates the innate immune response which then induces the adaptive immunity. Stimulation of different TLRs leads to diverse biological responses as various adaptor proteins are recruited to them which results in induction of different transduction pathways (Vural&Kehrl, 2014). One of the most extensively studied Toll-like receptors is TLR4. In 1999 MD2, myeloid differentiation factor 2, was shown to bind to LPS and confer its responsiveness to TLR4. The 18-25 kDa MD2 protein has been demonstrated to be the LPS co-receptor which is essential for the normal function of TLR4 and the subsequent activation of NF-kB (O'Neill *et al*, 2013) (Figure 1.4). NF-kB is a transcription factor involved in inflammation, immune response regulation, differentiation, and apoptosis. In resting cells, NF-kB is in the cytoplasm and is bound to the IkB inhibitor. Upon stimulation, IkB gets phosphorylated by the IkB kinase (IKK) complex which results in polyubiquitination and degradation of IkB. NF-kB translocates to the nucleus and induces the expression of various genes involved in inflammation and apoptosis (Sollberger *et al*, 2014).

After TLR stimulation, MyD88 mediates the recruitment of IRAK-4 followed by IRAK-1/2 (Figure 1.5). This complex interacts with TRAF6 which induces Lys63linked polyubiquitination of target proteins, including IRAK-1 (Lys63-linked polyubiquitin chains play a role in the formation of signalling complexes), or the generation of free Lys63-
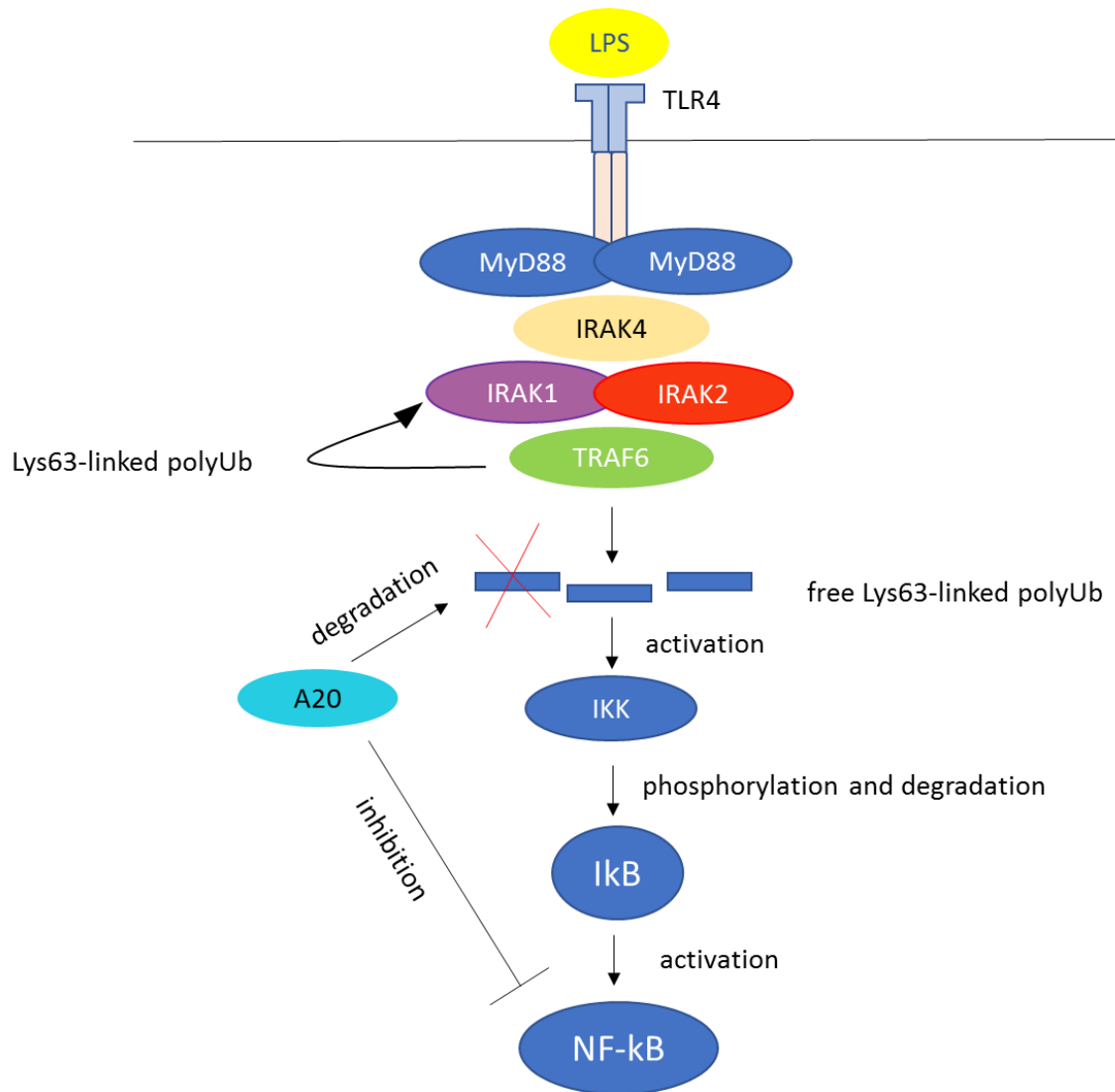
Figure 1.5 The TLR4 signalling pathway and role of A20 in NF-kB inhibition. The TLR4 stimulation involves the recruitment of various protein complexes (shown in coloured boxes) which induces Lys63-linked polyubiquitination and generation of free Lys63-linked polyubiquitin chains which in turn leads to the activation of the IKK complex. The IKK complex phosphorylates the IkB complex resulting in its degradation and subsequent activation of NF-kB. A20 cleaves Lys63-linked chains which leads to negative regulation of NF-kB and suppression of the TLR4 signalling.

linked polyubiquitin chains which are involved in the induction of a series of proteins, leading to the activation of the IKK complex and the subsequent NF-kB signalling. Excessive induction of the TLR pathway is linked to the development of inflammatory disorders. Therefore, cells have regulatory mechanisms to ''fine-tune'' TLR signalling. The ubiquitin-modifying enzyme A20 cleaves Lys63-linked chains and promotes the generation of Lys48-linked chains (Lys48-linked chains target proteins for degradation), resulting in negative regulation of NF-kB and suppression of the TLR signalling (Inomata *et al*, 2012; Duong *et al*, 2015). However, a negative regulatory system, if sustained, inhibits the response of the host to invasive pathogens. Therefore, immune suppression by A20 must be tightly regulated under stress conditions. Interestingly, autophagy has been shown to sequester A20 for degradation in tissue macrophages, thus inducing NF-kB activation. This allows macrophages to release chemokines and recruit neutrophils. It has been demonstrated that mice lacking autophagy in myeloid cells are prone to fungal infection due to impaired neutrophil recruitment (Kanayama *et al*, 2015).

1.2.v The inflammasome

The inflammasome is composed of a pathogen recognition receptor (PRR) of the NOD-like receptor (NLR) family such as NLRP1, NLR family pyrin domain containing 3 (NLRP3), NLR family CARD domain containing protein 4 (NLRC4), or the DNA-sensing absent in melanoma 2 (AIM2) (Denes *et al*, 2012). The cytosolic NLR family of PRRs function to sense and respond to stresses in the intracellular compartments. NLR members are classified based on their domain structure. The N-terminus can include a pyrin domain (PYD), a caspase-recruitment domain (CARD),

or a baculovirus inhibitory repeat (BIR) domain. The central nucleotide-binding oligomerization domain (NACHT) is common for all NLR members, followed by a C-terminal leucine-rich domain (LRR). The LRR domain is involved in the PAMP/DAMP sensing, whereas the N-terminal domain is essential for the recruitment of other inflammasome proteins, such as ASC and procaspase-1 (Denes *et al*, 2012). NLRP3 is the most characterised inflammasome complex which recognises a wide range of structurally diverse stimuli, such as pathogens, pore-forming toxins, ATP, monosodium urate crystals, cholesterol crystals, LPS, MDP, and bacterial RNA. In contrast, NLRP1 is activated by anthrax lethal toxin; NLRC4 is induced by several Gram-negative bacteria; AIM2 is stimulated by cytosolic doublestranded DNA (Franchi *et al*, 2009; Shi *et al*, 2012; Deretic, 2012).

Upon detecting cellular threat, NLRP3 oligomerises and exposes an N-terminal PYD domain for interaction with the PYD domain of the adaptor apoptosisassociated speck-like protein ASC (which relocates upon inflammation from the nucleus to the cytosol), which in turn recruits procaspase-1, resulting in its activation and cleavage of the precursor proIL-1beta into its active form (Qiao *et al*, 2012; Gurung&Kanneganti, 2015). Caspase-1 was described in 1989 as an inflammatory protease which induces the pro-inflammatory cytokines IL1beta and IL-18 (Sollberger *et al*, 2014). Pathogen and endogenous signals stimulate the procaspase-1 zymogen which results in auto-cleavage and the production of the active heterodimer consisting of two 10- and 20-kDa subunits, which can activate proIL-1beta and proIL-18 (Franchi *et al*, 2009) (Figure 1.6).

The NLRP3 inflammasome is induced through different receptor signalling pathways, such as TLRs. The stimulation of the Toll-like receptors and the subsequent activation of NF-kB is crucial for the transcriptional upregulation of both NLRP3 and proIL-1beta because their basal levels are inadequate for the inflammasome function. Moreover, NLRP3 is maintained in the cytosol in a ubiquitinated state which, upon stimulation, is capable of oligomerization after deubiquitination. In contrast, ASC and procaspase-1 are not adequate concentrations in the steady state (Sutterwala *et al*, 2014). The fact that proIL1beta levels are usually low requires its transcriptional upregulation which, as already described, is mediated by TLR stimulation and NF-kB activation. However, for the NLRP3 to function efficiently, a microbial ligand alone is not sufficient. An additional signal is required to activate the inflammasome, which can be extracellular ATP, bacterial toxins, or certain crystals (Franchi *et al*, 2009). An exception is the induction of the inflammasome by the TLR4 ligand LPS under conditions in which autophagy is compromised (Saitoh *et al*, 2008).
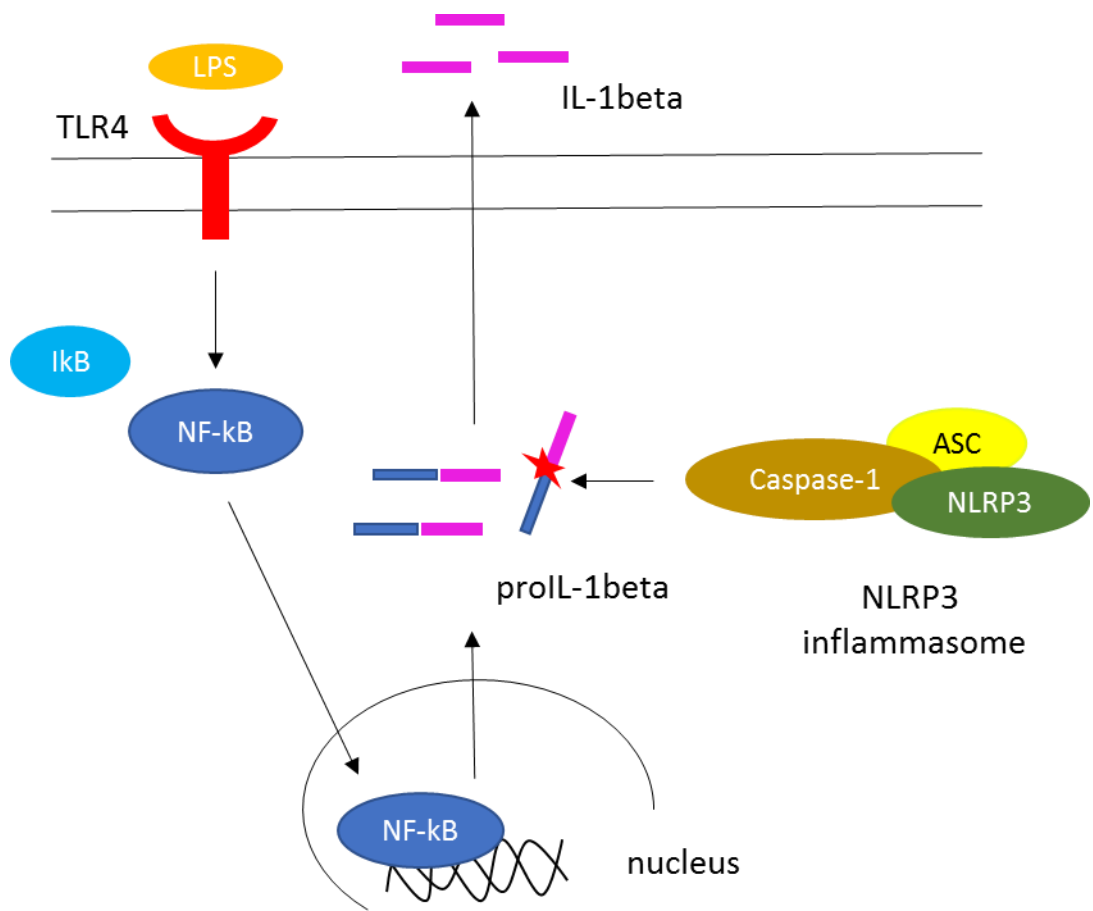
Figure 1.6 NLRP3 assembly and IL-1beta production and secretion. Upon stimulation, NLRP3 interacts with the adaptor apoptosis-associated speck-like protein ASC which in turn recruits caspase-1, resulting in its activation and cleavage of the precursor proIL-1beta (blue + purple) into its active IL-1beta form (purple). The cleavage site is marked with a red asterisk. NF-kB is also shown as it modulates proIL-1beta, as well as NLRP3, ASC and caspase-1 gene expression levels.

1.2.vi Caspase-8

Caspase-8 has long been recognised for its role in apoptosis. However, new evidence has shown the essential function of this protease in the regulation of inflammation. It has been demonstrated that caspase-8 is involved in NFkB activation and for direct or indirect cleavage of proIL-1beta, with or without the help of caspase-1. Different studies have demonstrated the role of caspase-8 in the release of pro-inflammatory cytokines. Murine B cells lacking caspase-8 expression exhibit compromised phosphorylation and nuclear translocation of the p65 subunit of NF-kB, resulting in decreased IL-6, TNF and IFN-beta levels after LPS treatment. Another function of caspase-8 is to activate caspase-1 which can then cleave proIL-1beta and proIL-18. *In vitro* studies have shown that caspase-8 cleaves caspase-1, leading to the full activation of caspase-1 and the subsequent induction of proIL-1beta and proIL-18 in response to LPS and ATP. It has also been reported that both caspases act synergistically to activate proIL-1beta but the molecular mechanisms underlying this function remain to be described (Man&Kanneganti, 2016). Other studies have demonstrated the binding of caspase-8 to ASC, suggesting that the protease is an active member of the inflammasome, however, the exact role of caspase-8 in the inflammasome induction remains unknown (Guo *et al*, 2015).

1.2.vii IL-1beta

IL-1beta is a pleiotropic, pro-inflammatory cytokine which is involved in the initiation of the innate immune response (Harris, 2013; O'Neill *et al*, 2013; Hailey *et al*, 2009). Although it is secreted by various cell types, the majority of studies focus on its production by immune cells, such as

monocytes and macrophages (Denes *et al*, 2012). IL-1beta was reported to play a crucial role in T-cell activation and the activation of the acute phase response (O'Neill *et al*, 2013). Systemic consequences of IL-1beta production include fever, hypotension and vasodilatation, whereas locally, the cytokine induces the expression of adhesion molecules on mesenchymal and endothelial cells which facilitates the recruitment of immune cells. The recruited lymphocytes and myeloid cells are then activated which enhances the inflammatory response (Gaidt&Hornung, 2017).

Proteins such as IL-1beta, IL-18 or fibroblast growth factor (FGF)-2 serve extracellular functions but they lack a signal peptide which would allow their endoplasmic reticulum (ER)/Golgi-dependent secretion. However, these proteins get secreted through mechanisms which are poorly understood, termed unconventional protein secretion (Sollberger *et al*, 2014).

Although crucial in the immune response, over-generation of IL-1beta can result in both acute (sepsis) and chronic (diabetes, rheumatoid arthritis, and artherosclerosis) disease. Therefore, its expression, production and secretion are tightly regulated. IL-1beta is synthesized as a biologically inactive 269residue precursor (31 kDa) protein, termed proIL-1beta. Caspase-1 and caspase-8 have been shown to cleave proIL-1beta to generate the 153-residue active form from the C-terminal domain. Two cleavage sites in proIL-1beta have been reported: Asp272Gly28 and Asp1162Ala117 (Figure 1.7). The cleavage starts at Asp272Gly28 followed by Asp1162Ala117, resulting in the production of the 17 kDa active form of IL-1beta which is then exported by a non-conventional secretion mechanism. Interestingly, proIL-1beta is

protease sensitive along the entire amino acid sequence, including the section which forms the mature cytokine. IL-1beta, however, is protease resistant under the same conditions. Moreover, the biologically inactive N-terminus inhibits the folding of the C-terminal domain but maintains the protein in a conformation which is primed to fold quickly after cleavage (Hailey *et al*, 2009).

1.3 Structure and function of Atg16L1

As already discussed, the potential link between Atg16L1 and inflammation was made when a T300A mutation in Atg16L1 was found to be a risk allele Crohn's disease. The protein is encoded by the *Atg16L1* gene which is located on chromosome 1 or 2 in mice or humans, respectively, and contains 607 amino acids. Atg16L1 expressed by mammals contains an N-terminal domain that binds Atg5 followed by a coiled coil domain (CCD) attached via a linker region to a larger C-terminal WD (tryptophan-aspartate) domain containing 7 WD repeats (Mizushima *et al*, 2003) (Figure 1.8).

The Atg5 binding domain binds the Atg5-Atg12 conjugate via Atg5, and selfassociations between CCD of Atg16L1 generate a large 800kDa complex that is required for conjugation of phosphatidylethanolamine (PE) to LC3 (Fujita *et al*, 2008). The CCD also provides a binding site for the PtdIns(3)P effector protein WIPI2b ensuring localised incorporation of lipidated LC3 into the autophagosome membrane (Dooley *et al*, 2014). Binding of Atg16L1 to WIPI2b requires glutamate residues E226 and E230 in the Atg16L1 CCD which bind arginines R108 and R125 exposed on the surface of WIPI2b. Deletion of either E226 or E230 in Atg16L1 abrogates binding to WIPI2b, and expression of WIPI2b lacking
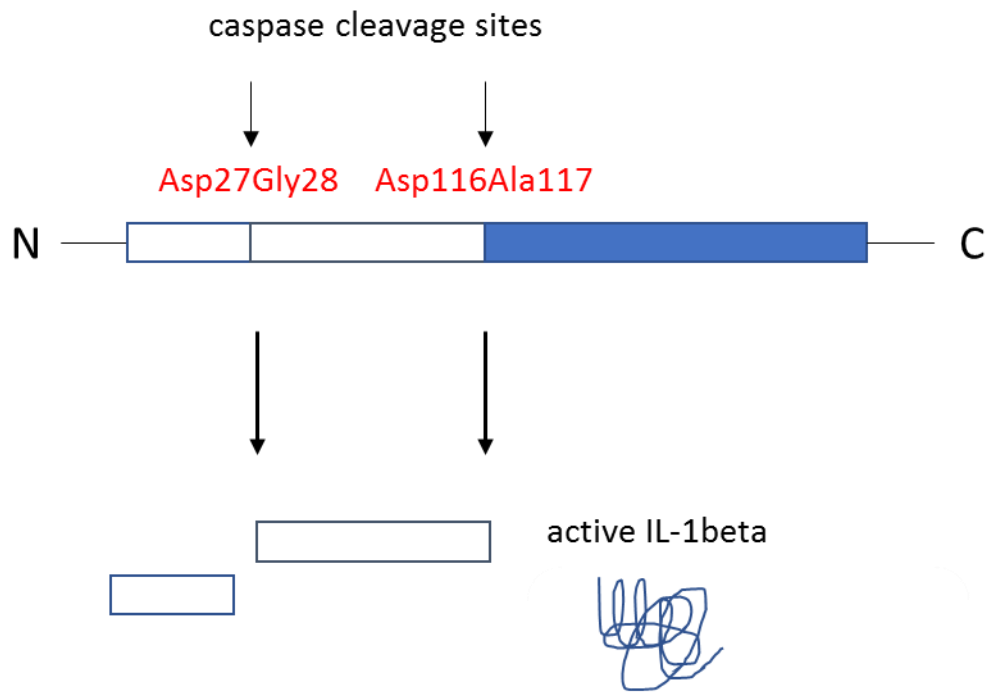
Figure 1.7 Schematic representation of proIL-1beta and caspase-1 cleavage sites. White boxes indicate the inactive part of the protein, whereas the blue box represents that part of proIL-1beta which, after caspase cleavage (cleavage sites are highlighted in red), folds to form the active IL-1beta (blue).
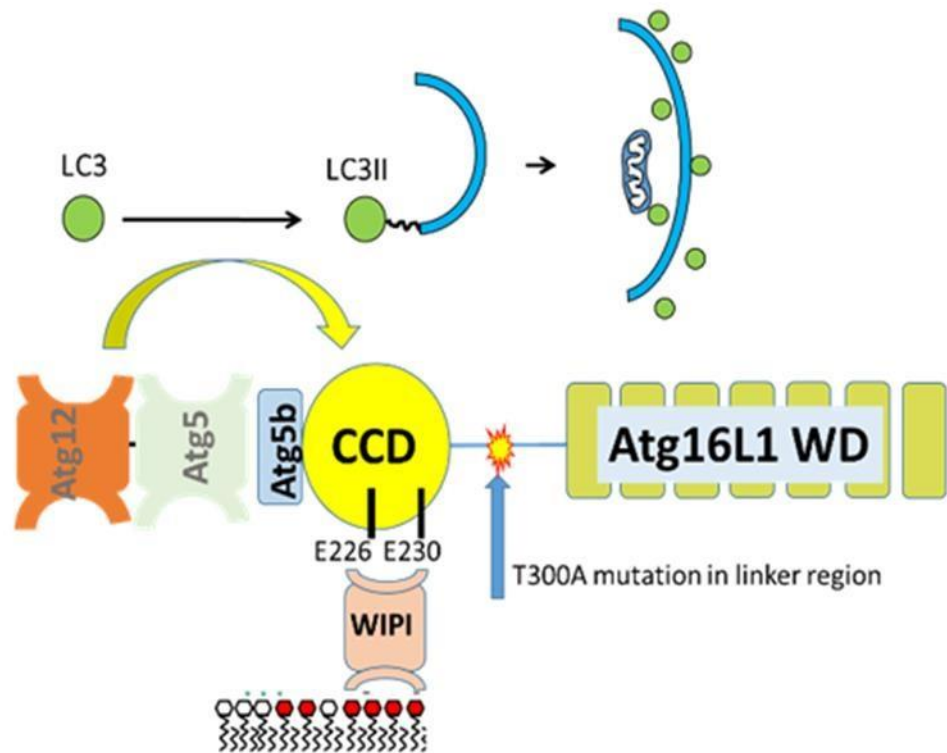
Figure 1.8 Structure and function of mammalian Atg16L1. Atg16L1 consists of an N-terminal Atg5-binding (Atg5b) domain followed by a coiled coil domain (CCD) which is attached by the C-terminal WD domain via a linker region containing the Crohn's disease risk allele T300A (indicated with an asterisk). Glutamate residues E226 and E230 in the CCD are required for the binding of Atg16L1 to WIPI2b, thus ensuring the incorporation of LC3-II into the autophagosome membrane. The interaction between the CCD with both Atg5-Atg12 and WIPI2b is required for LC3-I lipidation and autophagosome formation. [Figure provided by Tom Wileman].

R108 and R125 is unable to reconstitute LC3 recruitment to autophagosomes in WIPI2b depleted cells (Dooley *et al*, 2014) (Figure 1.8). The direct interaction between the CCD of Atg16L1 with both the Atg5-12 conjugate and the PtdIns(3)P effector protein WIPI2b is therefore required for LC3 conjugation to PE and autophagosome formation.

The CCD of Atg16L1 provides binding sites for Atg5 and WIPI2b, but the precise role played by the large C-terminal WD domain of Atg16L1 is unknown. The seven WD repeat domains generate a circular □-propeller (Bajagic *et al*, 2017) that is thought to provide a rigid scaffold to co-ordinate assembly of multiple protein complexes, and it is generally believed that the 800kD Atg5-12:16L1 complex provides a platform for protein:protein interactions important for autophagy. Several proteins that bind the WD domain of Atg16L1 are linked to pathogen clearance suggesting that the WD domain has evolved in higher eukaryotes to link autophagy to pathogen clearance and inflammation. These include pattern recognition receptors, such as TLR2 and NOD-like receptor NOD2, and TRIM20 which inhibits inflammasome-mediated activation of IL1beta (Boada-Romero *et al*, 2013; Kimura *et al*, 2015; Bajagic *et al*, 2017). The WD domain of Atg16L1 also binds the cytoplasmic tail of transmembrane protein TMEM59 which directs LC3 to endosomes containing Staphylococci (Boada-Romero *et al*, 2016).

The work of Murthy *et al* (2014) place T300A CD risk allele in the linker region of Atg16L1. This increases sensitivity of Atg16L1 to caspase-3-mediated processing and is generally believed to compromise autophagy. Interestingly, cleavage at this site preserves the Atg5 binding and CC domain and the E226 and E230 glutamates required for

binding to WIPI2b (Figure 1.9). This raises the possibility that cleavage of Atg16L1 within the linker region may affect functions other than autophagy, and given the binding of the WD domain to TLR2, NOD2, TRIM20 and TMEM59 this may involve pathways important for pathogen recognition and clearance and inflammation.

1.4 LC3 associated phagocytosis (LAP)

The phagocytic activity (the ability to ''eat'' or ''ingest'') of immune cells, such as macrophages, dendritic cells and neutrophils is crucial for the normal function of the innate immunity. The engulfment of a pathogen results in the generation of an intracellular vesicle, called the phagosome, which in common with autophagosomes, fuses with lysosomes (Figure 1.10). Degradation in lysosomes can kill pathogens, allowing specialised MHC-II antigen presentation compartments to expose peptides derived from pathogen proteins to T-cells to increase immune responses (Crotzer&Blum, 2009).

Recent studies have demonstrated that LC3, the major membrane protein of the autophagosome, can play a role during phagocytosis by an autophagyrelated pathway called LC3-associated phagocytosis (LAP) (Lai&Devenish, 2012). During LAP, LC3 is conjugated to the cytoplasmic face of the phagosomes and this may accelerate the targeting of phagosomes containing pathogens to lysosomes for degradation. LAP is activated following stimulation of Toll-like receptors, such as TLR1, TLR2, TLR4, and TLR6 and the engulfment of particles, which results in the recruitment of a subset of autophagy proteins to the phagosome. Although both autophagy and LAP involve the recruitment of class III PI3K, the Atg12-Atg5-Atg16L1 and LC3.
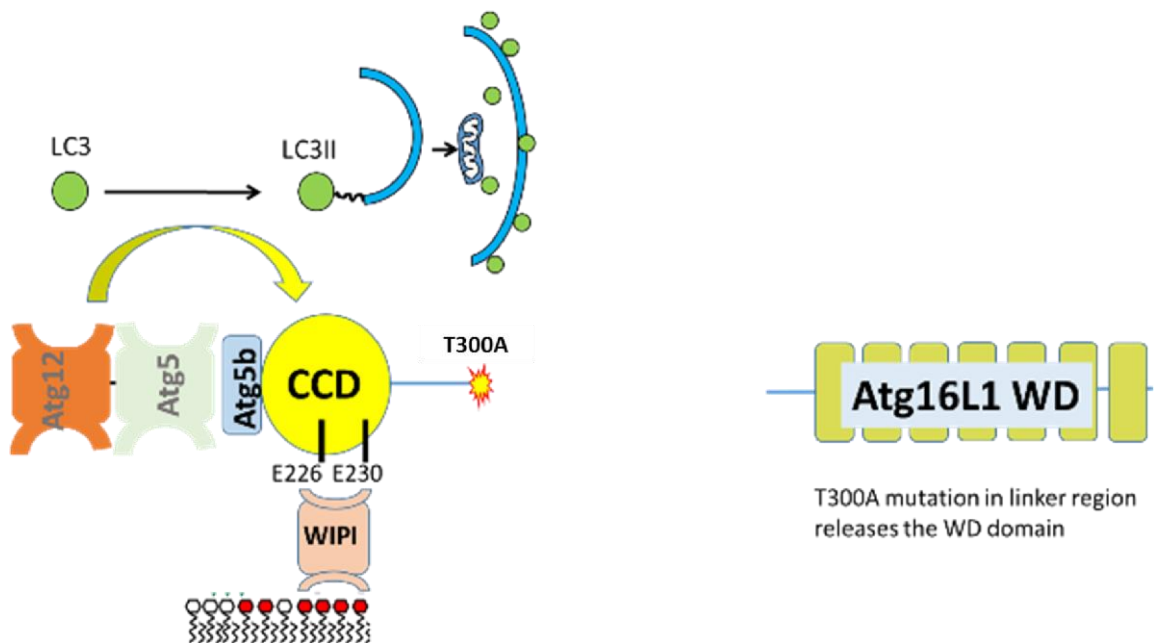
Figure 1.9 Crohn's disease risk allele T300A sensitizes Atg16L1 to caspase-3 cleavage. Crohn's disease T300A variant is located in the linker region of Atg16L1 and is associated with increased sensitivity to caspase-3-mediated processing. The cleavage preserves the Atg5 binding and CC domains and E226 and E230 residues required for interaction with WIPI2b. [Figure provided by Tom Wileman].
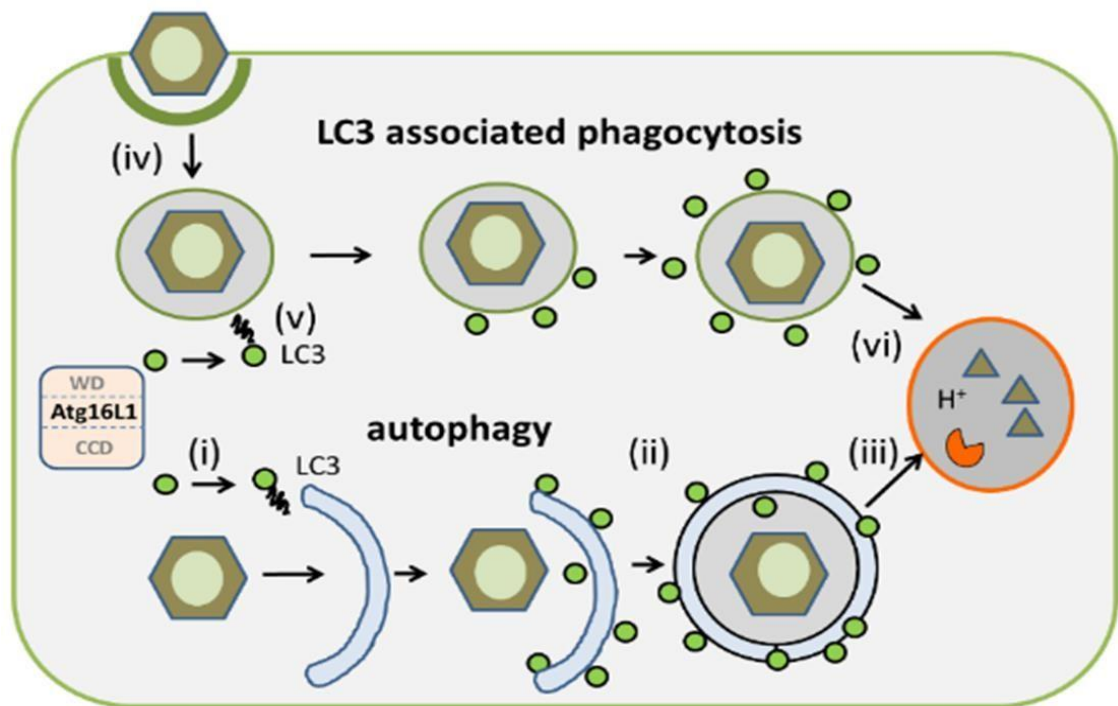
Figure 1.10 Pathways by which pathogens can be degraded. i) Autophagy targets intracellular pathogens for degradation by enclosing them into an LC3recruited double-membrane, an autophagosome **(ii)**; **(iv)** The engulfment of an extracellular pathogens is termed LC3-associated phagocytosis (LAP) and results in the formation of an LC3-recruited single-membrane structure, a phagophore, which encapsulates the pathogen **(v)**. Aurophagosomes **(iii)** and phagosomes **(vi)** fuse with a lysosome leading to the pathogen clearance. conjugation systems, they are mechanistically distinct processes. Autophagy requires ULK1 and VPs34 during the formation of a pre-initiation complex, and these are not needed for LAP. LAP on the other hand requires a Beclin regulatory protein called Rubicon, UVRAG and reactive oxygen species (ROS). [Figure provided by Tom Wileman].

Importantly for this project Atg16L1 is required for autophagy and LAP (Martinez *et al*, 2015).

During autophagy, the V-ATPase maintains autophagy flux by acidifying endolysosomal compartments and enabling the activity of the lysosomal hydrolases. Lysosomotropic compounds, however, inhibit autophagy and enhance the activation of LAP. The Na^+/H^+ ionophore monensin raises the lysosomal pH and blocks autophagy. Monensin enhances LAP by LC3-induced lipidation onto endolysosomal compartments, a process driven by osmotic imbalances within these compartments (Florey *et al*, 2015).

1.4.i Autophagy and LAP in inflammation

Pathogen recognition receptors sense bacterial components and induce signal-transduction pathways which results in the production of inflammatory mediators, such as cytokines, interferons, and chemokines. The strict regulation of inflammation is crucial for the host because insufficient or excessive inflammation can cause damage and disease. It is becoming increasingly clear that intracellular degradation systems play an essential role in the regulation of the immune response by degrading inflammatory mediators (Shibutani *et al*, 2015). This can involve degradation of pathogens, or degradation of proteins involved in inflammatory signalling. Both autophagy and LAP are effector mechanisms downstream of TLR stimulation which are involved in pathogen recognition and degradation, and the subsequent modulation of the immune response (Deretic, 2012; Martinez *et al*, 2015) (Figure 1.11).

1.5 Summary

Atg16L1 is required for both autophagy and LAP but the role played by the WD domain of Atg16L in these processes, and the control of inflammation 'in vivo' is not known. The observation that the T300A mutation associated with Crohn's disease can lead to the release of the WD domain by caspase-3 suggests theWD domain may be required for autophagy to suppress inflammation. Alternatively, the WD domain may be important for controlling inflammation through LAP, but none of these possibilities has been tested directly.

Autophagy and LAP require Atg16L1 for recruitment of LC3 to membranes, and tissue-specific knock out of Atg16L1 would result in loss of both pathways. Systemic loss of autophagy proteins, including Atg16L1, results in postnatal death because mice are unable survive the transient starvation that occurs when mice transfer from placental nutrition to feed on milk. The WD domain of Atg16L1 is missing in yeast, even so the Atg5 binding domain and CCD (Atg5b-CCD) are sufficient for autophagy and viability. This made it possible that the Atg5b-CCD may be sufficient for autophagy in higher eukaryotes such as mice. This study has analysed mice expressing the Atg5b-CCD of Atg16L1, but lacking the linker and WD domains (Atg16L1^{E230}) (Figure 1.12). These mice, activate autophagy, survive postnatal starvation and grow at the same rate as littermate controls. The mice are also fertile and provide a source of mice able to provide macrophages to test the role played by the Atg5b-CCD and the WD domains of Atg16L1 in controlling inflammation *in vivo*.
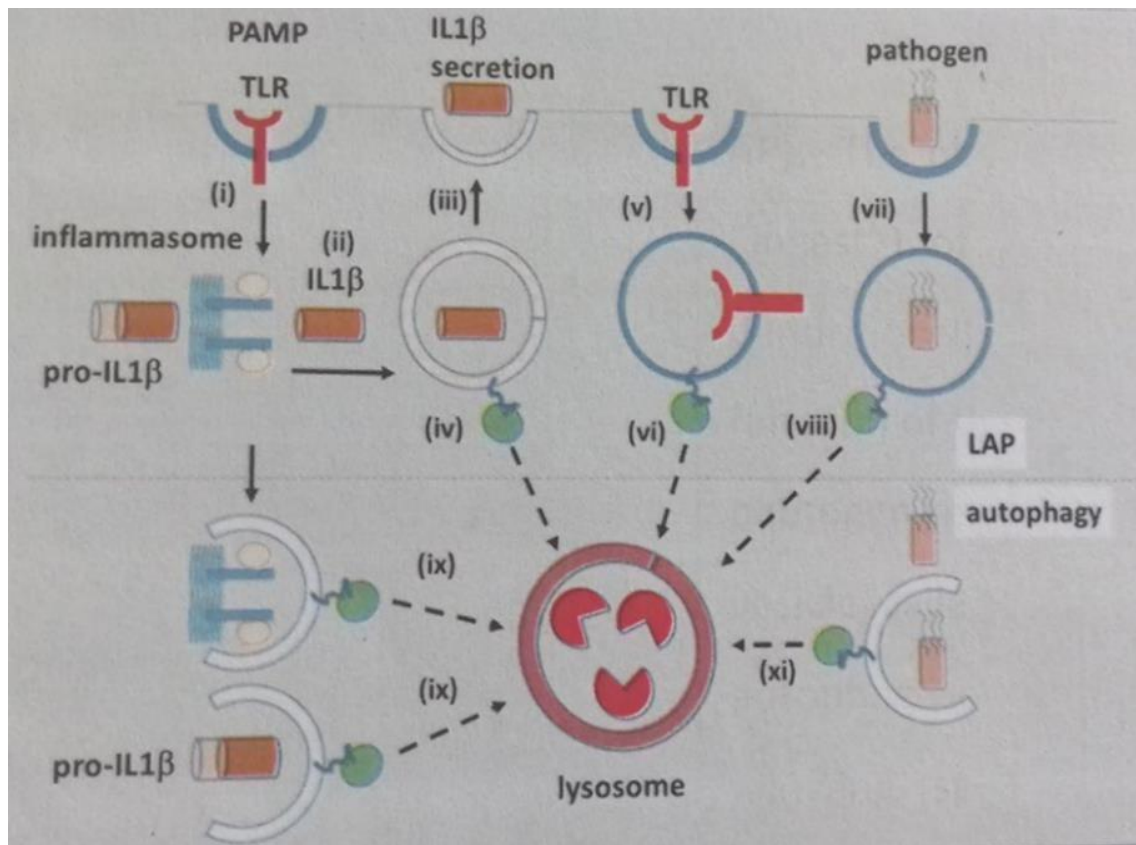
Figure 1.11 Possible mechanisms of autophagy and/or LAP inflammatory suppression in macrophages. TLR4 signalling (i) results in assembly of the inflammasome and conversion of proIL-1beta to IL-1beta **(ii).** IL-1beta is secreted by a pathway that may involve membrane vesicles **(iii)** or transporters that could be targeted for covalent attachment of LC3-II and delivery to lysosomes by LAP **(iv)**. TLR receptors can be removed from the plasma membrane by endocytosis **(v)** and signalling attenuated by targeting endosomes containing receptors via LAP **(vi)**. Pathogens entering cells in phagosomes **(vii)** are targets for LAP resulting in rapid delivery to lysosomes for degradation **(viii)**. At the same time inflammasome components **(ix)** and IL-1beta **(x)** can be removed from the cytoplasm by autophagy, as can pathogens that enter the cytosol **(xi)**. [Figure provided by Tom Wileman].
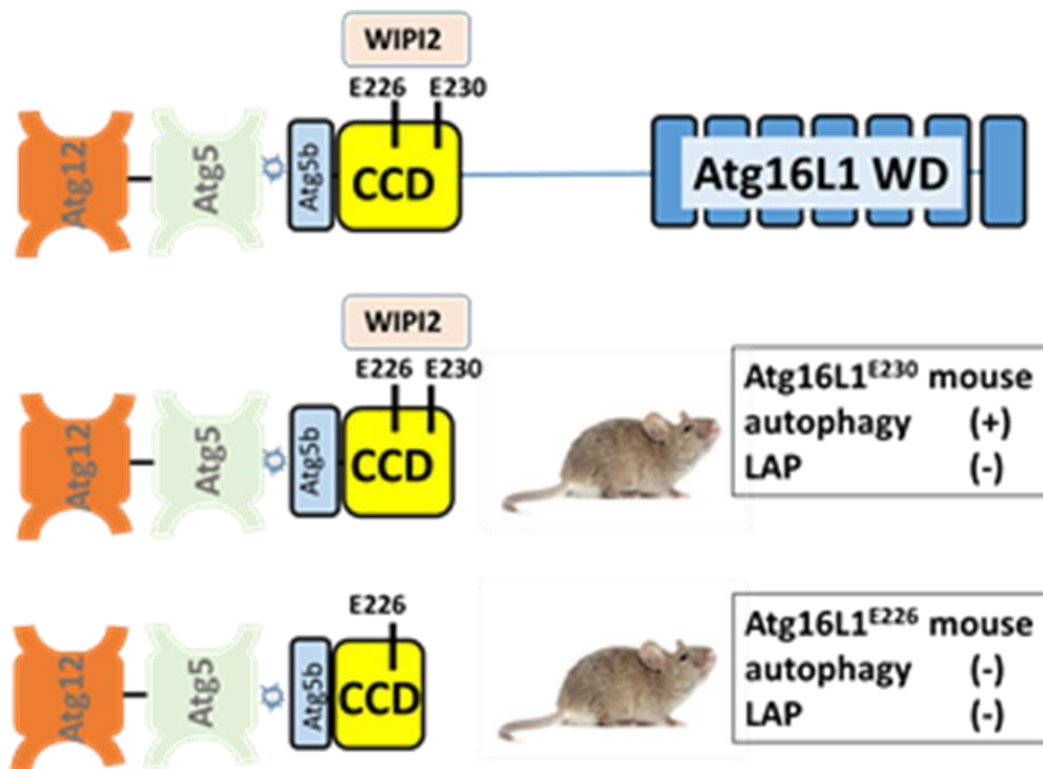
Figure 1.12 Summary of mouse phenotype with regard to Atg16L1 domain expression. i) Full length Atg16L1 expresses both the Atg5:CC domain and the WD domain, therefore wild type mice are autophagy and LAP-positive; **ii)** Atg16L1^{E230} mice express glutamate residues E226 and E230 which are essential for WIPI2b binding and autophagy but lack the WD domain and are therefore LAP-deficient; **iii)** Atg16L1^{E226} mice lack the E230 residue in the CC domain as well as the WD domain and are therefore autophagy- and LAP-deficient. [Figure provided by Tom Wileman].

1.6 Specific aims

Aim 1.   To determine the role played the Atg5b-CCD and WD domain of Atg16L1 during LAP.

Aim 2.   To determine the role played the Atg5b-CCD and WD domain of Atg16L1 in controlling IL-beta production by macrophages.

Aim 3.   To determine the role played the Atg5b-CCD and WD domain of Atg16L1 during M1 and M2 polarisation.

Hypothesis:

The published observation that the T300A mutation associated with Crohn's disease can lead to the release of the WD domain by caspase-3 cleavage leads us to hypothesise that the Atg16L1^{E230} mouse can be used as a Crohn's model. Additionally, the WD domain may be required for autophagy to suppress inflammation and inhibit macrophage M1 polarization.

Chapter 2

Materials and Methods

2.1 Mouse models

Two mouse models were used: Atg16L1^{E226} and Atg16L1^{E230} (see Chapter 3). All mice were maintained in accordance with Home Office regulations under specific pathogen free conditions in individually ventilated cages. Mice were weaned at approximately 3 weeks of age and separated by gender. Mice were ear tagged and ear biopsy taken for genotying. Maintenance animals no longer required were sacrificed by exposure to increasing CO_2 in line with Home Office Schedule 1 guidelines.

2.2 Genotyping

After the mice were bred and the new puppies were born, small ear biopsies were taken for genotyping. Each biopsy was lysed in 0.1 M Tris HCl pH=8.5 (Sigma, RES3098T-B7), 0.2M NaCl (Sigma, S7653), 0.005M EDTA (VWR, 60-00-4), 0.2% SDS (Sigma, L3771), 100 ug/ml proteinsase K (VWR, PAV3021) at 55°**C** overnight for tissue dissociation. Touchdown PCR was performed on the samples containing the lysed biopsies (diluted 1:10 with water), the primer sets (20 pM) (290: 5' CAAATATGCCTTCAGAACTG 3'; 291: 5' GCTGTAGTTCCAATCCCTAA 3'; 338: 5' TCGATGCTAGCCTACTATTC 3') and a reagent mixture (25 uM dNTP mix (Thermo Fisher, R0191), home-made 10x buffer, home-made DNA polymerase (diluted 1:10 with water) using a standard PCR thermocycler (Veriti, Applied Biosystems). The PCR programme was as follows: 95°C for 3 min; (x10) 95°C for 45 sec, 65°C (decreases 1°C/cycle) for 45 sec, 72°C for 1 min; (x25) 95°C for 45 sec, 55°C for 45 sec, 72°C for 1 min; 72°C for 10 min; 4°C on hold. PCRs were run on a 2% agarose

gel, then stained in an ethidium bromide containing TAE buffer (Sigma, T6025) and imaged on UVP Imager.

2.3 Bone marrow extraction

The mice were sacrificed by cervical dislocation. The abdomen and hind legs were sterilised with 70% ethanol. An incision was made in the midline of the abdomen, then legs were cut using scissors and muscle was removed by a blade. The femur and the tibia were separated at the knee joint. The bones were cut at both ends and flushed with RPMI-1640 (Sigma, R8758)using a 10 ml syringe and a 25gauge needle. The bone marrow was then passed through a cell strainer and collected into a 50 ml Falcon tube. The cells were then spun at 850 g at 4°C for 5 min. The supernatant was discarded and cell pellet was re-suspended in 14 ml of fresh RPMI-1640. M-CSF (Peprotech, 315-02) was then added to the cell suspension at a concentration of 30 ng/ml and cells were cultured in petri dishes for 6 days in an incubator (5% CO_2, 37°C). The medium was changed on day 3.

2.4 Culture media and reagents

The bone marrow-derived macrophages (BMDM) were grown in RPMI-1640 (Sigma) containing M-CSF (30 ng/ml) (Peprotech) with 10% fetal calf serum (FCS) (Sigma, 12133C) and 1% penicillin/streptomycin (PenStrep) (Gibco by Life Technologies, 15140122) at 37°C with 5% CO_2. Cells were detached using phosphate-buffered saline (PBS). The culture medium was removed and the cells were washed twice with pre-warmed PBS. Ice cold PBS (7 ml per dish) was added to the dishes which were then incubated in the fridge for 30 min. Detached cells were then transferred into 50 ml Falcon tubes and dishes were washed with ice

cold PBS to collect the remaining cells. The tubes were then spun at 850g at 4°C for 5 min. The supernatants were discarded and the cell pellets were re-suspended in either 1) RPMI-1640 containing M-CSF. Cells were counted and seeded for experiments; or 2) freezing medium containing 90% pre-warmed FCS and 10% DMSO (Sigma, D8418). Cells were frozen at -80 °C for future use.

BMDMs were stimulated with LPS 100 ng/ml (Sigma, L4130) and 100 ng/ml IFN-gamma (Peprotech, 315-05) for 24h to induce M1 polarization, or 10 ng/ml IL-4 (Peprotech, 214-14) and 20 ng/ml IL-13 (Peprotech, 210-13) for 24h to induce M2 polarization. To investigate inflammasome activation, cells were treated with 1 μg/ml LPS (Sigma) for 4h, followed by 150 μM BzATP (Sigma-Aldrich, B6396) for 30 min. To investigate IL-1beta secretion in response to TLR stimulation, BMDMs were treated with LPS (1 μg/ml) (Sigma-Aldrich), flagellin (10 μg/ml) (Sigma-Aldrich, SRP8029), CpG (10 μg/ml) (Invivogen, 1585), and MDP (10 μg/ml) (Sigma-Aldrich, A9519) to activate TLR4, TLR5, TLR9, and NOD2, respectively.

2.5 Flow cytometry

Bone marrow-derived macrophages were cultured at 5×10^5 cells/well in a 48well plate overnight at 37°C with 5% CO_2 in M-CSF (30 ng/ml) containing RPMI-1640. Cells were detached (see ''Culture media and reagents'') and resuspended in 0.5 ml of 5% FCS PBS. 0.5 μl of anti-mouse CD16/CD32 antibody (Fc block antibody) (eBioscience, 14-0161-81) was added (diluted 1:400) and the cells were incubated for 10 min. Anti-mouse F4/80 Antigen APC (eBioscience, 17-4801-80) and Anti-Mouse CD11b FITC (eBioscience, 11-0112-82), 0.5 μl each, were added

(diluted 1:400) and the cells were incubated for 30 min in the dark. The samples were spun at 850 g for 5 min, washed once and re-suspended in 600 μl of 5% FCS PBS. Unstained cells were used as a control. The cells were characterized using Beckman Coulter Cytoflex.

2.6 Immunofluorescence

BMDMs were cultured at 50 000 cells/well on microscope glass coverslips (13 mm, No 1, VWR, 631-0149) in 24-well plates and subjected to treatment time courses. The RPMI-1640 was removed, the cells were washed with 1xPBS and then fixed in ice cold 100% MeOH (-20°C, 10 min) (Sigma, 322415). The cells were washed three times with 1xPBS and blocked in 5% goat serum (Sigma-Aldrich), 0.3% Triton X-100 (Sigma-Aldrich, 9002-93-1), 1% bovine serum albumin (BSA) (VWR) in PBS for 30 min. The primary antibody (Table 1) was prepared in antibody dilution buffer (0.3% Triton X-100 and 1% BSA in PBS). The cells were incubated with the primary antibody overnight at 4°C and then washed three times with 1xPBS, 5 min. The secondary antibody (Table 1) was prepared in antibody dilution buffer. The cells were incubated in the secondary antibody for 2h at room temperature, then washed three times in 1xPBS, 5 min and stained in 4', 6-diamidino-2-phenylindole (DAPI) (Thermo Scientific, 62248) for 10 min at room temperature. The coverslips were then mounted onto microscope slides (VWR, 631-1551) with Fluoromount G (VWR, 100502-406) for imaging (Zeiss, Axio Vision fluorescence imager, 63x objective setting).

2.7 Analysis of IL-1beta in cell culture supernatants

2.7.i Cell culture

BMDMs were cultured at 80 000 cells/well in 48-well plates and either left in culture medium (untreated, control macrophages) or treated with LPS (100 ng/ml) (Sigma-Aldrich) for 4h and BzATP (150 μM) for 30 min. The supernatants were then collected and IL-1beta levels were measured using Luminex (eBioscience).

2.7.ii Luminex Multiplex Assay

Concentrated 50x IL-1beta Simplex beads (eBioscience, EPX01A-26002-901) were diluted in water at a final concentration 1x. The beads were then vortexed for 30 sec. 50 μl of the magnetic beads attached to antibodies were added to the appropriate wells of a 96-well flat bottom plate and incubated for 2 min to allow their accumulation on the bottom of each well. The wells were then washed with 120 μl of wash buffer (Hand-Held Magnetic plate washer was used for the washing steps) (eBioscience). The IL-1beta standard was diluted in culture medium according to manufacturer's protocol to prepare the top concentration (4 800 pg/ml). 4-fold serial dilutions were made to create the standard curve for a total of 7 points. 50 μl of standards/samples were added to the beadcontaining wells. The plate was sealed and incubated with shaking for 2h at room temperature. The wells were washed 3 times with 120 μl of wash buffer. 25 μl/well of IL-1beta detection antibody was added, plates were sealed and incubated with shaking for 30 min at room temperature. After 3x120 μl washes with wash buffer, 50 μl/well of Streptavidin-PA was added and plates were sealed and incubated with shaking for 30 min at room temperature.

Once again, the wells were washed 3x120 µl of wash buffer after which 120 µl/well of reading buffer was added. The plate was sealed and incubated with shaking for 5 min at room temperature, and then read on Luminex®100/200.

2.8 Analysis of IL-1beta in murine serum samples

2.8.i *In vivo* LPS challenge

Mice were injected intraperitoneally with either PBS (control) or LPS (10 mg/kg) (Sigma, L2630) and blood samples were collected 90 min post injection. The whole blood was allowed to clot at room temperature for 20 min. To remove the clot, the samples were then spun at 2000 g at 4°C for 10 min. The resulting supernatant (blood serum) was transferred to a clean Eppendorf and used for Luminex analysis of IL-1beta levels (see Analysis of IL-1beta in cell culture supernatants).

2.9 ProIL-1beta ELISA

2.9.i Preparation of lysates from cultured bone marrow-derived macrophages

BMDMs were cultured at 80 000 cells/well in a 48well plate overnight at 37°C with 5% CO_2 in M-CSF (30 ng/ml) containing RPMI-1640. They were then either left in the culture medium (untreated, control macrophages) or treated with LPS (100 ng/ml) (Sigma-Aldrich) for 24h. After the incubation, the medium was removed and the cells were washed with PBS. 100 µl of ice cold ProcartaPlex cell lysis buffer (eBioscience, EPX-99999-000) was added to each well and incubated for 5 min. The cells were then scraped, transferred to a clean Eppendorf tube and spun at

14 000 g at 4°C for 10 min. The supernatants were transferred to a clean Eppendorf and assayed or stored at -80°C.

2.9.ii Enzyme Linked Immunosorbent Assay (ELISA)

ELISA was conducted according to manufacturer's protocol (ELISA Ready-SetGo, eBioscience, discontinued). In brief, Corning Costar (9018) ELISA plates were coated with 100μl of proIL-1beta capture antibody in 1xcoating buffer. The plates were sealed and incubated overnight at 4°C. The wells were then aspirated and washed three times with 250 μl wash buffer. The residual liquid was removed by blotting the plates on absorbent paper. To block the wells, 200 μl of 1xELISA Diluent was added and the plates were incubated at room temperature for 1h. The wells were aspirated and 100 μl of each sample was added per well. The plates were sealed and incubated at room temperature for 2h. The wells were aspirated and washed 5 times with 250 μl wash buffer. After adding 100 μl/well of biotinylated detection antibody, the plates were sealed and incubated at room temperature for 1h. The wells were aspirated and washed 5 times with 250 μl wash buffer. 100 μl/well of Avidin-HRP was added and the plates were incubated at room temperature for 30 min. The wells were aspirated and washed 7 times with 250 μl wash buffer. 100μl/well of TMB solution was added and the plates were incubated at room temperature for 15 min. 50 μl/well of stop solution was added and plates were read at 450 nm using (the values were corrected to the background of 570 nm). Mouse proIL-1beta recombinant protein was used to create a standard curve. The standard was diluted according to manufacturer's protocol (eBioscience) to prepare the top concentration (3 000 pg/ml). 2-fold serial dilutions were made to create the standard curve for a total of 8

points. 100 μl/well of each standard was added to the appropriate wells. The concentration of proIL-1beta in each sample was calculated using the standard curve.

2.10 Caspase-Glo® 1/8 Inflammasome Assay

BMDMs were cultured at 50 000 cells/well in a 96-well plate overnight at 37°C with 5% CO_2 in M-CSF (30 ng/ml) containing RPMI-1640. They were then either left in culture medium (untreated, control macrophages) or treated with LPS (1 μg/ml) for 4h which was followed by a 30 min treatment with BzATP (150 μM) (Sigma-Aldrich). The plate was then removed from the incubator and allowed to equilibrate at room temperature for 5 min. 100 μl of Caspase-Glo® 1/8 reagent (Caspase-Glo® 1 buffer was added to ZWEHD substrate; Caspase-Glo® 8 buffer was added to Caspase-Glo® 8 substrate) (Promega, G9951 and G8200) was added to each well and the contents were mixed by using a plate shaker at 500 rpm for 30 sec. The plate was incubated at room temperature for 1h and read at 560 nm using a Wallac plate-reading luminometer. Blank reactions (containing culture medium but no cells) were used to measure the background luminescence associated with the culture medium and Caspase-Glo® 1/8 reagent. The values for the blank reactions were subtracted from those obtained for the experimental cells.

2.11 Mouse proIL-1beta _pcDNA3.1+N-eGFP

Mouse proIL-1beta _pcDNA3.1+N-eGFP was generated by GenScript. This plasmid contains full length proIL-1beta tagged at the N-terminus with enhanced green fluorescent protein (eGFP).

2.11.i Starter culture preparation and plasmid isolation

The proIL-1beta plasmid (4 μg) was re-suspended in 40 μl of water. After a brief vortex, 4 μl of the plasmid were added to 50 μl of DH5α *E.coli*. The sample was incubated on ice for 30 min, heated at 42°C for 50 sec, incubated on ice for 2 more minutes, then added to 900 μl of SOC medium (Invitrogen, 15544034). The medium was incubated with shaking at 37°C for 2h. LB agar plates (with ampicillin, 100 μg/ml) were spread with 100 μl of the SOC medium and incubated overnight at 37°C for 14-16h. A single colony was selected and inoculated in 150 ml of liquid LB medium with ampicillin (100 μg/ml). After a 14-16h incubation at 37°C in shaking condition, the LB was transferred into a 50 ml Falcon tube which was then spun at 6000g for 15 min. The supernatant was discarded and the plasmid isolation was conducted according to the manufacturer's protocol (Macherey-Nagel). In brief, the pellet was re-suspended in 8 ml of resuspension buffer+Rnase A (NucleoBond®Xtra Midi kit, 740410-10). After a brief vortex, 8 ml of lysis buffer was added to the suspension. The tube was incubated at room temperature for 5 min. NucleoBond®Xtra column was equilibrated with 12 ml of equilibration buffer which was allowed to empty by gravity flow. 8 ml of neutralization buffer was added to the suspension and was mixed by inverting the tube. The lysate was loaded onto the column which was then washed with 5 ml of equilibration buffer. The column filter was removed and the column was washed with 8 ml of wash Buffer. The plasmid DNA was eluted with 5 ml of pre-heated elution buffer and collected in a 50 ml Falcon tube. 3.5 ml of room temperature isopropanol was added to precipitate the DNA. The sample was

vortexed and spun 15 000 g at 4°C for 30 min. The supernatant was removed and 2 ml of room temperature 70% ethanol was added to the pellet. The sample was spun at 15 000 g at room temperature for 5 min. The ethanol was discarded and the pellet was allowed to air dry for 10 min. The plasmid DNA pellet was re-suspended in 300 μl of sterile water. The concentration was measured using a nanodrop spectrometer.

2.11.ii Restriction digest

The mouse proIL-1beta pcDNA3.1+N-eGFP plasmid (300 ng) was digested using KpnI and EcoRI (Figure 2.1). The digestion was performed in water bath at 37°C for 40min. The plasmid was run on a 1% agarose gel (restriction digestion conducted by GenScript).
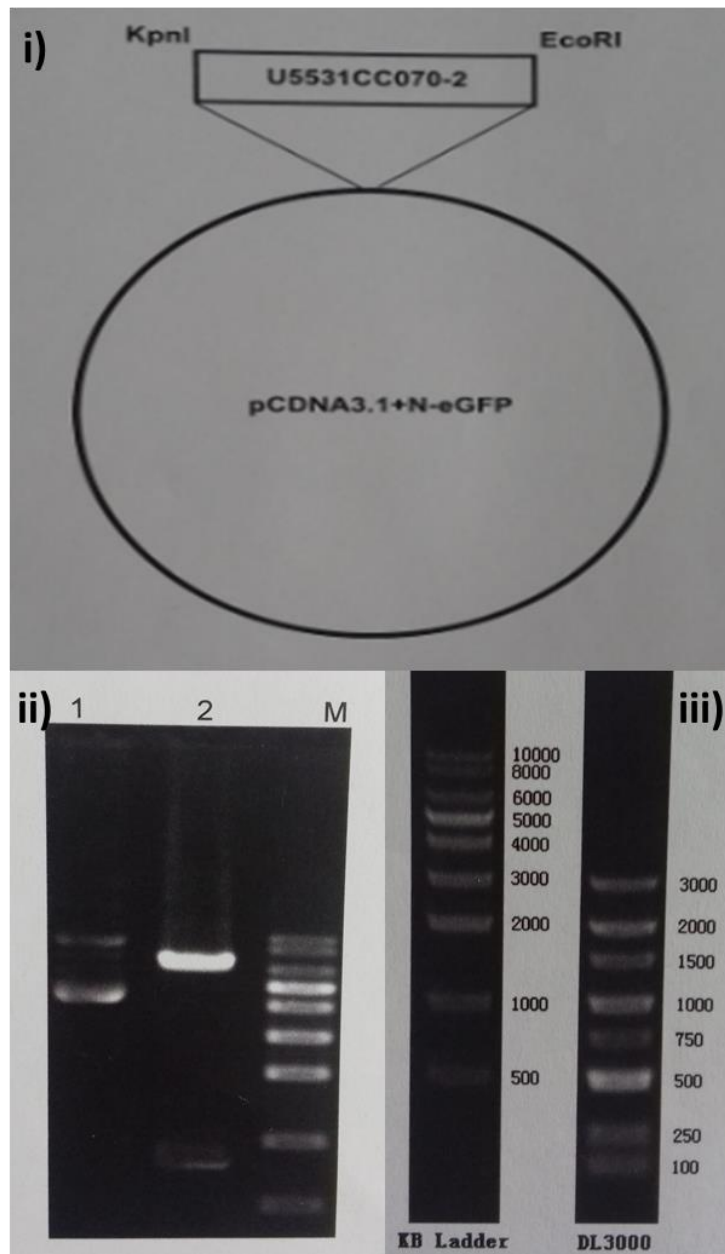
Figure 2.1: Pro-IL1β-GFP plasmid map and restriction digest validation of plasmid. (i) A cartoon of the plasmid and the gene of interest pro-IL1β ligated into plasmid DNA using KpnI and EcoRI; **(ii)** 300ng plasmid DNA, lane 1, was ran on a 1% agarose gel, 300ng plasmid DNA after digestion using KpnI and EcoRI restriction enzymes, lane 2. Lane M is a base-pair ladder for size, expanded version shown in **(iii)**. Lane 2 shows the gene of interest approximately 800bp (lower band) and empty plasmid 7000bp (upper band).

2.11.iii HEK293A cell culture

Human Embryonic Kidney 293 cells (HEK293A) (Thermo Fisher, R70507) were chosen to use with the mouse proIL-1beta pcDNA3.1+N-eGFP plasmid due to their high transfection efficiency. The cells were cultured in high glucose Gibco™ DMEM (Fisher Scientific, 41965062) in T75 flasks and split 1:3 every 2 to 3 days.

2.11.iv Mouse proIL-1beta pcDNA3.1+N-eGFP plasmid transfection

HEK293A cells were cultured at 15 000 cells/well on glass coverslips (13 mm, No 1, VWR) in a 24-well plate. The transfection was conducted using Lipofectamine® LTX with Plus™ reagent (ThermoFisher Scientific, 15338100) according to the manufacturer's protocol. In brief, the following recipe was followed (volumes indicated/well): 1.4 μl of Lipofectamine was mixed with 50 μl of Optimem in a 1.5 ml Eppendorf. In a separate 1.5 ml Eppendorf 1.05 μl of plasmid DNA (2 μg) was mixed with 0.65 μl of Plus reagent and 50 μl of Optimem. The contents of the two tubes were mixed, vortexed and incubated at room temperature for 10 min. 100 μl of the mixture was added per well.

The plate was incubated at 37°C with 5% CO_2 for 24h.

2.12 Protein analysis

2.12.i Cell lysis

For the protein expression analysis, BMDMs were cultured at 500 000 cells/well overnight at 37°C with 5% CO_2 in M-CSF (30ng/ml) containing RPMI-1640 in a 12 well-plate, and subjected to treatment time courses. The cells were washed once with 1xPBS which was then discarded. 30 μl of Tissue Protein Extraction Reagent (T-PER) (Thermo Fisher, 89842) was

added per well. The cells were then scraped and the cell lysates were transferred to clean Eppendorf tubes. The lysates were incubated on ice for 30 min and then centrifuged at 16 000 g at 4°C for 10 min. The supernatants were transferred to clean Eppendorf tubes and stored at -80°C or used for Western blotting.

2.12.ii Bradford assay

The Bradford assays were conducting using the Bio-Rad protein kit II (Bio-Rad, 5000002). A bovine serum albumin (BSA) standard was diluted according to the manufacturer's protocol (Bio-Rad) to prepare the top concentration (150 μg/ml) which was then used to create the standard curve for a total of 7 points. 10 μl of each BSA standard were loaded in a 96-well plate. The samples were diluted 1:10 with nuclease-free water and 10 μl of each were used for the assay. The Bio-Rad protein assay dye reagent was made up in water at a dilution of 1:5. 190 μl of the dye were added to both standards and samples to a total volume of 200 μl/well. The plate was incubated at room temperature for 5 min and read on BMG Omega reader (595nm). The sample volumes to be loaded onto the Western blotting gels were calculated to make 10 μg/μl.

2.12.iii Western blotting

Equal volumes of protein sample and RunBlue LDS sample buffer (Expedeon, B31010) were mixed and heated at 93°C for 4 min. The Blue SDS run buffer (Expedeon, NXA05160) was diluted 1:8 in water. Precast 4-12% SDS gels (Expedeon, NXG41212) and All Blue standards (Bio-Rad, 1610373) were used for the assay. The gels were run at 140V for 90 min. The samples were transferred onto nitrocellulose membranes (Bio-Rad) by wet transfer containing 25 mM Tris base, 190 mM glycine, 20%

methanol and 0.05% SDS. The transfers were run at 200mA at 4°C for 85 min. The membranes were blocked for 1h in 5% skim milk (Sigma, 70166) Tris-buffered saline and Tween® 20 (Sigma-Aldrich, P9416) (TBST) at room temperature. The blocked membranes were stained with primary antibodies in 3% skim milk (Table 1) overnight at 4°C. The stained membranes were washed in TBST 5x5 min at room temperature, then stained with secondary antibodies (Table 1) at room temperature for 2h. The membranes were washed in TBST 5x5 min and PBS 2x1 min, and then imaged on ChemiDoc XRC+ Imaging System (BioRad).

Antibody	Application	Company
Mouse anti-actin, 58169 dilution 1:1000	WB	Cell Signalling Technology
Rabbit anti-Atg16L1, 8089 dilution 1:1000	WB	Cell Signalling Technology
Rabbit anti-LC3, 4108 dilution 1:500	WB, IF	Cell Signalling Technology
Rabbit anti-NLRP3, 15101 dilution 1:1000	WB	Cell Signalling Technology
Rabbit, anti-A20, 5630 dilution 1:1000	WB	Cell Signalling Technology
Mouse anti-caspase-1, 14-9832-82 dilution 1:1000	WB	eBioscience
Mouse anti-caspase-1, sc-398715 dilution 1:500	IF	Santa Cruz
Anti-rabbit HRP-conjugated secondary antibody, 7074 dilution 1:10 000	WB	Cell Signalling Technology
Anti-mouse HRP-conjugated secondary antibody, 7076 dilution 1:10 000	WB	Cell Signalling Technology
AlexaFluor 488 goat anti-rabbit IgG, R37116 dilution 1:10 000	IF	Thermo Fisher
AlexaFluor 594 donkey anti-rabbit IgG, R37119 dilution 1:10 000	IF	Life Technologies

Table 1. Primary and secondary antibodies used for immunofluorescence and western blotting.

2.13 Gene expression analysis

2.13.i RNA extraction

BMDMs were cultured at 500 000 cells/well overnight at 37°C with 5% CO_2 in M-CSF (30ng/ml) containing RPMI-1640 in a 12 well-plate and treated according to the experimental needs. The cells were washed once with 1xPBS which was then discarded. 100 μl Trizol reagent (Ambion by Life Technologies, 15596026) was added to each well. The cells were scraped and the samples were transferred to clean Eppendorf tubes. 20 μl chloroform was added to each sample to help the homogenization. The tubes were shaken vigorously for 15 sec, incubated at room temperature for 2 min, and then spun at 12 000g at 4°C for 15 min. The aqueous phase of the samples was removed and placed into a new tube. 50 μl 100% isopropanol was added to the samples which were then incubated at room temperature for 10 min and spun at 12 000g at 4°C for 10 min. The supernatants were discarded and the RNA pellets were washed with 100 μl 75% ethanol. The samples were vortexed and spun at 7 500g at 4°C for 5 min. The wash was discarded and the pellets were air dried for 10 min, then re-suspended in 15 μl Rnase-free water and incubated in a heat block at 57°C for 15 min.

2.13.ii RNA clean-up

The RNA samples were cleaned using Rneasy MinElute cleanup kit (Qiagen, 74204). The sample volume was adjusted to a volume of 100 μl with Rnase-free water. 350 μl buffer RLT and 250 μl 100% ethanol were added. The samples were then mixed well, transferred to an Rneasy MinElute spin column placed in a 2 ml collection tube, and spun at 10 000 g at room temperature for 15 sec. The wash was discarded and 500

μl buffer RPE was added to the spin column. The samples were spun at 10 000 g at room temperature for 15 sec, 500 μl 80% ethanol was added each of them, followed by a 2 min spin at 10 000 g. The flow-through was discarded and the columns were spun again at full speed for 5 min to dry the spin column membranes. The Rneasy MinElute spin columns were placed in new 1.5 ml collection tubes. 14 μl Rnase-free water was added to the column membranes, then the tubes were spun at full speed for 1 min to elute the RNA.

A nanodrop spectrometer was used to measure the RNA concentration.

2.13.iii Reverse transcription (cDNA synthesis)

The reverse transcription was done according to Table 2. The mixture was heated at 65°C for 5 min and then chilled on ice. 4 μl 5xFirst strand buffer and 2 μl 0.1M DTT were added to the mixture which was then incubated at 25°C for 2 min. 1 μl Superscript II was added, followed by a 2-hour incubation at 42°C and a 15-minute incubation at 70°C.

2.13.iv Primer design and optimization

The primers were designed using Primer3 software and purchased from Sigma-Aldrich unless otherwise stated (Table 3).

Gradient PCR was performed to determine the optimum annealing temperature of each primer set: initial denaturation: 95°C for 30 sec; cycling stage (x40): 95°C for 5 min, temperature gradient for 15 sec, 72°C for 10 min. The PCR products were run on a 2% agarose gel containing ethidium bromide (Figure 2.2i). After the optimum annealing temperature was determined, the qRT-PCR amplification efficiency was estimated which indicates the rate at which the PCR amplicon is generated. A standard curve and a 2-fold dilution

Reagent	12 µl reaction
RNA	1 µg
Random primers (Promega)	1 µl
dNTPs (10mM)	1 µl
RNAaseIn (Promega)	1 µl
dH$_2$O	up to 12 µl

Table 2. Reverse transcription reagent mixture.

Primer	Sequence	Annealing temperature
IL-1beta	5' GAGCCCATCCTCTGTGACTC 3'	60°C
	5' CGACAGCACGAGGCTTTT 3'	
IL-6	5' CCTCTCTGCAAGAGACTTCCAT 3'	60.5°C
	5' AATTAAGCCTCCGACTTGTGAA 3'	
Ptgs2	5' AGCCAGGCAGCAAATCCT 3'	58.5°C
	5' ACAGTTTTCACCATAGAATCCAGTC 3'	
Arg1	5' ACGTAGACCCTGGGGAACA 3'	60°C
	5' CCAGCAGGTAGCTGAAGGTC 3'	
Chil3	5' GTGTTCTGGTGAAGGAAATGC 3'	60°C
	5' TCAGGGATCTTGTACCCAGACT 3'	
NLRP3	5' ATGCTGCTTCGACATCTCCT 3'	60°C
	5' AACCAATGCGAGATCCTGAC 3'	
A20	5' TCGCGCTGTTCCACTTGTTA 3'	60°C
	5' GCGTTGATCAGGTGAGTCGT 3'	
18S	(Qiagen)	60°C
	(Qiagen)	

Table 3. Primers used for qRT-PCR

series of cDNA were used to verify the efficiency of the PCR reaction (Figure 2.2ii). Only primer sets with efficiencies between 90% and 110% were used for qRT-PCR (Figure 2.2iii).

2.13.v qRT-PCR

qRT-PCR was carried out using 2x qPCRBIO SyGreen mix (PCR Biosystems, PB20.11-05) (Table 4).

The real-time PCR programme was as follows: holding stage: 50°C for 2 min, followed by 95°C for 10 min; cycling stage (x35): 95°C for 15 sec, followed by the specific primer annealing temperature (Table 4) for 45 sec; melt curve stage: 95°C for 15 sec, 60°C for 1 min, 95°C for 30 sec and 60°C for 15 sec. The melt curves were analyzed to determine if the qRT-PCR had produced single, specific product (Figure 2.2iv). The gene expression values were calculated using the relative copies method and normalized to 18S. The PCR was carried out in a 7500 Real-Time PCR System (Applied Biosystems, Grand Island, NY).

2.14 Seahorse

The Seahorse XFp metabolite analyzer was used to measure oxygen consumption (OCR) and proton production (ECAR) from BMDMs isolated from wild type or mutant mice. The flux plate (Figure 2.3) is loaded with specific inhibitors in each port (four ports above each well) that allow selective application of either substrates or inhibitors of glycolysis or oxidative phosphorylation. The flux plate sits above the cell culture plate that has eight wells containing adherent cells in six wells, two wells are used as control wells. The substrates and inhibitors are injected at specific time points, to examine their effect upon cell metabolism. For

example, experiments lasted approximately 100 minutes with detection of either OCR or ECAR every 12 minutes, appropriate substrates or inhibitors were injected sequentially at time points 20, 45 and 70 minutes thereby allowing approximately 25 minutes to determine any effect. The Seahorse detects changes in either OCR or ECAR by fluorescent sensor probes that run down through the flux plate in close proximity to the adherent cell layer. The Seahorse XF Cell Mito Stress Test (Agilent, 103015-100) kit was used to examine different parameters of respiration; basal respiration, proton leak and ATP production, whilst the Seahorse glycolysis stress test (Agilent, 103017-100) was used to examine; glycolytic reserve, glycolytic capacity and glycolysis.

i)

| | 60°C | 61°C | 62°C | 63°C | 64°C | negative control |

ii)

NLRP3

y = -3.3028x + 20.416
R² = 0.9979

iii)

Amplification Plot

ΔRn vs Cycle

iv)

Melt Curve

Derivative Reporter (-Rn) vs Temperature (°C)
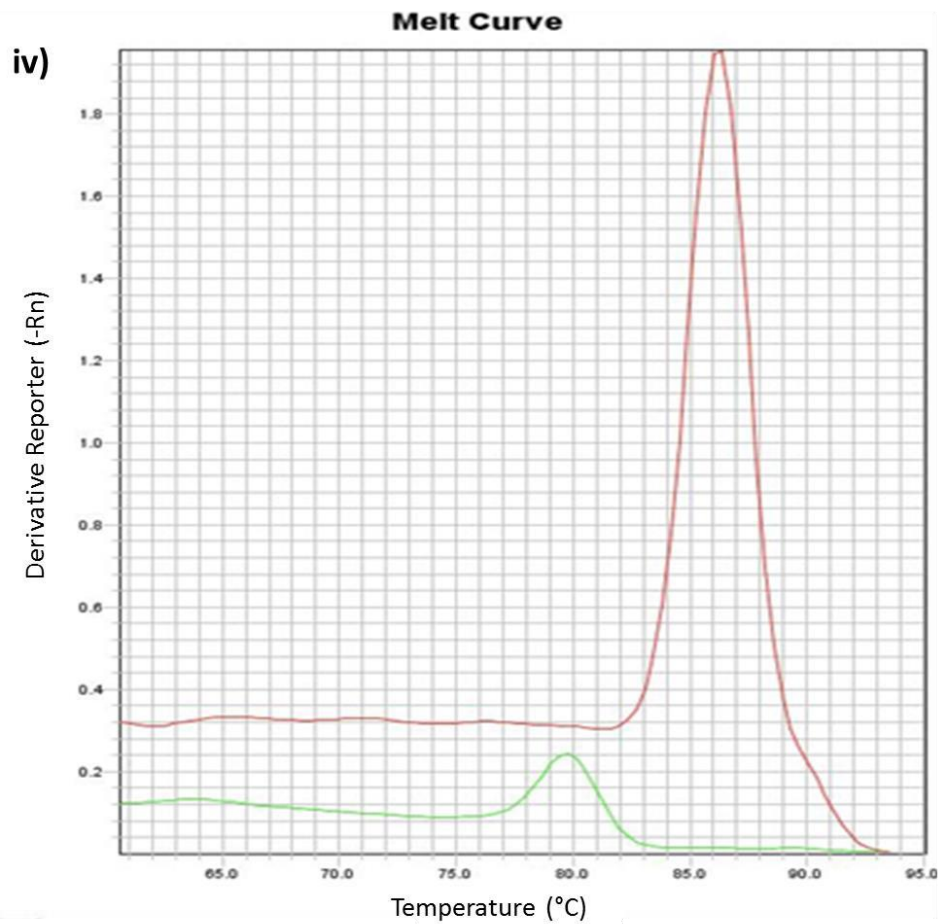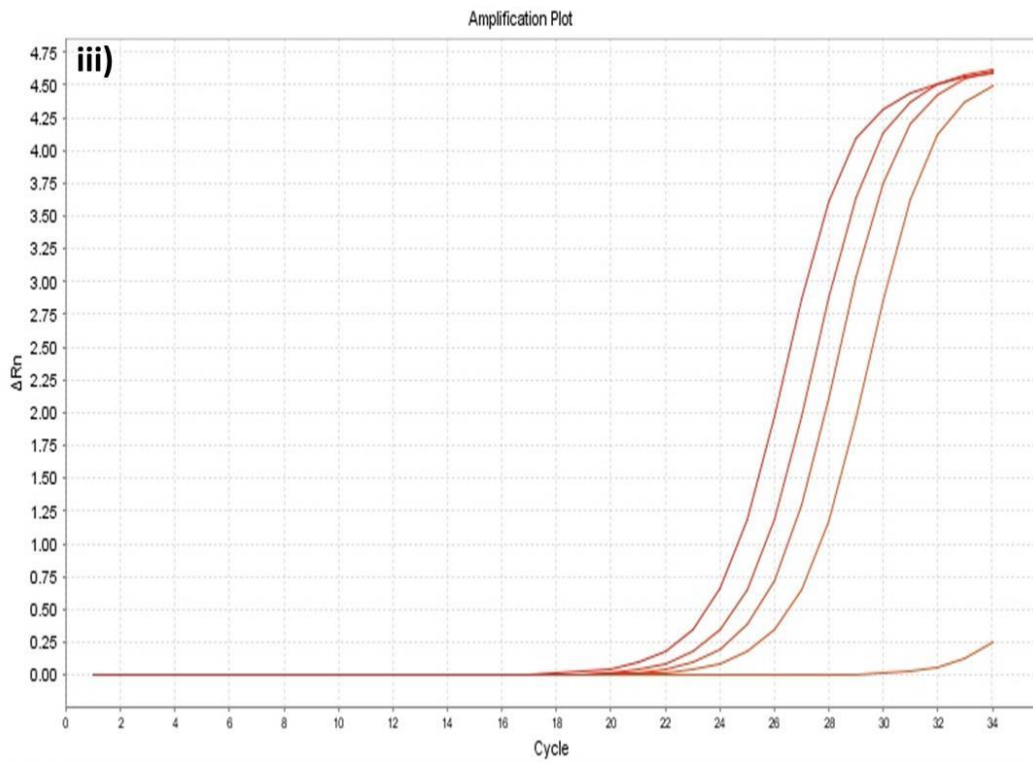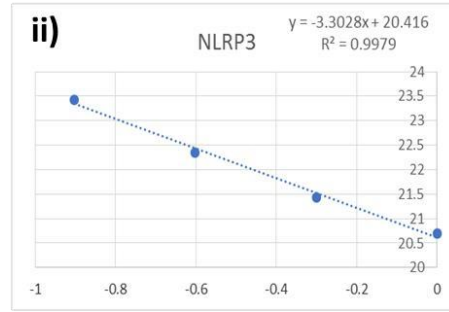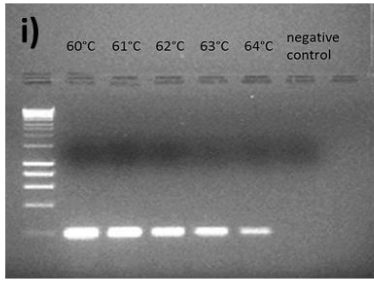
Figure 2.2. Example validation of primer set to be used for qPCR. (i) Annealing temperature was determined using endpoint PCR over the indicated annealing temperature range (60-64°C) and products ran on a 1% agarose gel. Thereafter, the primer efficiency in a qPCR **(ii)** reaction was calculated at the annealing temperature (60°C) using serial dilutions of cDNA and plotting the Ct value versus Log concentration, the slope of the curve (3.3) was used to determine the efficiency (100.8%). The Ct values of serially diluted cDNA was derived from amplification curves **(iii)**. Finally, the melt curve was examined **(iv)** to ensure a single product (red) for the primer set and no product (also see **(i)**) in the no-template control (green) sample.

Reagent	20µl reaction
2x qPCRBIO SyGreen Mix	10µl
Forward primer (10 µM)	0.8µl
Reverse primer (10 µM)	0.8µl
Template cDNA (0.5µg)	2µl
dH$_2$O	6.4µl

Table 4. qRT-PCR reagent mixture.
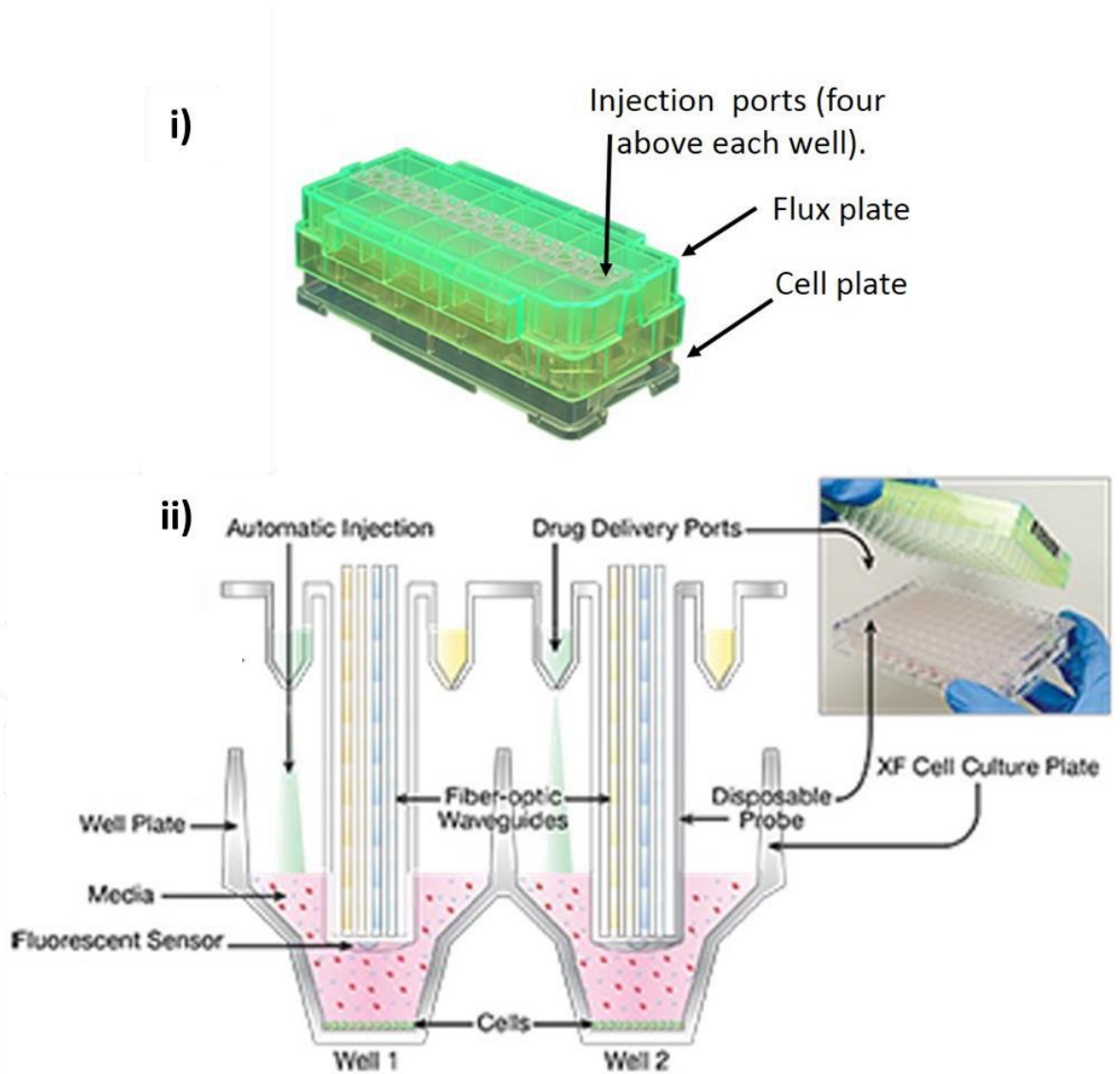
Figure 2.3 Seahorse Flux and Cell plates used in mitochondrial or glycolysis stress tests. (i): Flux plate (green) with injection ports sits on top of the cell culture plate (bottom clear). **(ii)** Zoom in schematic of the Seahorse well plate and sensor for detection of oxygen or protons at the detection probe tip, using proprietary fluorescence technology, and is utilised during the mitochondrial or glycolytic stress tests respectively. These fluorescence measures are then used to calculate separate areas of respiration for graphing as histograms [Images taken from Agilent Technologies].

2.14.i Glycolysis stress test

The glycolysis stress test measured the basic metabolic profile of the BMDM cells derived from wild type and Atg16L1^{E230} and Atg16L1^{E226} mutant mice. Glycolytic activity was determined from the extracellular acidification rate (ECAR, Figure 2.4).

The indicated injection of saturating amounts of glucose (10mM, Figure 2.4) enabled glycolysis to be determined through its conversion from glucose to pyruvate (Figure 2.5) by the subsequent detection of protons or extracellular acidification (ECAR). Injection of oligomycin (1μM), allowed the glycolytic capacity to be determined and indicated the maximum rate of glycolysis as oxidative phosphorylation would have been blocked and thus cells were forced to utilise glycolysis to make ATP. It further enabled the glycolytic reserve to be calculated by subtracting glycolysis from glycolytic capacity, the glycolytic reserve indicated a cells ability to respond to an energetic demand (stress event).

The final injection of 2-deoxyglucose (50mM), a competitive inhibitor of glucose hexokinase, competitively blocks glycolysis, and allowed the nonglycolytic acidification to be identified.
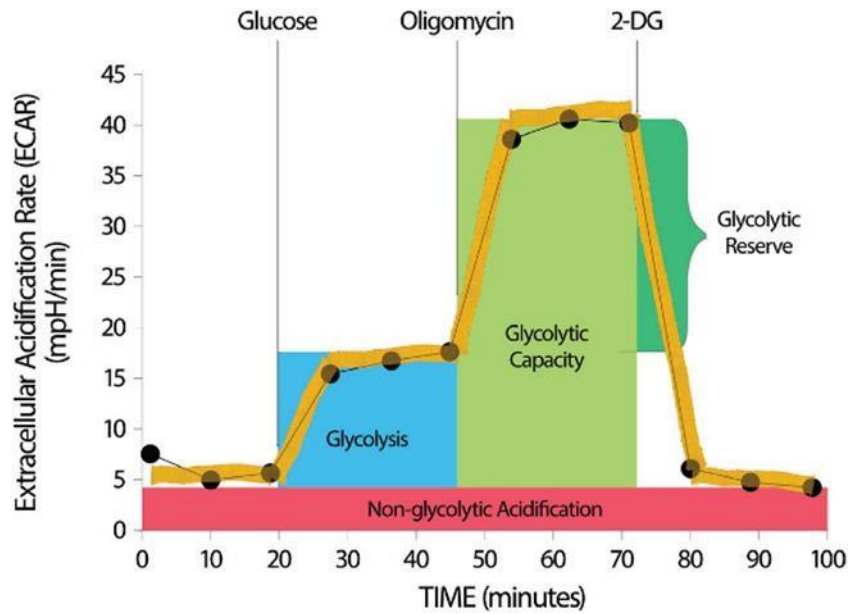
Figure 2.4 Example protocol of the glycolysis stress test. Schematic of the time course of the glycolysis stress test showing changes in ECAR in response to addition of; glucose (10mM) at time point 20 minutes, oligomycin (1μM) at time point 45 minutes and 2-deoxyglucose (50mM) at time point 70 minutes. These data allow measures of glycolysis (blue area), glycolytic capacity (green area) and glycolytic reserve (dark green area) to be determined [Taken from Agilent Technologies].
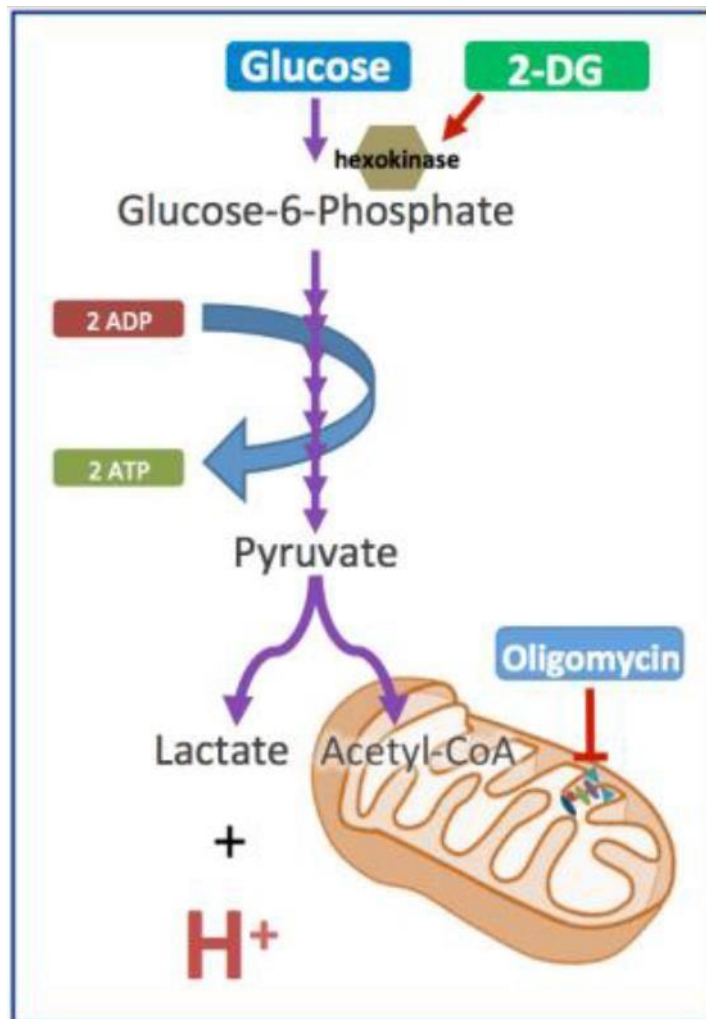
Figure 2.5 Abbreviated schematic of glycolysis. During glycolysis glucose is utilised as a substrate to generate 2ATP, generating protons which are detected by the probe and plotted as ECAR. Here glucose is applied to initiate ATP production, oligomycin is added to remove OXPHOS to force the cells to utilise glycolysis alone as an ATP source and finally 2-DG is added to block the first enzyme (glucose hexokinase) in the glycolytic pathway thereby allowing non-specific acidification to be determined [Taken from Agilent Technologies].

2.14.ii Mitochondrial stress test

The oxygen consumption rate (OCR) was determined as a measurement of oxidative phosphorylation (OXPHOS, Figure 2.6). Oxidative phosphorylation (OXPHOS) is the generation of a proton gradient by electron transport chain subunits, this proton gradient is then utilised to power the production of ATP (Figure 2.7).

Basal respiration indicates (Figure 2.6) normal energetic demand of a cell under basal conditions. The decrease in oxygen consumption in response to oligomycin (1μM) indicated the portion of respiration being utilised to drive ATP production. Subsequent injection of the un-coupler FCCP (1μM), that collapses the proton gradient, forces the cells into maximum oxygen consumption by complex IV (as if an energy demand or stress has been imposed), giving a measure of maximal respiration through the consumption of available substrates (e.g. fats, amino acids, sugars). This further allows the spare respiratory capacity to be calculated by subtracting maximal respiration from basal respiration, which indicated the ability of a cell to respond to an energetic demand whilst indicating how close a cell is already to that theoretical maximum respiration. Injection of rotenone and antimycin-A (0.5μM) block all remaining electron transport chain function and indicated the oxygen consumption that was non-mitochondrial. The difference between the non-mitochondrial oxygen consumption and oxygen consumed during ATP production allowed the proton leak to be calculated, a higher proton leak indicated greater mitochondrial damage.

At the experiment end, the six wells of the tissue culture plate were washed twice with PBS and thereafter 20μl lysis buffer was applied. The

cell culture plate was left on ice for 30 minutes before each well being scrapped and the
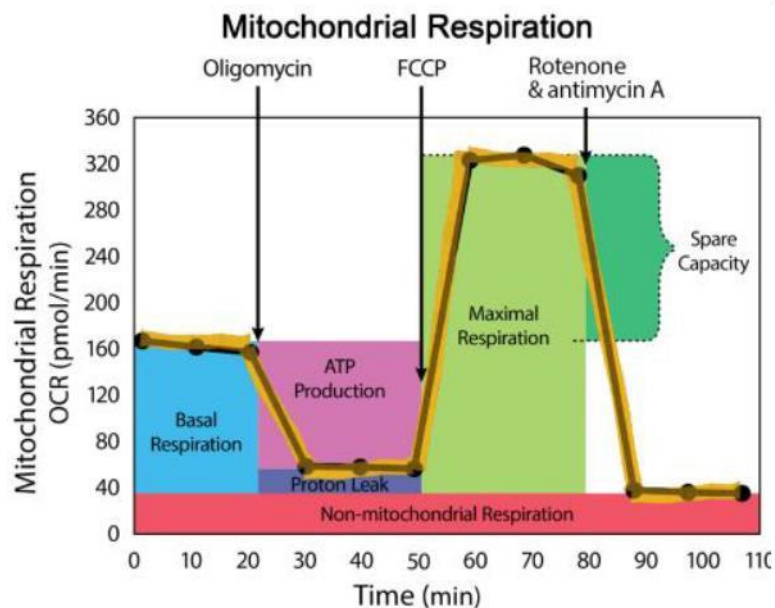
Figure 2.6 Example protocol of the mitochondrial stress test. Schematic of the time course of the mitochondrial stress test showing changes in mitochondrial OCR in response to sequential addition of; oligomycin (1μM), FCCP (1μM) and finally rotenone combined with antimycin-A (0.5μM) at time points 20, 50 and 80 minutes respectively. These data allow the determination of basal respiration (blue area), ATP production (magenta area), proton leak (purple area), maximal respiration (green area) and spare respiratory capacity (dark green area) [Taken from Agilent Technologies].
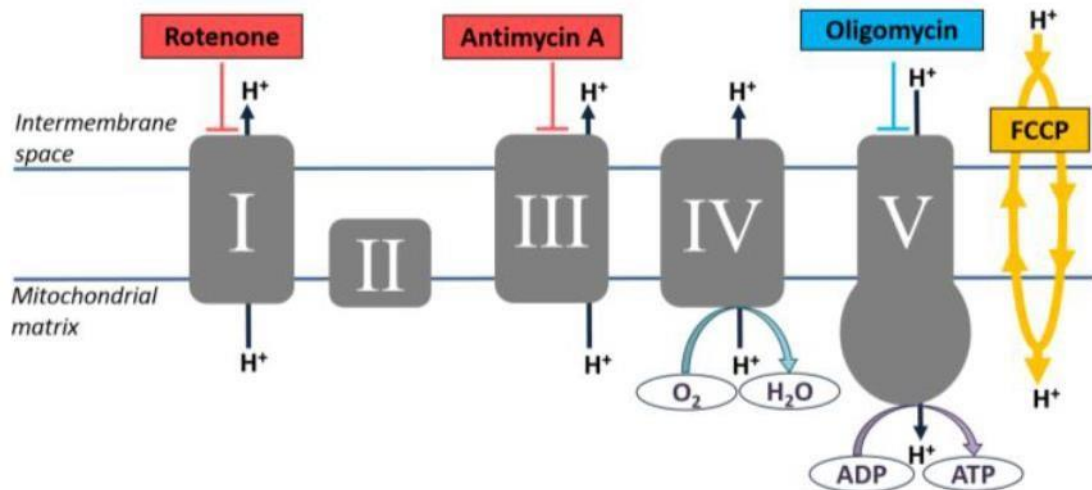
Figure 2.7 Schematic of the electron transport chain. The scheme shows the key sites of proton pumps within the electron transport chain and the location of mitochondrial stress test antagonist action upon each electron transport chain subunit. Oligomycin blocks complex V (ATP synthase), FCCP is an uncoupler and collapses the proton gradient whilst rotenone a complex I inhibitor and antimycin-A a complex III inhibitor shut down the remaining mitochondrial respiration [Taken from Agilent Technologies].

lysis buffer placed in an Eppendorf tube for bath sonication at 4°C for 5 minutes. Thereafter, the tubes were centrifuged for 8 minutes at 11000g, the supernatant being taken and placed in a fresh tube for subsequent protein determination using the Bradford method (see western blot section for Bradford description).

Experiments were undertaken in triplicate (or as indicated) to enable average data to be calculated, plotted and analysed using Student's T-Test. The Seahorse report generator automatically calculates the required respiratory parameters for both the glycolysis and mitochondrial stress tests using the supplied Wave software (Version 2.4.0; Agilent Technologies). The generated Wave report was exported to Excel where the data for each test and area of interest was pooled and averaged for subsequent plotting. The p values < 0.05 were considered statistically significant.

2.15 Statistical analysis

The results were derived from three independent experiments unless otherwise stated. The statistical analysis was done with GraphPad Prism v5 using one-way ANOVA unless otherwise stated. The p values < 0.05 were considered statistically significant (* < 0.05; ** < 0.01; *** < 0.001; **** < 0.0001).

Chapter 3

Genotyping Atg16L1^{E226} and Atg16L1^{E230} mouse models

3.1 Introduction and aims

Mammalian Atg16L1 is a key protein that regulates autophagosome biogenesis. Defects in *Atg16L1* are associated with susceptibility to inflammatory bowel disease, as well as colorectal cancer and chronic obstructive pulmonary disease (Chen *et al*, 2015). Atg16L1 consists of an N-terminal region which binds Atg5 and a coiled-coil domain (CCD) which mediates self-oligomerization and acts as interaction site for different proteins involved in the autophagy pathway, such as WIPI2b (Mizushima *et al*, 2003) Atg16L1 also contains a structural motif of 40 amino acids (often terminating in a Trp-Asp (W-D) dipeptide), the WD domain which is exclusively present in mammals. The absence of this domain in yeasts indicates that it is not crucial for bulk autophagy. This has been demonstrated by Mizushima and colleagues (2003) in a truncated mouse Atg16L1 variant in which the absence of the WD domain did not affect canonical autophagy.

It has been reported that defects in the LAP pathway resulting from the absence of key protein components, such as rubicon and NADPH oxidase-2, lead to increased inflammatory cytokine production, thus implicating LAP in the control of inflammation (Martinez *et al*, 2016). Other studies suggest that it is autophagy that suppresses and regulates inflammasome activation and limits the production of pro-inflammatory cytokines. It has been shown that macrophages lacking the CC domain of Atg16L1 produce and secrete increased levels of IL-1beta and IL-18 when stimulated with LPS, lipopolysaccharide, which mimics bacterial infection (Saitoh *et al*, 2008).

To further investigate the functions of the CCD and WD domains of Atg16L1 in the innate immunity, appropriate mouse models had to be established. That was done by Julia Maryam Arasteh during the course of her PhD. As already mentioned, the Atg16L1^{E226} model, carries a stop codon after glutamate 226 which prevents the expression of glutamate at position 230 and the binding to WIPI2b, a modulator of autophagosome elongation through interaction with Atg16L1 (Dooley *et al*, 2014). The Atg16L1^{E230} model carries a stop codon at the end of the CC domain which contains glutamate residues E226 and E230 which are required for WIPI2b binding. Therefore, both mouse models lack the WD domain of Atg16L1. Having these two models, we could investigate the role of the Atg16L1 domains in inflammation and innate immunity.

After the mouse models were established, mice had to be genotyped for their genetic make-up to be verified. Heterozygous mice were not used for experiments. Homozygous as well as littermate control mice were included in the studies.

3.2 Atg16L1^{E226} and Atg16L1^{E230} genetic background

Atg16L1 is the mammalian homologue of the yeast *Atg16*. The only structural difference between the two is the absence of the WD domain in the yeast equivalent which only consists of 150 amino acids (aa). In the mouse genome *Atg16L1* is located on chromosome 2 and consists of 19 exons which code for 623 aa. The CC domain of Atg16L1 spans 79-230 aa and includes the first 6 exons of the gene, whereas the WD domain spans 320-607 aa and includes exons 10-19 (Uniprot).

To establish a mouse model which does not have the WD domain but has an intact CC domain (Atg16L1^{E230}), stop codons had to be inserted.

Since exon 6 contains the last amino acids which encode the CC domain, two stop codons as well as a neomycin cassette were introduced after exon 6 to terminate the production of the linker region and the WD domain (Figure 3.1). In the

Atg16L1^{E230} mouse, the CC domain contains glutamate residues E226 and E230 which are involved in the interaction with WIPI2b. In the Atg16L1^{E226} mouse model, the TAGTAG stop codons were introduced at position 226 of the CC domain to remove residues E226 and E230 and block the binding of the resultant form of Atg16L1 with WIPI2b and disrupt autophagy (Figure 3.1).

3.2.i Mouse genotyping

The genetic make-up of the mice had to be verified before they were sacrificed and used for experiments. As already mentioned, heterozygous mice were not included in the studies but were used for breeding. To classify the mice as control wild type, heterozygous or mutant, we genotyped DNA samples extracted from ear biopsies (as described in Methods). The primers used for the PCR reactions were designed to amplify specific regions adjacent to exon 6 giving different sized products depending on the mouse genotype (as described in Methods) (Figure 3.2). The first primer set binds to the intronic sequences which are adjacent to exon 6, thus amplifying the whole exon. In case of a wild type sequence (Figure 3.2i), the size of the amplicon is 291 bp because it only contains exon 6 and small parts of the adjacent introns. In the presence of stop codons, the product size is 639 bp because the sequence contains a neomycin cassette which is inserted straight after exon 6 but before the reverse primer site (Figure 3.2ii and 3.2iii). Homozygous mice have a single band at 639 but heterozygotes
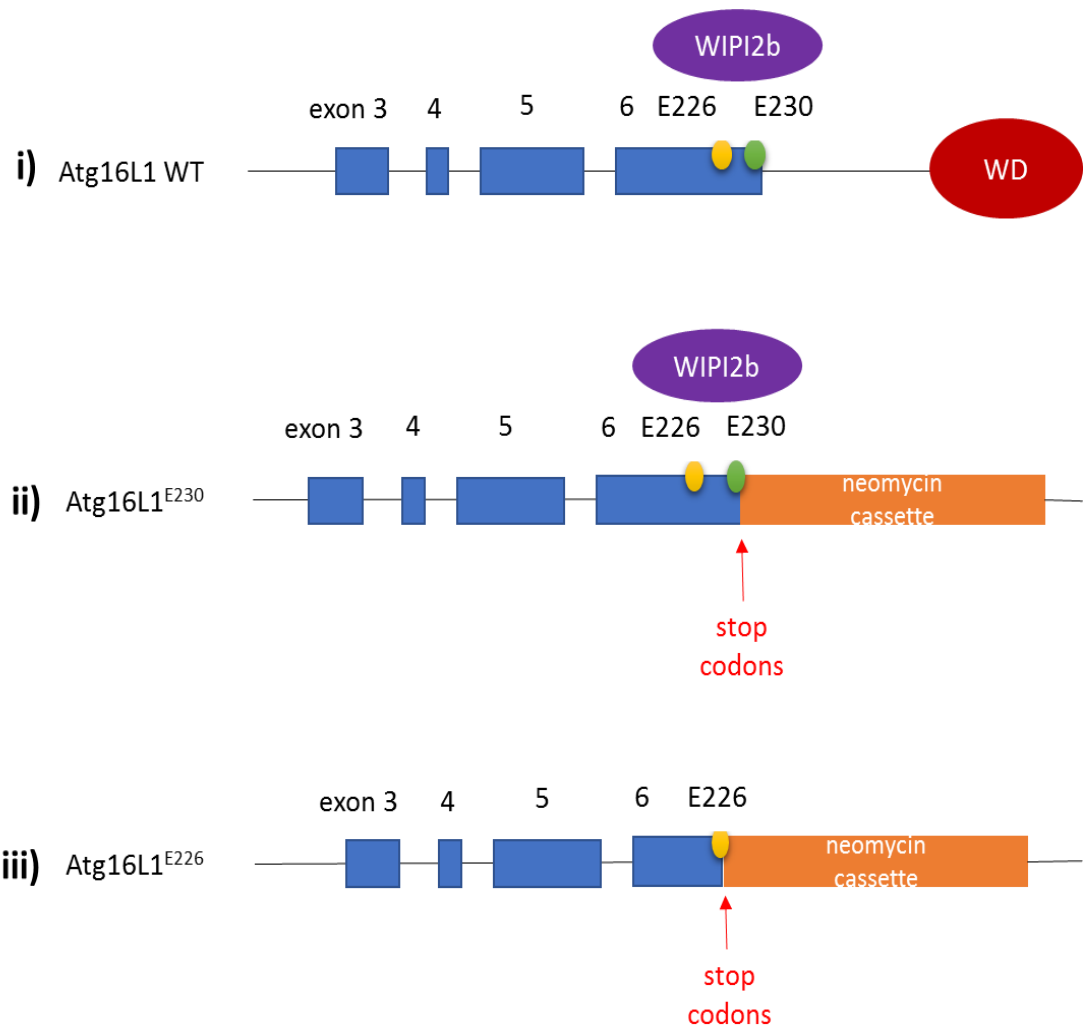
Figure 3.1 Atg16L1 WT, Atg16L1^{E226} and Atg16L1^{E230} genetic background. i) The CCD of the wild type Atg16L1 contains both glutamate residues E226 and E230 which are involved in WIPI2b binding. The control mice also have the WD domain which attached to the CCD via a linker region; **ii)** Atg16L1^{E230}. Two stop codons and a neomycin cassette are introduced after exon 6 of the CC domain which retains the E226 and E230 residues involved in the WIPI2b binding. The WD domain of Atg16L1 is absent; **iii)** The CCD of Atg16L1^{E226} is missing the glutamate residue at position 230 which blocks the binding with WIPI2b. The WD domain of Atg16L1 is absent. Atg16L1^{E226} and Atg16L1^{E230} mouse models were established by Julia Maryam Arasteh.

have both the 291 and the 639 (Figure 3.2iv and 3.2v). To distinguish between the Atg16L1^{E226} and Atg16L1^{E230}, an extra primer set was used. The CCD of the Atg16L1^{E230} mouse contains an extra 4 amino acids. Since each amino acid is encoded by 3 nucleotides, the DNA sequence of *Atg16L1* in the Atg16L1^{E230} mouse model is 12 nucleotides longer than the one in the Atg16L1^{E226}. To distinguish between the two mouse models, the reverse primer of the second primer set (290x338) binds to the DNA sequence of exon 6 which is present in the Atg16L1^{E230} but absent in the Atg16L1^{E226} (Figure 3.2iii). Thus, in case of an Atg16L1^{E230} animal, the PCR reaction shows a product with an amplicon size of 179 bp, but no amplification is observed for Atg16L1^{E226} (Figure 3.2v). Once their genotype was verified, the appropriate mice were sacrificed and bone marrow was extracted from the lower legs (femurs and tibias) for the experimental purposes described in this thesis.

3.2.ii Determination of the effect of genotype upon phenotype by performing protein expression analysis

To verify the genotype of the mice, bone marrow-derived macrophages were used to analyse the protein expressed by wild type and mutant Atg16L1 mice. Cells were probed for Atg16L1 as well as LC3, a key protein involved in autophagosome formation and an accepted autophagosome marker. Macrophages were also stained for LC3 after HBSS starvation to evaluate autophagy.

As expected, full length Atg16L1 was observed in the wild type cells but not in the Atg16L1^{E226} or Atg16L1^{E230} which only expressed the CCD of the protein (Figure 3.3i). As already described, both Atg16L1^{E226} and Atg16L1^{E230} lack the WD domain but have an intact CCD. The stop codon

after glutamate 226 does not compromise the antibody binding and the CC domain can still be detected but after longer exposure.

3.3 Ability of Atg16L1^{E226} and Atg16L1^{E230} to generate autophagosomes

As already described, mammalian LC3 is an essential component of autophagy. Following synthesis, LC3 is cleaved by cysteine protease-Atg4 to form LC3-I which is dispersed throughout the cytoplasm. In response to starvation, LC3-I is conjugated to phosphatidylethanolamine to form LC3-II which binds the newly formed autophagosomes and is a marker for autophagosome formation. Figure 3.3ii shows generation of the 14 kDa LC3-II following starvation of bone marrow-derived macrophages from control and Atg16L1^{E230} mice but the 14kDa band was not produced in macrophages from Atg16L1^{E226} macrophages expressing the CCD that lacks protein residues required for WIPI2b binding. Unlike the control and Atg16L1^{E230} macrophages which showed LC3-I/LC3-II conversion, Atg16L1^{E226} cells presented with accumulation of LC3-I, probably due to compromised autophagy which reduces degradation of LC3 in lysosomes.

i)

Atg16L1 WT

exon 3   exon 4   exon 5   exon 6

primer 290   primer 291

product:
291 bp

ii)

stop
codons

Atg16L1^{E226}

exon 3   exon 4   exon 5   exon 6   Neomycin cassette

primer 290   primer 291

product:
639 bp

iii)

stop
codons

Atg16L1^{E230}

exon 3   exon 4   exon 5   exon 6   Neomycin cassette

primer 290   primer 338   primer 291

product:
179 bp

product:
639 bp

iv)

Atg16L1^{E226} genotyping

290 & 291

L   1   2   3   4   5   6   7

800 bp
600 bp
400 bp

200 bp
Genotype:

WT (+/+)   WT (+/+)   Heterozygous (+/-)   Heterozygous (+/-)   WT (+/+)   Mutant (-/-)   Mutant (-/-)

v)

Atg16L1^{E230} genotyping

290 & 291   290 & 338

L   1   2   3   1   2   3

800 bp
600 bp
400 bp
200 bp

Genotype:

Mutant (-/-)   Heterozygous (+/-)   WT (+/+)   Mutant (-/-)   Heterozygous (+/-)   WT (+/+)

93

Figure 3.2 Annealing sites of primers 290, 291 and 338 used for genotyping.i) Full length Atg16L1. Primers 290 and 291 bind to the intronic sequences adjacent to exon 6 and result in a 291 bp product; **ii)** Atg16L1^{E226} mouse. The insertion of a neomycin cassette after exon 6 results in the generation of a 639 bp product; **iii)** Atg16L1^{E230} mouse. An extra 338 primer which binds to the sequence of exon 6 which is present in the Atg16L1^{E230} but absent in the Atg16L1^{E226} is used to distinguish between the two. An Atg16L1^{E230} animal results in the generation of a 179 bp product; **iv)** and **v)** Representative genotyping images.

3.4 Comparison of major phenotypes of Atg16L1^{E226} and Atg16L1^{E230} mice

It has been shown that autophagy-deficient *Atg5-/-* mice show minimal abnormalities at birth but have lower body weight than that of wild-type mice. However, although they do not display any abnormal phenotypes, *Atg5-/-* neonates died within 1 day of delivery (Kuma *et al*, 2004). A few studies have reported similar neonatal lethality in *Atg3-/-*, *Atg7-/-*, *Atg12-/-*, and *Atg16L1/-* mice (Komatsu *et al*, 2005; Malhotra *et al*, 2015; Sou *et al*, 2008; Saitoh *et al*, 2008). Similarly, the autophagy-compromised Atg16L1^{E226} mice were smaller compared to control and Atg16L1^{E230} mice, however, no neonatal
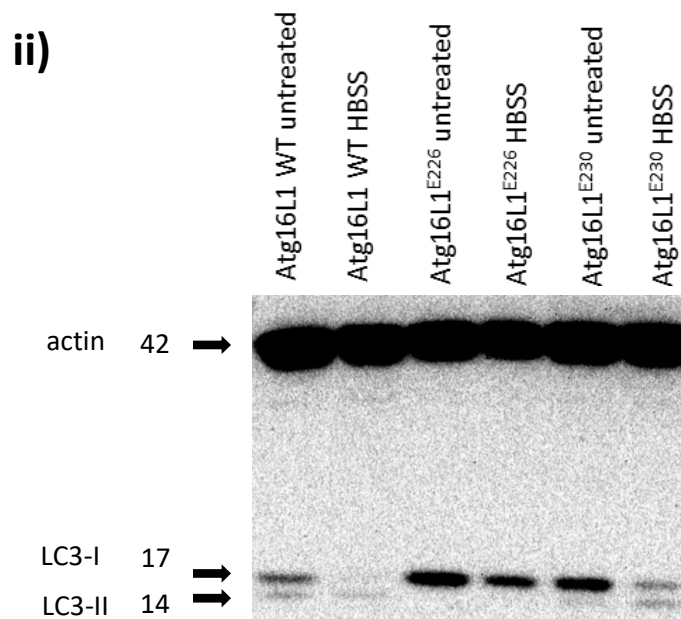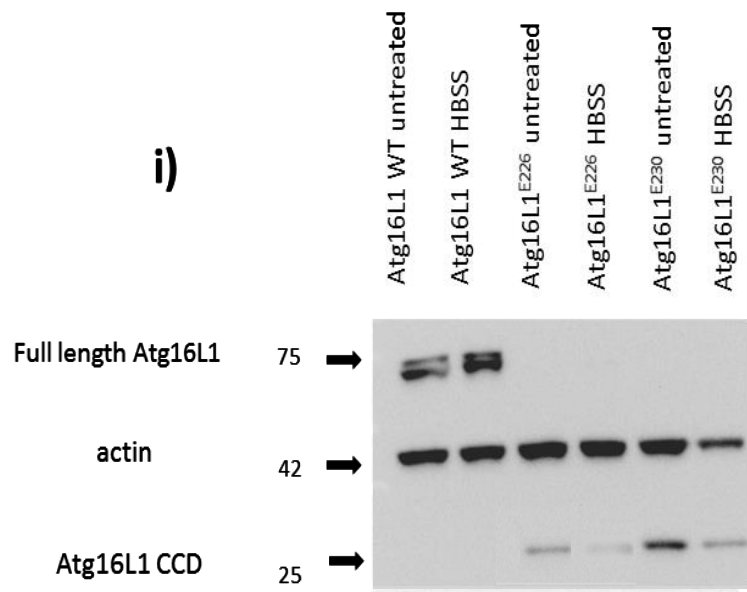
Figure 3.3 Role played by the Atg5 binding and CC domains of Atg16L1 in autophagy. BMDMs were cultured in growth medium (fed) or HBSS (starved) to induce autophagy. Cell lysates were then blotted with the antibodies to detect **i)** Atg16L1 or **ii)** LC3. Actin was used as a control. (n=3).

lethality was observed. A recent study by Yoshii and colleagues (2016) has demonstrated that re-expression of Atg5 in the brain is sufficient to rescue *Atg5-/-* mice from neonatal lethality, suggesting that neuronal dysfunction is the main cause of death of *Atg5-/-* mice. Interestingly, although rescued from lethality, these mice presented with various anatomical abnormalities, such as enlarged liver, spleen, and lymph nodes, with varying inflammatory changes. Abnormalities were also observed in the reproductive organs (Yoshii *et al*, 2016). In this study, a comparison of major phenotypes of Atg16L1^{E226} and Atg16L1^{E230} was performed. Whole body weight of sacrificed mice was measured (Figure 3.4). The adult Atg16L1^{E230} mice containing an intact CC domain and capable of starvation-induced autophagy had an average body weight of 28 grams similar to littermate controls (25 grams). The Atg16L1^{E226} mice were some 25% smaller at 18 grams. Interestingly, the liver was enlarged in the Atg16L1^{E226} model weighing on average 2.5 grams compared to 1.5 grams for Atg16L1^{E230} and littermate controls, which was indicative of possible inflammation (Figure 3.4). No obvious size differences were observed in the rest of the organs, such as brain, heart, lungs, kidneys or intestines. However, the autophagy-compromised Atg16L1^{E226} mice were infertile and therefore only heterozygous mice were used for breeding. The Atg16L1^{E230} mice were fertile and healthy.

## 3.5 Atg16L1^{E230} mice are deficient in LC3 associated phagocytosis

The data above show that the phenotype of the Atg16L1^{E230} mouse was virtually indistinguishable from wild type littermate controls. This showed that the WD domain of Atg16L1 was not required for maintaining tissue homeostasis in the major internal organs of the mouse. All that was needed was an N-terminal Atg5-binding and CC

domain capable of binding WIPI2b. Recent studies have revealed a pathway related to autophagy called LC3 associated phagocytosis (LAP) which results in the translocation of LC3 from the cytosol to the limiting membrane of phagosomes containing pathogens. To evaluate the role played by the WD domain of Atg16L1 in LAP macrophages isolated from Atg16L1^{E230} mice were starved with HBSS to induce autophagy or treated with polystyrene beads and monensin to trigger LC3-associated phagocytosis (LAP) (Figure 3.5). In this experiment monensin causes osmotic stress in the phagosome which provides a signal for LC3 translocation (Florey *et al*, 2015). Untreated cells did not show puncta. However, under HBSSstarved conditions, autophagosome formation was observed in wild type as well as Atg16L1^{E230} macrophages. As expected, Atg16L1^{E226} macrophages were unable to produce LC3 puncta due to compromised autophagy. When BMDM were also incubated with polystyrene beads and monensin, LC3 was recruited to the beads in wild type macrophages but not macrophages cultured from the Atg16L1^{E230} mouse. The results show that the WD domain of Atg16L1 is required for LAP.
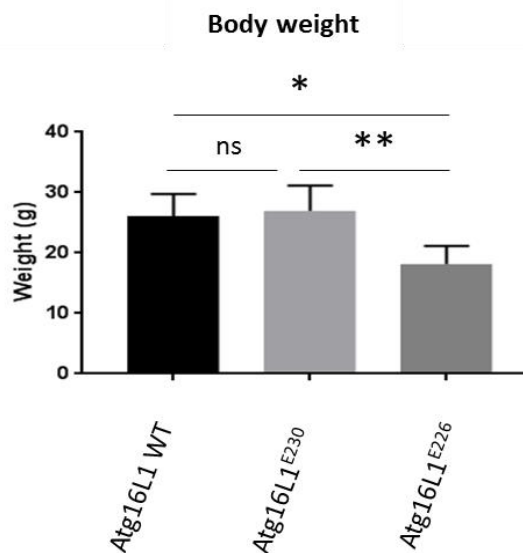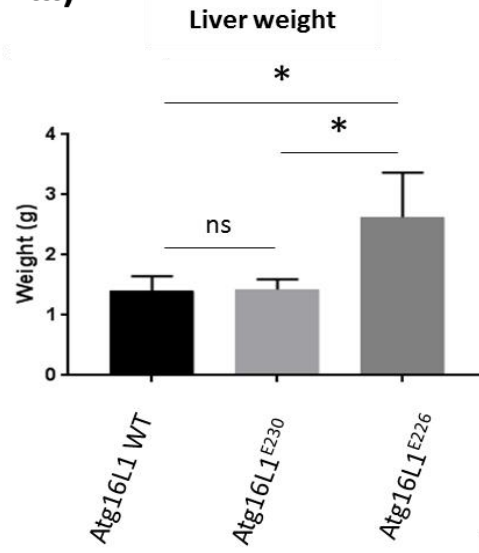
Figure 3.4 Comparison between wild type, Atg16L1^{E226} and Atg16L1^{E230} mice. i), ii) and **iii)** represent body size, body weight and liver weight, respectively. The *p* values < 0.05 were considered statistically significant (* < 0.05; ** < 0.01). Also shown are the error bars in **i)** and **ii)**. (n=3).

| | Growth medium (fed) | HBSS (starved) | Polystyrene beads + monensin |
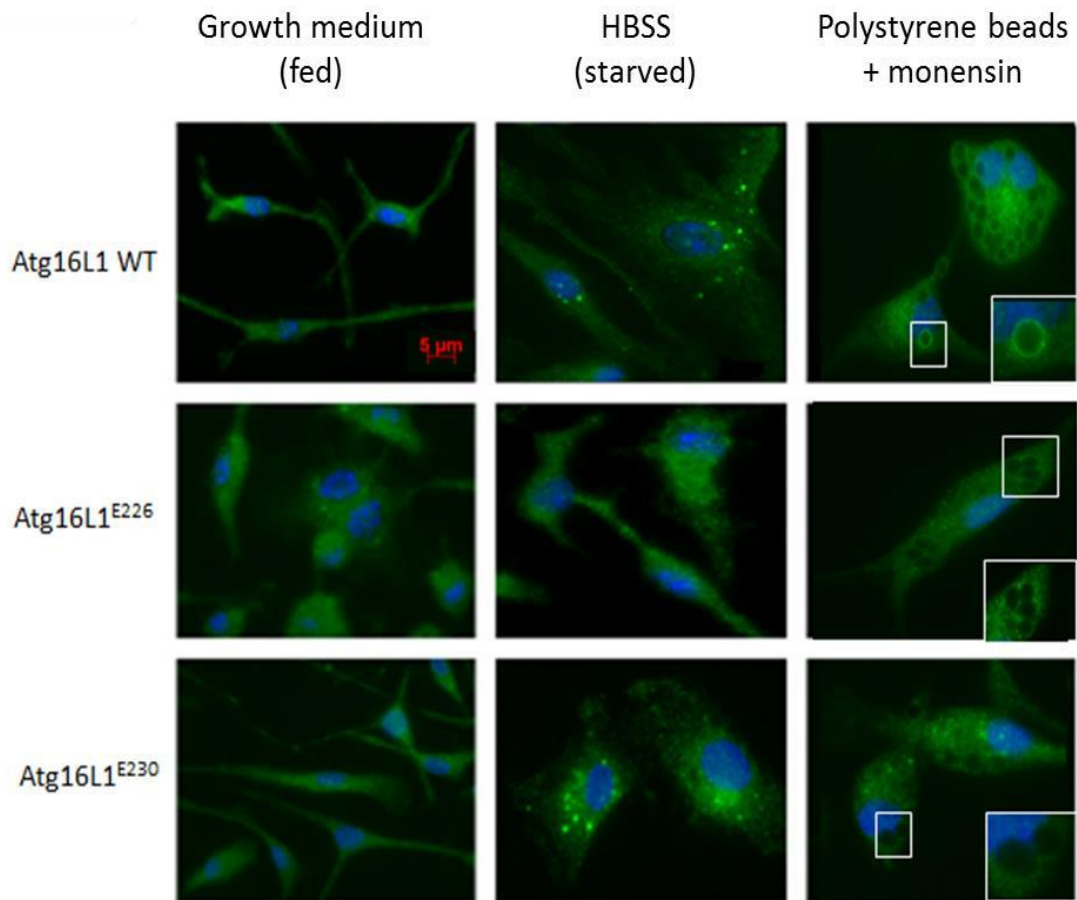
Figure 3.5 Role played by the Atg5 binding and CCD of Atg16L1 in autophagy and LAP. BMDMs were cultured in growth medium (fed), treated with HBSS (starved) to induce autophagy, or with polystyrene beads and monensin to induce LAP. Cells were then probed for LC3. The white boxes show areas of the cell containing polystyrene beads. The zoomed-in images on the righthand side show that LC3 recruitment was observed in wild type but not macrophages cultured from Atg16L1^{E226} or Atg16L1^{E230} mice. (n=3).

Chapter 4 Mechanism of suppression of IL-1beta production by Atg16L1

4.1 Introduction and aims

Interleukin-1beta (IL-1beta) is a potent pro-inflammatory cytokine that is essential for host-defence responses to infection and injury. It is a member of the IL-1 family and is one of the most vastly studied cytokine molecules. IL-1beta is secreted predominantly by cells of the immune system, such as macrophages and dendritic cells, and is produced as an inactive precursor, termed proIL-1beta, in response to recognition of lipopolysaccharide (LPS), a pathogen associated molecular patterns (PAMPs) carried by Gram negative bacteria and recognised by TLR4 (Lopez-Castejon&Brough, 2011; Mosser&Edwards, 2008; Harris *et al*, 2017). IL-1beta is essential for the adequate immune response to pathogen stimuli and is associated with exacerbated damage during chronic inflammation and acute tissue injury (Lopez-Castejon & Brough, 2011).

Recent studies indicate that the WD domain of Atg16L1 may supress pro-inflammatory cytokine production. One study suggests that the T300A mutation associated with Crohn's disease, which is located in the linker region of the protein, generates a caspase-3 cleavage site that would result in removal of the WD domain following activation of caspase-3 during inflammation (Murthy *et al*, 2014). Another study demonstrates that LAP defects resulting from knock-out of rubicon in myeloid cells leads to an acute elevation of pro-inflammatory cytokine levels (Martinez *et al*, 2016).

The aim of the current study is to evaluate the role of the Atg16L1 WD domain played in autophagy and LAP, and to investigate whether the

CCD is enough to suppress inflammation and cytokine production in response to LPS.

4.2 LPS-induced autophagy

As described in the previous chapter above, the Atg16L1^{E230} mouse lacks the linker and WD domains of Atg16L1 but retains the Atg16L1^{E230} residue required for autophagy. Interestingly, macrophages isolated from the Atg16L1^{E230} mouse were autophagy positive but were found to be deficient in LAP when challenged with polystyrene beads and monensin. The Atg16L1^{E226} mouse model carries a stop codon after the glutamate residue 226, which prevents the expression of the second glutamate at position 230 and is therefore deficient in both autophagy and LAP.

LPS is reported to activate autophagy via TLR4 signalling (Deretic, 2012). To verify the ability of LPS to activate autophagy and recruit LC3 to autophagosome, BMDMs were treated with LPS (100 ng/ml) for 24h. The results were similar to those observed after cell starvation (Figure 4.1i). WT and Atg16L1^{E230} BMDMs generated LC3 puncta whereas Atg16L1^{E226} macrophages did not show formation of puncta and were unable to activate autophagy in response to LPS. LC3-I/LC3-II conversion was investigated by Western blot of cell lysates taken from BMDMs before and after LPS treatment (Figure 4.1ii). Both WT and Atg16L1^{E230} macrophages showed that the LC3-I levels decreased after LPS challenge suggesting degradation through autophagy. It was not possible to see LC3-II, the reasons are not clear but may result from rapid degradation of LC3-II once it is attached to autophagosomes that then fuse with

lysosomes. This is supported by the higher levels of LC3-I in the Atg16L1^{E226} BMDMs that lack autophagy.

Taken together, the results show that the CC domain of Atg16L1 is sufficient to maintain autophagy in response to LPS.

i)

	HBSS (starved)	LPS
Atg16L1 WT		
Atg16L1^{E226}		
Atg16L1^{E230}		

ii)

Lanes: Atg16L1 WT untreated, Atg16L1 WT LPS, Atg16L1^{E226} untreated, Atg16L1^{E226} LPS, Atg16L1^{E230} untreated, Atg16L1^{E230} LPS

actin — 50, 37

LC3-I — 17

LC3-II — 14

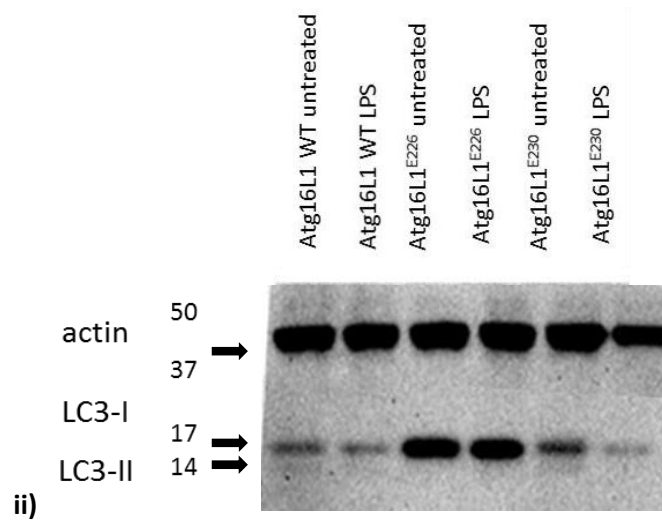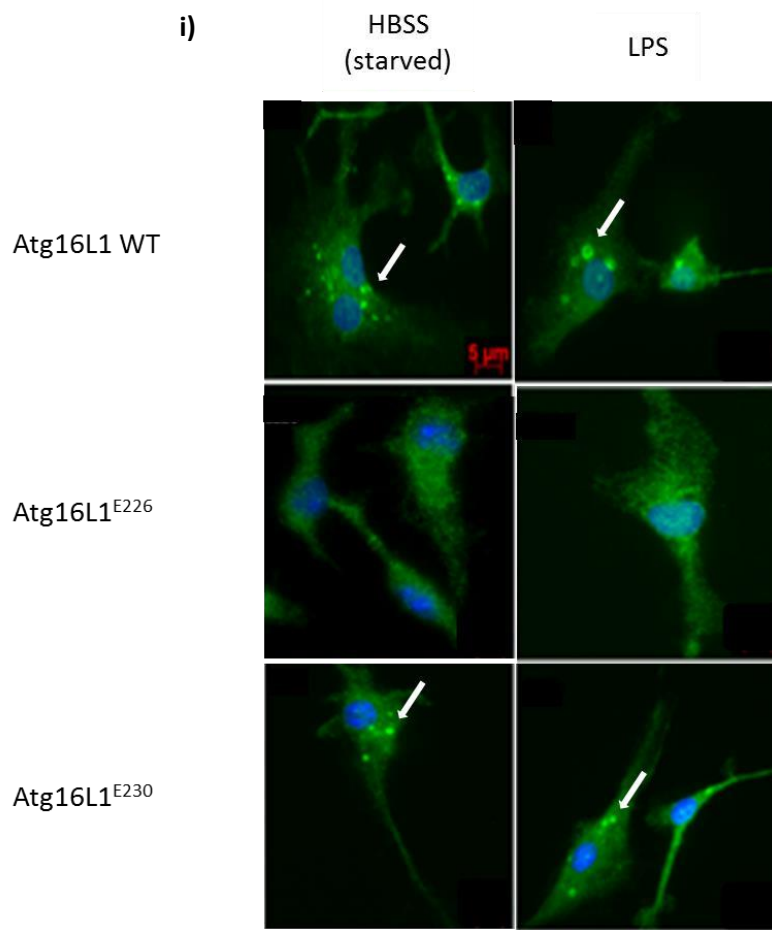**Figure 4.1 LPS-induced autophagy. i)** BMDMs were cultured in HBSS (starved) or treated with LPS (100 ng/ml) to induce autophagy. Cell were then probed for LC3 (arrows show LC3-recruited puncta) (n=3); **ii)** BMDMs were cultured in growth medium (fed) or treated with LPS (100 ng/ml) to induce autophagy. Cell lysates were then blotted with the indicated antibodies. (n=3).

4.3 Deficient autophagy results in a significant IL-1beta increase *in vitro* and *in vivo*

Saitoh and colleagues (2008) have shown that loss of the CC domain of Atg16L1 in BMDMs results in greatly increased secretion of IL-1beta. In addition, as already mentioned, other studies implicate LAP in suppression of IL1-beta (Martinez *et al*, 2016). The availability of mice defective in autophagy and LAP (Atg16L1^{E226}) and mice with selective loss of LAP (Atg16L1^{E230}) allowed us to dissect the role of autophagy and LAP in IL-1beta production and secretion further.

IL-1beta secretion was investigated *in vitro* using BMDMs treated with LPS for 4h followed by a 30 min treatment with BzATP to activate the NLRP3 inflammasome. Supernatants were then collected and analysed for IL-1beta (Figure 4.2). Unstimulated cells showed low cytokine levels which were similar between the genotypes. LPS stimulation, however, resulted in a significant in IL-1beta secretion rising to 50 pg/ml for wild type controls. There was a dramatic increase to 250 pg/ml for the autophagy-deficient Atg16L1^{E226} macrophages. The Atg16L1^{E230} BMDMs showed elevation of IL-1beta to 125 pg/ml but this was not significantly different from WT.

To investigate if the same trend would be observed *in vivo*, mice were injected peritoneally with either PBS (control mice) or LPS (10 mg/kg). The procedure was conducted by Dr Devina Divekar. Blood samples were collected 90 min post-injection to measure serum IL-1beta production. Results were consistent with the *in vitro* study showing drastically increased cytokine serum levels after the LPS-challenge. Again, the autophagy-deficient Atg16L1^{E226} mice had the most dramatic IL-1beta increase (Figure 4.3).
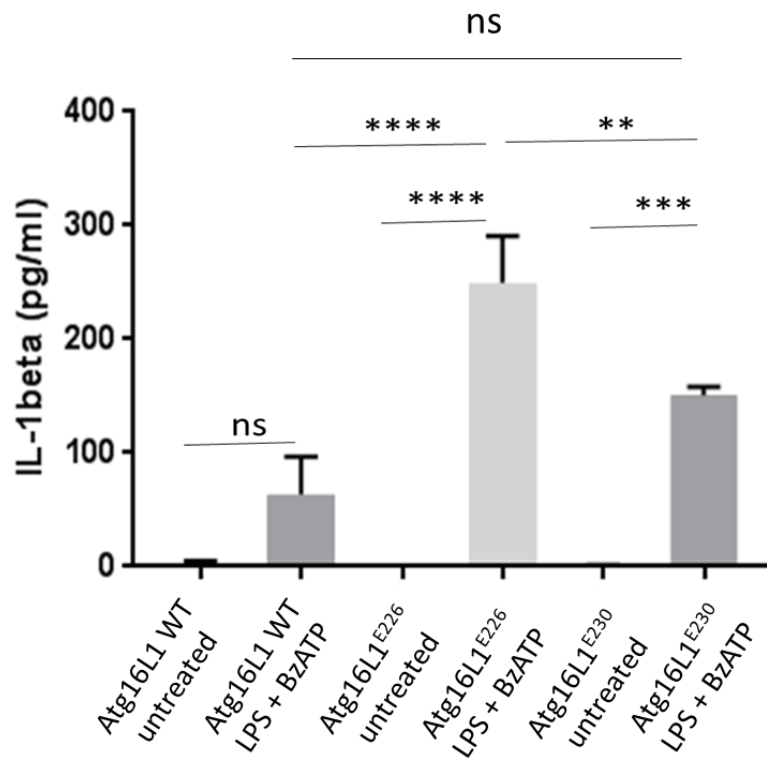
Figure 4.2 IL-1beta production in Atg16L1 WT, Atg16L1^{E226} and Atg16L1^{E230} BMDMs. IL-1beta production from macrophages stimulated with LPS (1 μg/ml) for 4h followed by BzATP (150 μM) for 30 min. The *p* values < 0.05 were considered statistically significant (ns – not significant; ** < 0.01; *** < 0.001; **** < 0.0001). (n=3).
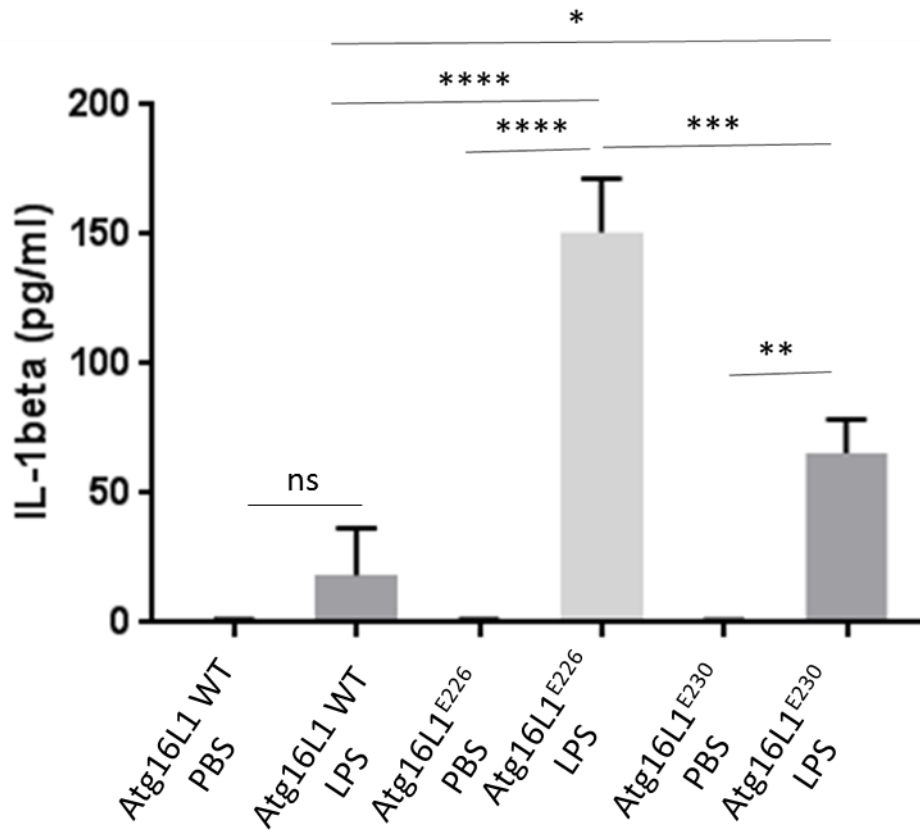
Figure 4.3 IL-1beta production in Atg16L1 WT, Atg16L1^{E226} and Atg16L1^{E230} mice. IL-1beta in blood serum 90 min post-injection with LPS (10 mg/kg). The *p* values < 0.05 were considered statistically significant (* < 0.05; ** < 0.01; *** < 0.001; **** < 0.0001). (n=3).

Harris and colleagues (2011) have shown that IL-1beta secretion in autophagy compromised dendritic cells is TLR4-dependent. In the study, 3methyladenine (3MA) was used to inhibit autophagy and to determine which

TLR ligands would increase IL1-beta secretion when autophagy was supressed. They tested several TLR ligands and showed that only the TRL4 ligand, LPS, could increase IL-1beta secretion. Similarly, we cultured and treated BMDMs with CpG to activate TLR9; flagellin to activate TLR5; and MDP to activate NOD2. Figure 4.4 shows that IL-1beta secretion was LPS-inducible. The observed IL-1beta levels were considerably lower than what was observed in the previous experiment where macrophages were treated with LPS only. The reason might be the number of cells used in this experiment - due to insufficient material, only 20 000 cells/well were cultured and treated with TLR ligands.

4.4 Levels of proIL-1beta protein are increased in macrophages cultured from the autophagy-deficient Atg16L1[E226] mouse

IL-1beta is produced as a 31 kDa precursor, termed proIL-1beta, which is cleaved upon stimulation, to form the 17 kDa active IL-1beta. Unlike IL-1beta, proIL-1beta accumulates in the cytosol and can be detected after cell lysis.

The finding that IL-1beta secretion was dramatically increased in the autophagy-deficient Atg16L1[E226] mouse led us to ask whether its precursor, proIL-1beta, was also abundant. BMDMs were cultured and stimulated with LPS (100 ng/ml) for 24h. Supernatants were removed, cells were lysed and analysed for proIL-1beta by ELISA (Figure 4.5).

Untreated cells showed basal levels of proIL-1beta (20 pg/ml) which increased to 250 pg/ml when macrophages were stimulated with LPS. Basal levels of pro-IL1beta in Atg16L1^{E226} BMDMs were similar to control (30 pg/ml) but increased dramatically to 750 pg/ml in response to LPS. In contrast, the response of Atg16L1^{E230} BMDMs to LPS was similar to controls. The findings that both IL- and proIL-1beta showed a significant elevation in the Atg16L1^{E226} but not Atg16L1^{E230} BMDMs led us to ask whether the observed differences were due to increased gene expression. Macrophages were cultured and stimulated with LPS (100 ng/ml) for 24h to induce *IL-1beta* transcription (Figure 4.6). Untreated BMDMs showed very low levels of *IL-1beta.* However, a dramatic increase in gene expression was observed after LPS treatment. Interestingly, no difference in IL-1beta transcription levels was observed between the genotypes.
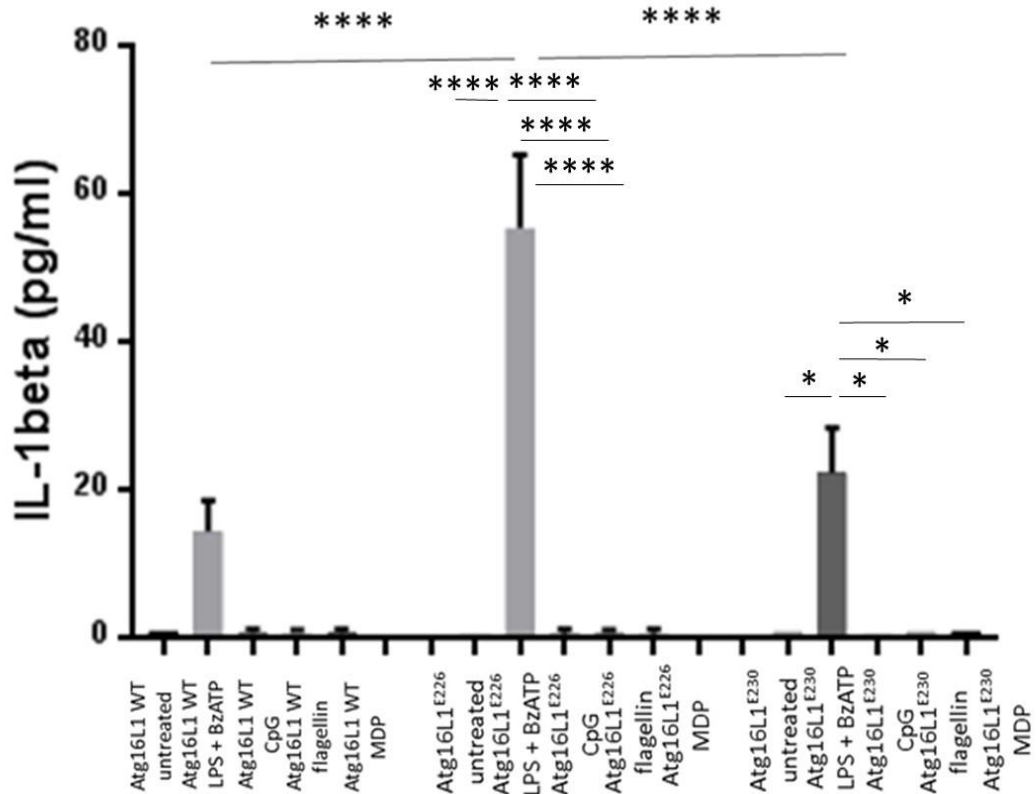
Figure 4.4 Role of TLR receptors in IL-1beta secretion from Atg16L1 WT, Atg16L1^{E226} and Atg16L1^{E230} BMDMs. Macrophages were cultured in growth medium (fed) or treated with LPS (1 µg/ml) for 4h and BzATP (150 µM) for 30 min, TLR4 ligand; CpG (10 µg/ml), TLR9 ligand; flagellin (10 µg/ml), TLR5 ligand; MDP (10 µg/ml), NOD2 ligand. The *p* values < 0.05 were considered statistically significant (* < 0.05; **** < 0.0001). (n=3).

Figure 4.5 ProIL-1beta production in Atg16L1 WT, Atg16L1[E226] and Atg16L1[E230] BMDMs. Cells were cultured in growth medium (fed) or treated with LPS (100 ng/ml) for 24h. Cell lysates were then analysed with ELISA. The *p* values < 0.05 were considered statistically significant (ns – not significant; * < 0.05; ** < 0.01; *** < 0.001). (n=3).

4.4.i ProIL-1beta is a substrate for autophagy

The observation that both proIL- and IL-1beta were dramatically elevated in the autophagy compromised Atg16L1^{E226} mouse model, together with the finding that there was no difference in the IL-1beta mRNA levels between the genotypes, suggested that proIL-1beta maybe a substrate for autophagy. TLR4 stimulation activates NF-kB, a transcription factor that regulates various cellular processes, such as immune and inflammatory responses, cell growth, apoptosis, and developmental processes. Activated NF-kB induces the transcription of IL-1beta which is translated into the inactive pro- form. ProIL1beta is then cleaved by caspases to form the active IL-1beta which is secreted outside the cell (Qiao *et al*, 2012; Baeuerle&Henkel, 1994). Autophagy, however, as an anti-inflammatory process, and may target proIL-1beta for degradation (Figure 4.7). This would explain why the BMDMs from the autophagy compromised Atg16L1^{E226} mouse generated high levels of proIL- and IL-1beta.

To provide evidence that autophagy targets proIL-1beta for degradation, proIL-1beta was tagged at the N-terminus with eGFP and expressed in cells to see if it co-localizes with autophagosome marker LC3. After a 24h transfection, cells were starved with HBSS for 3h to induce autophagy and the formation of autophagosomes was analysed by fluorescence microscopy using antibodies to LC3. Co-localisation between LC3 (red) and proIL-1beta (green) is shown in figure 4.8.
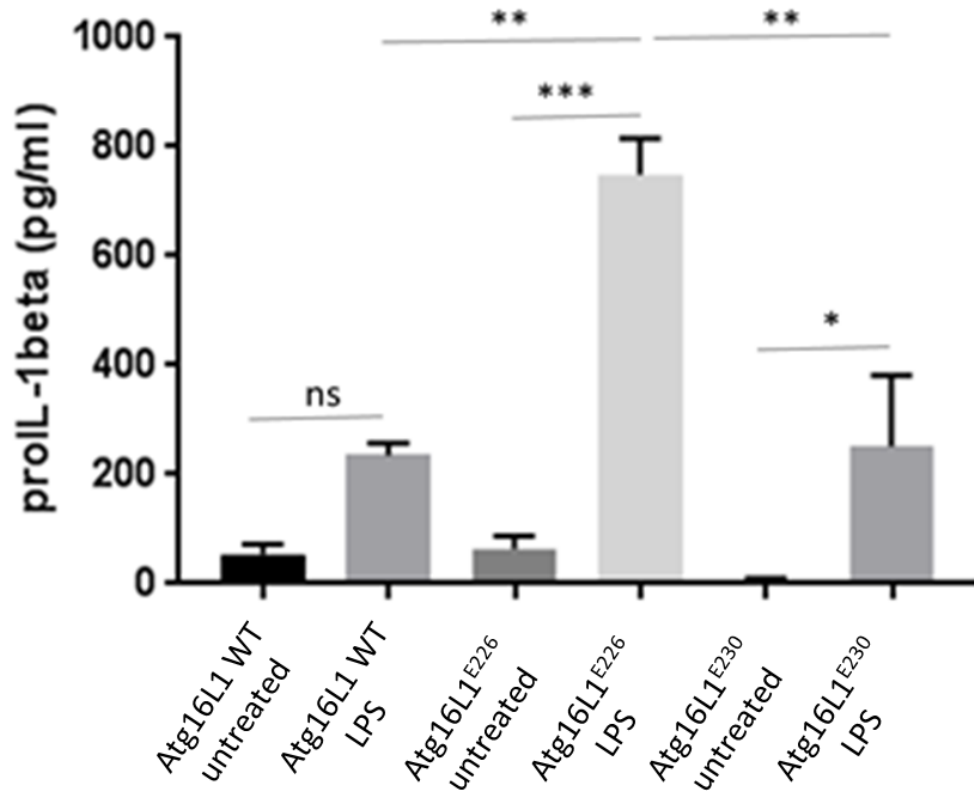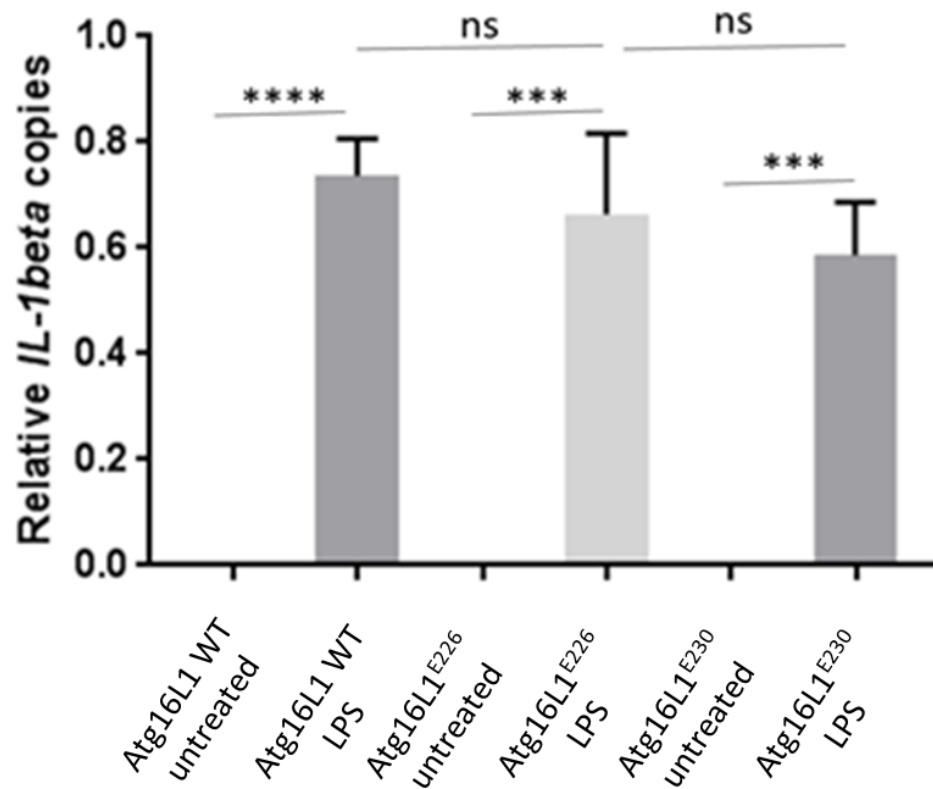
Figure 4.6 IL-1beta mRNA levels in Atg16L1 WT, ATg16L1^{E226} and Atg16L1^{E230} BMDMs. Macrophages were cultured in growth medium (fed) or treated with LPS (100 ng/ml) for 24h to induce IL-1beta gene expression. *IL-beta* mRNA levels were calculated using the ''relative copies'' method where the expression of the gene of interested was measured in relation to the expression of the *18S* gene. The *p* values < 0.05 were considered statistically significant (ns – not significant; *** < 0.001; **** < 0.0001). (n=3).
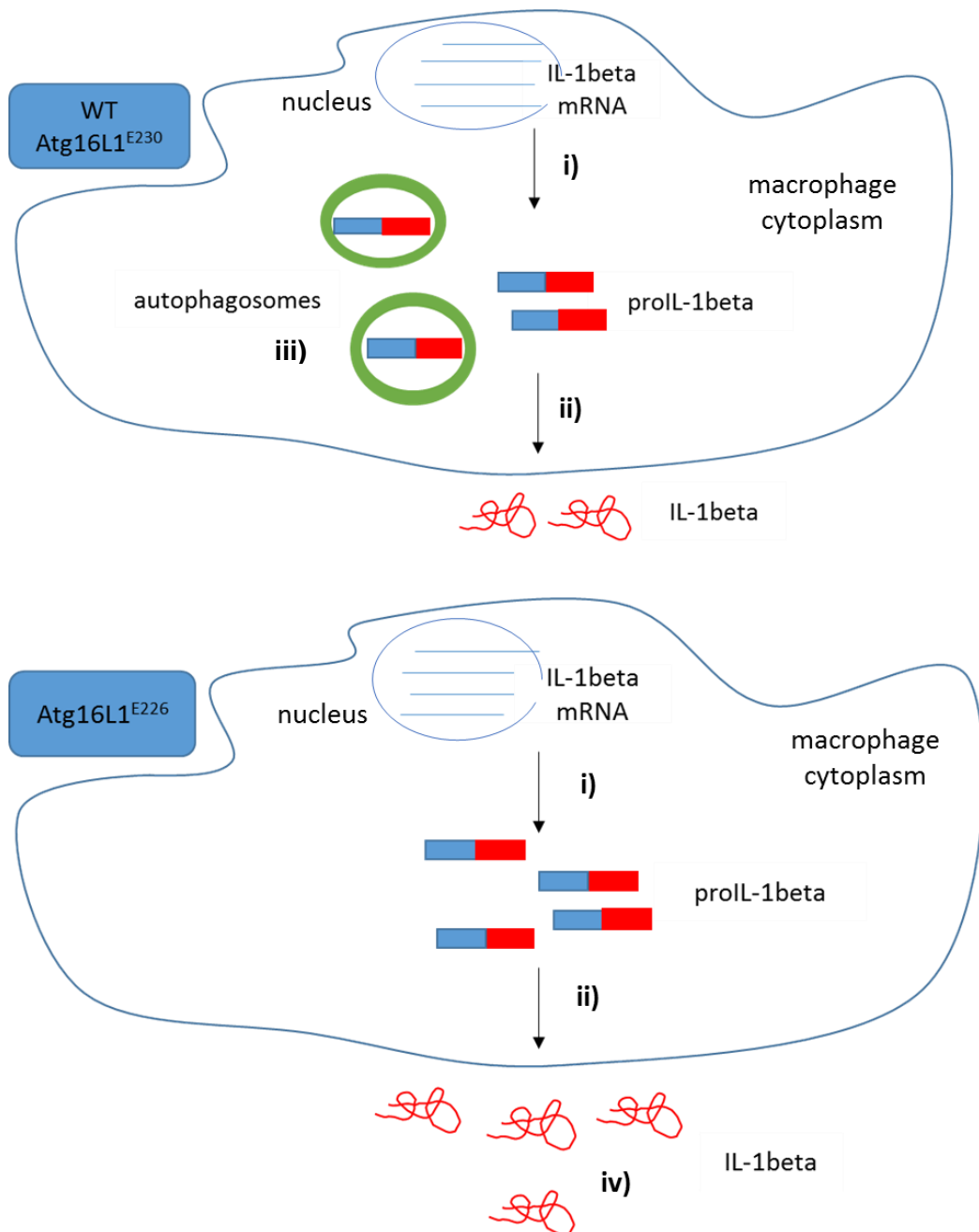
Figure 4.7 Schematic representation of the possible role played by autophagy in IL-1beta production and secretion. i) IL-1beta mRNA is translated into the inactive proIL-1beta precursor which gets cleaved to form the active IL-1beta which is then secreted outside the cell **(ii)**. Autophagy is an anti-inflammatory process which might target proIL-1beta for degradation **(iii)**, thus explaining the high pro- and IL-1beta levels in the autophagy compromised Atg16L1^{E226} macrophages **(iv)**.

In conclusion, our data suggest that levels of proIL-1beta and IL-1beta are raised in BMDMs from the Atg16L1^{E226} mouse because proIL-1beta is not removed by autophagy. In this model LPS-induced TLR4 signalling activates NF-kB and induces expression of IL-1beta mRNA. The mRNA is translated in the cytoplasm to generate proIL-1beta which is removed by autophagy. This pathway may have evolved to supress inflammation. The analysis further indicates that the Atg5 binding and CC domains of Atg16L1 are sufficient to suppress proIL-1beta levels, and that control of IL-1beta appears to be independent of the linker and WD domains of Atg16L1. Experiments in Figure 3.6 show that these domains are required for LAP. We can conclude therefore that LAP is not involved in suppression of IL-1beta production.
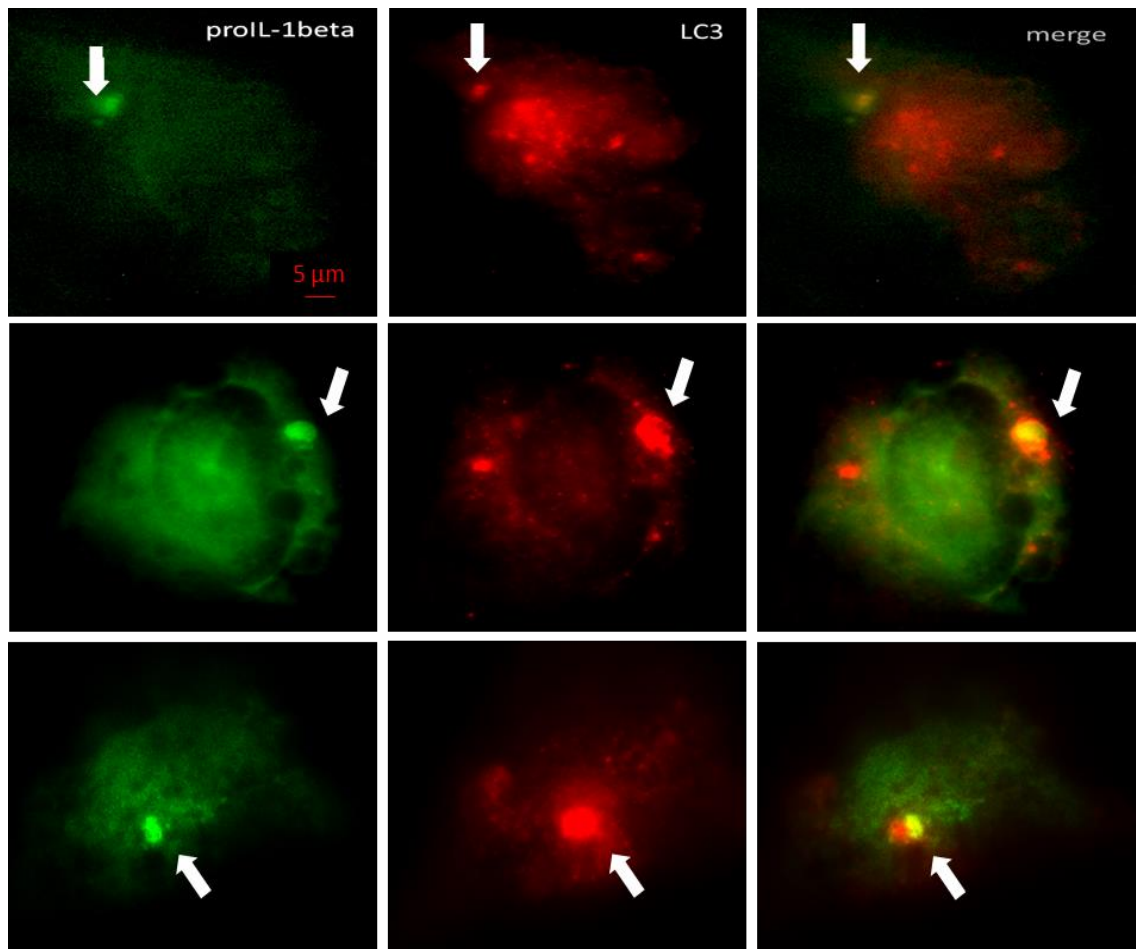
Figure 4.8 ProIL-1beta and LC3 co-localization. 293HEKA cells were transfected with proIL-1beta_pcDNA3.1+N-eGFP for 24h and starved with HBSS for 3h to induce autophagy. ProIL-1beta appears as green puncta. The cells were stained for LC3 which is seen as red puncta. The arrows indicate the location of proIL-1beta (first panel of images), LC3 (middle panel of images), as well as their co-localisation in the merged images. (n=3).

Chapter 5

Mechanism of suppression of inflammasome activation by Atg16L1

5.1 Introduction and aims

It has been reported that the major pathway for conversion of proIL-1beta to IL-1beta is the activation of caspase-1 by the inflammasome (Gurung&Kanneganti, 2015). Inflammasomes are multimeric protein complexes that assemble in the cytosol upon infection or after sensing PAMPs or DAMPs and can therefore be considered as innate immune system receptors (Guo *et al*, 2015). They consist of NLR family members and the adaptor apoptosis-associated speck-like (ASC) protein. Three inflammasomes have been characterized − NLRP1, NLRP3, and NLRP4 − with the main differences being the stimuli and the mechanisms of action (Franchi *et al*, 2009). Despite the differences, however, canonical inflammasomes serve as a platform for caspase-1 recruitment and activation (Guo *et al*, 2015).

Caspase-1 is a member of the intracellular cysteine protease family which induces inflammation through the activation of proinflammatory cytokines, such as IL-1beta and IL-18 (Franchi *et al*, 2009). Upon stimulation, the inactive zymogen pro-caspase-1 binds to ASC which results to its oligomerization and subsequent autoproteolytic cleavage into the enzymatically active heterodimer consisting of two 10 and 20 kDa subunits. Active caspase-1 cleaves the precursor proIL-1beta and generates the biologically active IL1beta (Guo *et al*, 2015).

It has been demonstrated that IL-1beta is also regulated by caspase-8. Although the mechanism of its activity is not fully understood, it is believed that caspase-8 regulates IL-1beta through pathways that are dependent upon the inflammasome. Studies have proposed that caspase-8 regulates NF-kB to modulate inflammation

(Gurung&Kanneganti, 2015). It has been shown that caspase-8 directly cleaves proIL-1beta at the same site as caspase-1 (Vince *et al*, 2012; Man&Kanneganti, 2016). It has also been suggested that caspase-8 is a part of the NLRP3 inflammasome and is involved in caspase-1 processing and cleavage (Gurung&Kanneganti, 2015).

A20, a suppressor of the NLRP3 inflammasome, has been shown to inhibit NFkB and restrict ubiquitination of proIL-1beta. It has been demonstrated that A20 co-precipitates with caspase-1 and caspase-8 and prevents spontaneous secretion of IL-1beta, thus preventing inflammatory diseases (Duong *et al*, 2015).

The aim of the current study is to investigate the role of autophagy and LAP in the activation of the inflammasome proteins with regards to IL-1beta induction and secretion.

5.2 Compromised autophagy results in increased caspase-1 and caspase-8 activity

Since both caspase-1 and caspase-8 cleave the precursor proIL-1beta to generate the active form of IL-1beta, we sought to investigate whether the increased IL-1beta levels in autophagy-compromised macrophages were due to increased caspase activity. BMDMs were incubated in growth medium or treated with LPS (1 μg/ml) for 4h followed by a 30 min incubation with BzATP (150 μM) to activate the NLRP3 inflammasome. Cells and supernatants were pooled to measure caspase activity in each genotype. The macrophages from the Atg16L1^{E226} mice showed high basal levels of caspase-1 and caspase8 compared to controls (Figure 5.1i and 5.1ii). The macrophages from the Atg16L1^{E230} mice showed raised basal caspase activity intermediate between

Atg16L1^{E226} and control. In each case, incubation with LPS and BzATP increased caspase-1 and caspase-8 activity, but the greatest increase was seen in BMDMs from Atg16L1^{E226} mice.

The big increase in caspase activity in the Atg16L1^{E226} mouse model raised the question whether caspase-1 and capsase-8 are substrates for autophagy upon LPS stimulation. To investigate this hypothesis, WT BMDMs, i.e. macrophages with intact autophagy, were stimulated with LPS (1 μg/ml) for 4h followed by a 30 min treatment with BzATP (150 μM). Cells were then immunostained for LC3 (green) and caspase-1 (red) (Figure 5.1iii). LC3 puncta were produced in the stimulated cells and caspase-1 was located to small punctate structures in the cytoplasm. However, no co-localization was observed between the two proteins, indicating that even though caspases mediate proIL-1beta cleavage and IL-1beta production, it was not possible to provide evidence for degradation of caspase-1 by autophagy. With the time available, it was not possible to investigate whether caspase-8 co-localizes with LC3 and is therefore a substrate for autophagy.

Taken together, our findings demonstrate that lack of autophagy results in a significant increase in caspase-1 and caspase-8 activity which is concordant with previous studies showing that deficiency in autophagy proteins, such as LC3 and beclin 1, activates caspase-1 (Nakahira *et al*, 2011). In the study, *Map1lc3-/-* and *Becn1+/-* peritoneal macrophages were used to investigate the role of autophagy in inflammasome activation. The results demonstrated that the mechanism by which autophagic proteins regulate caspase-1 activation was due to their contribution to mitochondrial quality control. Autophagy-compromised macrophages presented with abnormal mitochondria which produced

more ROS. Also, the study demonstrated a relationship between the generated mitochondrial ROS and the activity of caspase-1, showing that mitochondrial complex I inhibitor rotenone enhanced caspase-1 activation and IL-1beta secretion. The mechanism of caspase-8 activity is still unclear. As already discussed, caspase-8 has been revealed to be involved in caspase-1 activation as well as IL-1beta processing. It has also been suggested that both caspases work synergistically. Interestingly, Kovacs and colleagues (2011) have shown that autophagy compromised T-cells, deficient for beclin-1, accumulate caspase-8 aggregates. That might explain the increased caspase-8 activity in the autophagy negative Atg16L1^{E226} cells. The exact mechanisms, however, are yet to be elucidated No co-localization was observed between LC3 and caspase-1, indicating that while proIL-1beta may be sequestered into autophagosomes (Figure 4.8) it is segregated from caspase-1.
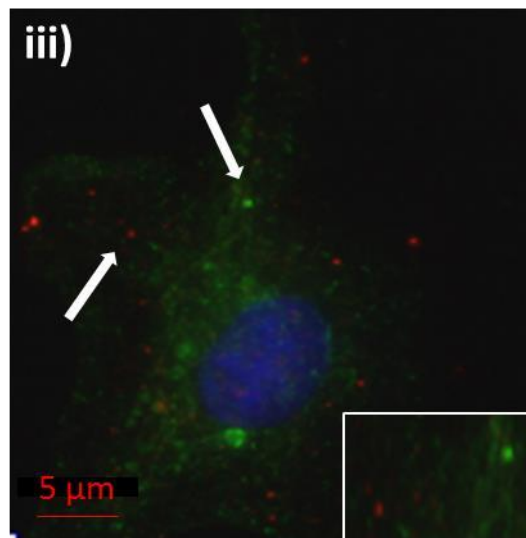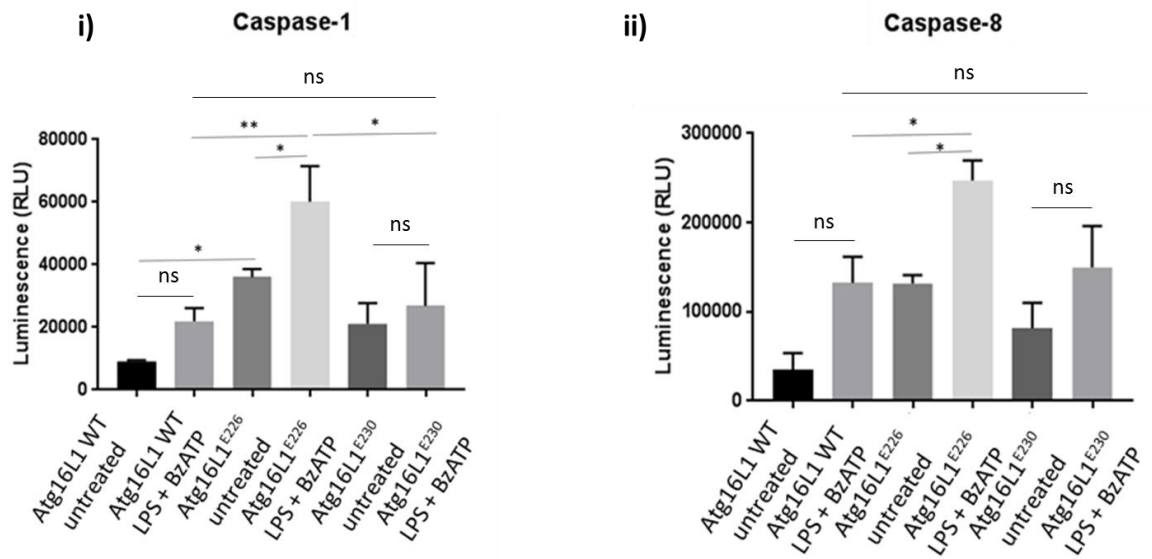
Figure 5.1 Caspase activity in Atg16L1 WT, ATG16L1^{E226} and Atg16L1^{E230} macrophages. i) and **ii)** BMDMs were cultured in growth medium or treated with LPS (1 μg/ml) for 4h, followed by BzATP (150 μM) for 30 min. Caspase activity is presented in relative light units (RLU). The *p* values < 0.05 were considered statistically significant (* < 0.05; ** < 0.01). (n=3); **iii)** WT BMDMs were stimulated with LPS for 4h (1 μg/ml), followed by treatment with BzATP (150 μM) for 30 min. Cells were then probed for LC3 and caspase-1. The arrows indicate the location of LC3 (green puncta) and caspase-1 (red puncta). The white box is a zoomed-in image of an area containing both LC3 and caspase-1. (n=3).

5.3 Deficient autophagy does not affect NLRP3 production and expression

NLRP3 is the most extensively investigated of the inflammasomes (Sutterwala *et al*, 2014). Upon stimulation, the main inflammasome protein, NLRP3 oligomerizes and interacts with the adaptor protein ASC which results in caspase-1 activation (Qiao *et al*, 2012). It has also been demonstrated that caspase-8 is also involved in NLRP3 induction (Chi *et al*, 2014). Therefore, we sought to assess NLRP3 expression in both Atg16L1^{E226} and Atg16L1^{E230} BMDMs. Macrophages were treated with LPS (1 µg/ml) for 4h before analysis by qRT-PCR (Figure 5.2i).

Gene expression was upregulated by LPS but no difference in upregulation was observed between genotypes. The analysis was repeated by Western blot (Figure 5.2ii). Consistent with the qRT-PCR results, levels of NLRP3 increased in response to LPS but no increase was observed in the Atg16L1^{E226} macrophages which suggests that NLRP3 is unlikely to be a substrate for autophagy. If that was the case, the protein expression would have been elevated in the autophagy-deficient cells.
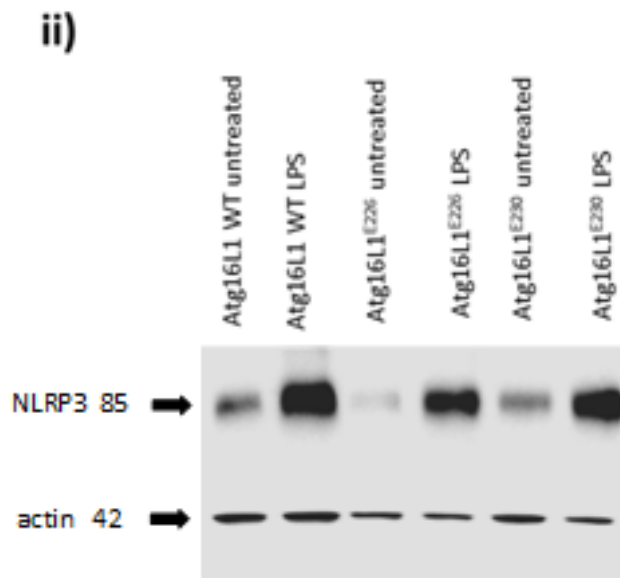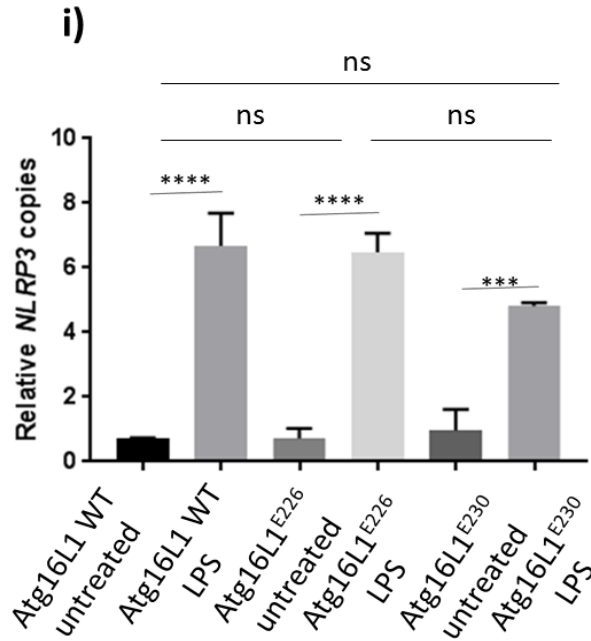
Figure 5.2 NLRP3 gene and protein expression in Atg16L1 WT, Atg16L1^{E226} and Atg16L1^{E230} BMDMs. i) Cells were cultured in growth medium or treated with LPS (1 µg/ml) for 4h before RNA extraction and analysis by qPCR. The *p* values < 0.05 were considered statistically significant (*** < 0.001; **** < 0.0001) (n=3); **ii)** Cells were cultured in growth medium or treated with LPS (1 µg/ml) for 4h. The cell lysates were then blotted for NLRP3. (n=3).

5.4 Autophagy compromised BMDMs show an increase in A20 expression

It has been reported that the ubiquitin-modifying enzyme A20 associates with caspase-1 and proIL-1beta and is recruited to the NLRP3 inflammasome. It has also been suggested that it restricts proIL-1beta ubiquitination through RIPK and prevents the spontaneous secretion of the biologically active IL-1beta (Duong *et al*, 2015). This made it possible that increased levels of IL-1b would be produced if A20 were degraded by autophagy. Therefore, the levels of A20 in both Atg16L1^{E226} and Atg16L1^{E230} were investigated. BMDMs were treated with LPS (1 μg/ml) for 4h before qRT-PCR and Western blotting (Figure 5.3). As seen for NLRP3 expression, mRNA levels for A20 were increased following incubation with LPS but the increases did not show any changes between the genotypes (Figure 5.3i). However, protein levels were increased in the autophagy-deficient Atg16L1^{E226} BMDMs (Figure 5.3ii). This suggests that A20 is a substrate for autophagy,and is consistent with previous studies that have demonstrated that A20 co-localizes with p62, an autophagic adaptor protein, in tissue macrophages and is sequestered for degradation in the autophagosome (Kanayama *et al*, 2015). The observations do not easily explain increased levels of IL-1beta, based on the model provided from Duong and colleagues (2015), where increased A20 would be expected to decrease processing of IL-1beta by caspase-1. There is, however, an important difference between activation of proIL1beta and levels of proIL-1beta protein. The results in figure 4.2 show increased levels of IL-1beta in BMDMs from Atg16L1^{E226} mice, suggesting that pro-IL1beta is degraded by autophagy. The observation that A20 binds proIL-1beta, and is also a substrate for

autophagy, raises the possibility that A20 may target proIL-1beta for autophagy. This could be tested by silencing A20 which should raise IL-1beta levels.

Taken together, our data demonstrate that the increase of IL-1beta levels in the Atg16L1^{E226} mouse model is due to increased caspase activity although caspase-1 does not seem to be a substrate for autophagy. NLRP3 did not show an expression elevation in the absence of autophagy. The increased levels of A20, however, suggest that it might be a target for autophagosomal degradation and a possible regulator of IL-1beta.
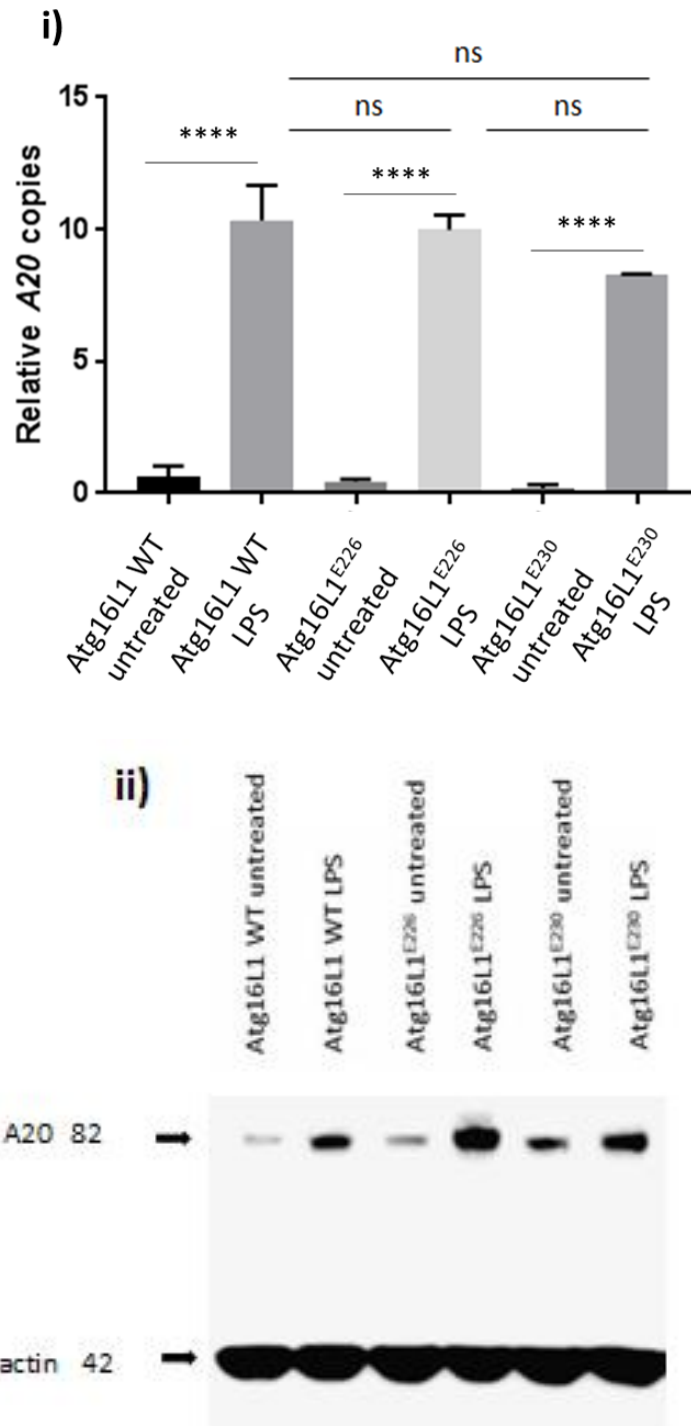
Figure 5.3 A20 gene and protein expression in Atg16L1 WT, Atg16L1^{E226} and Atg16L1^{E230} BMDMs. (i) Cells were cultured in growth medium or treated with LPS (1 µg/ml) for 4h before RNA extraction and analysis by qPCR. The p values < 0.05 were considered statistically significant (**** $<$ 0.0001). (n=3); **ii)** Cells were cultured in growth medium or treated with LPS (1 µg/ml) for 4h. The cell lysates were then blotted for A20. (n=3).

Chapter 6

Mechanism of regulation of macrophage homeostasis by Atg16L1

6.1 Introduction and aims

Macrophages are an essential component of the innate immune response and represent the first line of defence against pathogens. Moreover, they are involved in homeostasis, tissue remodelling, wound healing, and can affect tissue metabolism. On one hand, macrophages have extrinsic metabolic functions by releasing cytokines; on the other hand, their intrinsic metabolic functions shape their activation state. Upon environmental stimulation, they acquire distinct phenotypes (Biswas& Mantovani, 2012). In response to various signals, macrophages may undergo classical M1 or alternative M2 activation (polarization). The M1 polarized macrophages secrete high amounts of pro-inflammatory cytokines and are characterized with a high production of reactive nitrogen and oxygen intermediates. They are implicated in initiating and sustaining of inflammation whereas the M2 macrophages promote tissue repair and have immunoregulatory functions (Sica&Mantovani, 2012).

It has long been known that macrophage functions and metabolism are tightly connected (Biswas& Mantovani, 2012). An increasing number of studies have emphasized the significance of investigating the link between the metabolic state and the phenotype of immune cells (Galvan-Pena&O'Neill, 2014). Moreover, defining the mechanisms of macrophage metabolic activity and regulation is crucial to pathology (Biswas&Mantovani, 2012).

Loss of autophagy in macrophages and other myeloid cells *in vivo* is associated with increased inflammation. This has been referred to as a 'bystander or extrinsic autophagy'' by Lu and colleagues (2016) and well

as Park and colleagues (2016),and differs from intrinsic autophagy where autophagy protects against infection by degrading pathogens inside cells. In this model, loss of autophagy from macrophages and other myeloid cells increases proinflammatory responses and raises the inflammatory threshold *in vivo*. This can protect against infection because invading microorganisms encounter a pre-activated immune system, or lead to inflammatory disease if inflammation is not controlled, e.g. Crohn's disease.

The Atg16L1 [T300A] Crohn's disease model predicts that the T300A risk allele generates caspase-3 cleavage site that is cleaved by caspase-3 activated during inflammation. It is thought that this inactivates Atg16L1 leading to loss of autophagy and increased inflammation (Murthy *et al*, 2014). Caspase-3 cleavage removes the WD domain of Atg16L1 and leaves the Atg5 binding and CC domains of Atg16L1 intact. The work in the previous chapters studying BMDMs from Atg16L1[E230] mice has shown, however, that these domains of

Atg16L1 are sufficient to maintain autophagy and supress IL-1beta secretion. This chapter analyses the effects of loss of the WD domain on macrophage polarization, oxygen consumption and glycolytic activity.

6.2 Macrophage polarization

6.2.i Compromised autophagy skews macrophage polarization to an M1 phenotype

It has been shown that in response to various stimuli, immune cells rapidly adapt their metabolic profiles to defend the host and meet its needs. Upon intracellular or bacterial infection, or after IFN-gamma stimulation, macrophages obtain the M1 phenotype which is

characterised by the generation of various metabolites or cytokines, called M1 markers, involved in the killing of the pathogen (Galvan-Pena&O'Neill, 2014). Here we investigated the expression of two M1 markers: IL-6, an important mediator of the acute phase response which also stimulates the production of neutrophils and supports the growth of B cells (Hunter&Jones, 2015); and Ptgs2 (COX2), involved in the production of prostaglandins which play an essential role in inflammation (Morita, 2002).

BMDMs were incubated in growth medium or treated with LPS (100 ng/ml) and IFN-gamma (100 ng/ml) for 24h before qRT-PCR was performed (Figure 6.1). Untreated BMDMs showed very low basal levels of *IL-6* and *Ptgs2.* A dramatic increase in gene expression was observed after LPS and IFN-gamma stimulation but the greatest elevation was seen in BMDMs from Atg16L1^{E226} mice. Increases in *IL-6* and *Ptgs2* in the Atg16L1^{E230} cells were similar to controls.

6.2.ii Compromised autophagy inhibits M2 macrophage polarization

The M2 macrophages are associated with tissue repair, immunoregulation and chronic inflammation resolution (Sica&Mantovani, 2012). Exposure to fungi or parasites, or after stimulation with IL-4 or IL-13, macrophages obtain the M2 phenotype which is characterised by the production of metabolites, receptors and chemokines, called M2 markers, involved in pathogen clearance, tissue repair, or inflammation resolution (Roszer, 2015). The expression of two M2 markers: Arg1, a tissue healing regulator which also reduces the T-cell response; and Chil3, involved in inflammatory response which also displays a chemotactic activity for T lymphocytes (Roszer, 2015) were

analysed after incubation of BMDMs with IL-4 (10 ng/ml) and IL-13 (20 ng/ml) for 24h before qRT-PCR (Figure 6.2). Untreated cells showed low basal levels of the M2 polarization markers. After stimulation with IL-4 and IL-13, however, both *Arg1* and *Chil3* showed a significant expression decrease in the BMDMs from the autophagy-deficient Atg16L1^{E226} mouse. Both Atg16L1^{E230} and WT macrophages showed a 3-fold increase in the expression of Chil3 in response to treatment with IL-4 and IL-13. The same 3-fold pattern was observed in the Arg1 expression as well, however, the Chil3 levels in the Atg16L1^{E230} macrophages showed a decrease compared to the WT which might be due to the lower starting expression in the latter. Since the Atg16L1^{E230} macrophages are LAP-compromised, one possible speculation might be that LAP interacts with the Chil3 production pathway. Taken together, the results demonstrate that loss of autophagy leads to increased susceptibility to pro-inflammatory M1 phenotype, but this susceptibility is not caused by a loss of the WD domain of Atg16L1.

Figure 6.1 Gene expression levels of *IL-6* and *Ptgs2* in Atg16L1 WT, Atg16L1^E226 and Atg16L1^E230 BMDMs. Cells were treated with LPS (100 ng/ml) and INF-gamma (100 ng/ml) for 24h. The *p* values < 0.05 were considered statistically significant (* < 0.05; ** < 0.01; *** < 0.001; **** < 0.0001). (n=3).
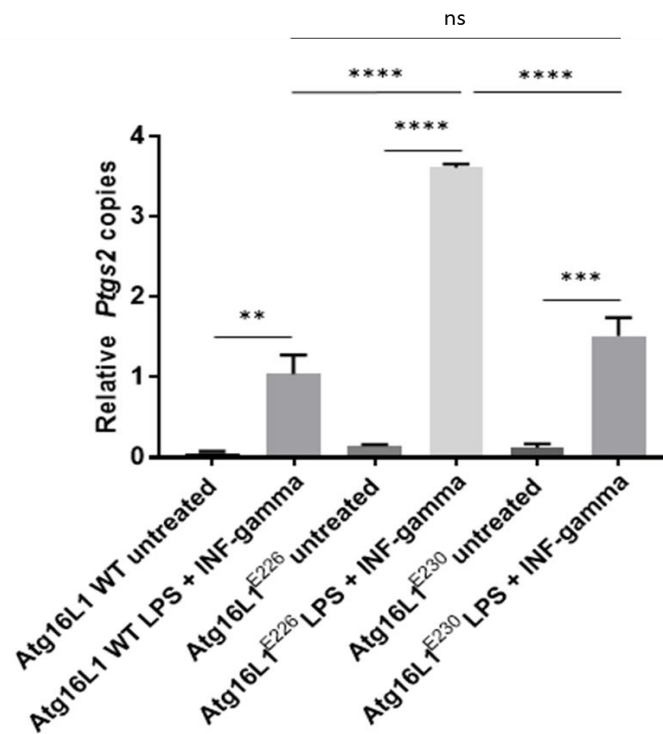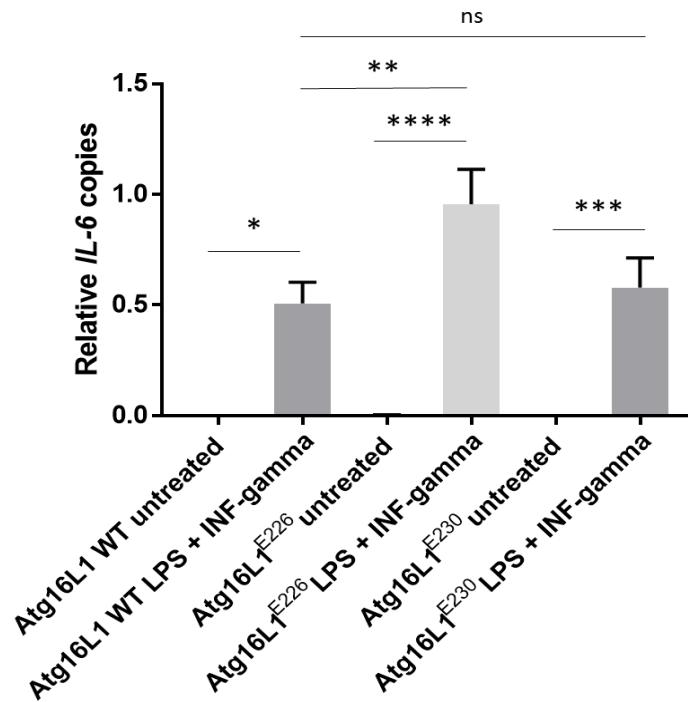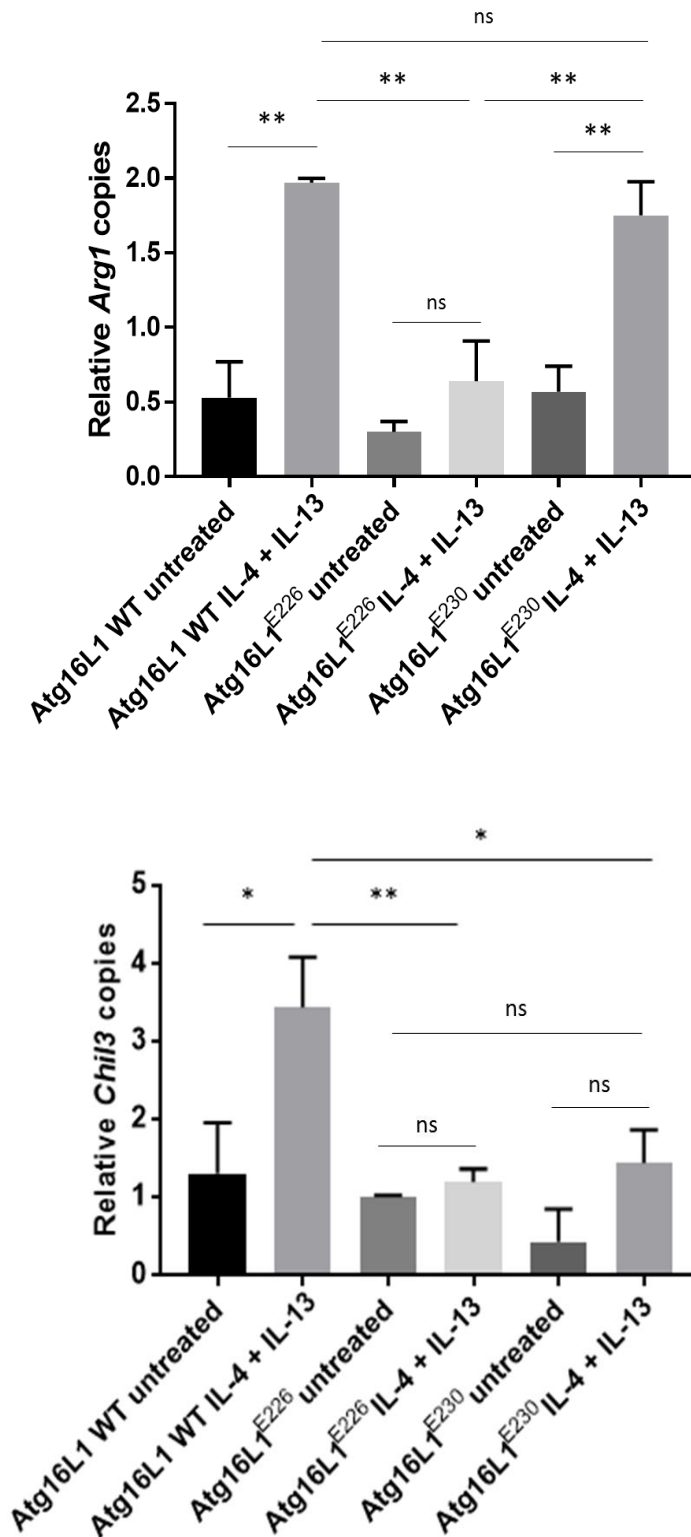
Figure 6.2 Gene expression levels of *Arg1* and *Chil3* in Atg16L1 WT, Atg16L1^E226 and Atg16L1^E230 BMDMs. Cells were treated with IL-4 (10 ng/ml) and IL-13 (20 ng/ml) for 24h. The *p* values < 0.05 were considered statistically significant (* < 0.05; ** < 0.01). (n=3)

6.3 Metabolic flux analysis of BMDM to determine any phenotypic differences in glycolysis and OXPHOS

The respiratory profile of the different genotypes was investigated using the stress tests to examine any differences in glycolytic and mitochondrial function thereby determining the two major energy-producing pathways in a cell. Differences in glycolytic function may identify alterations in how glucose is utilised between the genotypes by examining the maximum glycolysis capacity. Where differences in the mitochondrial function allow the determination of cellular metabolic function, for example it may highlight differences in mitochondrial leak or damage between the genotypes that would directly affect the amount of ATP generated per glucose molecule.

6.3.i Glycolysis stress test

Figure 6.3i-ii shows glycolytic metabolism for BMDMs derived from wild type, $Atg16L1^{E230}$ (top) and $Atg16L1^{E226}$ (bottom) mice respectively, analysis showed an increase in ECAR in response to a first injection of a saturating concentration of glucose (10mM), this enhanced ECAR indicated glycolysis under basal conditions (histogram figure 6.4i, iv). Thereafter, oligomycin was injected to block OXPHOS and shifted the cells into maximum glycolytic
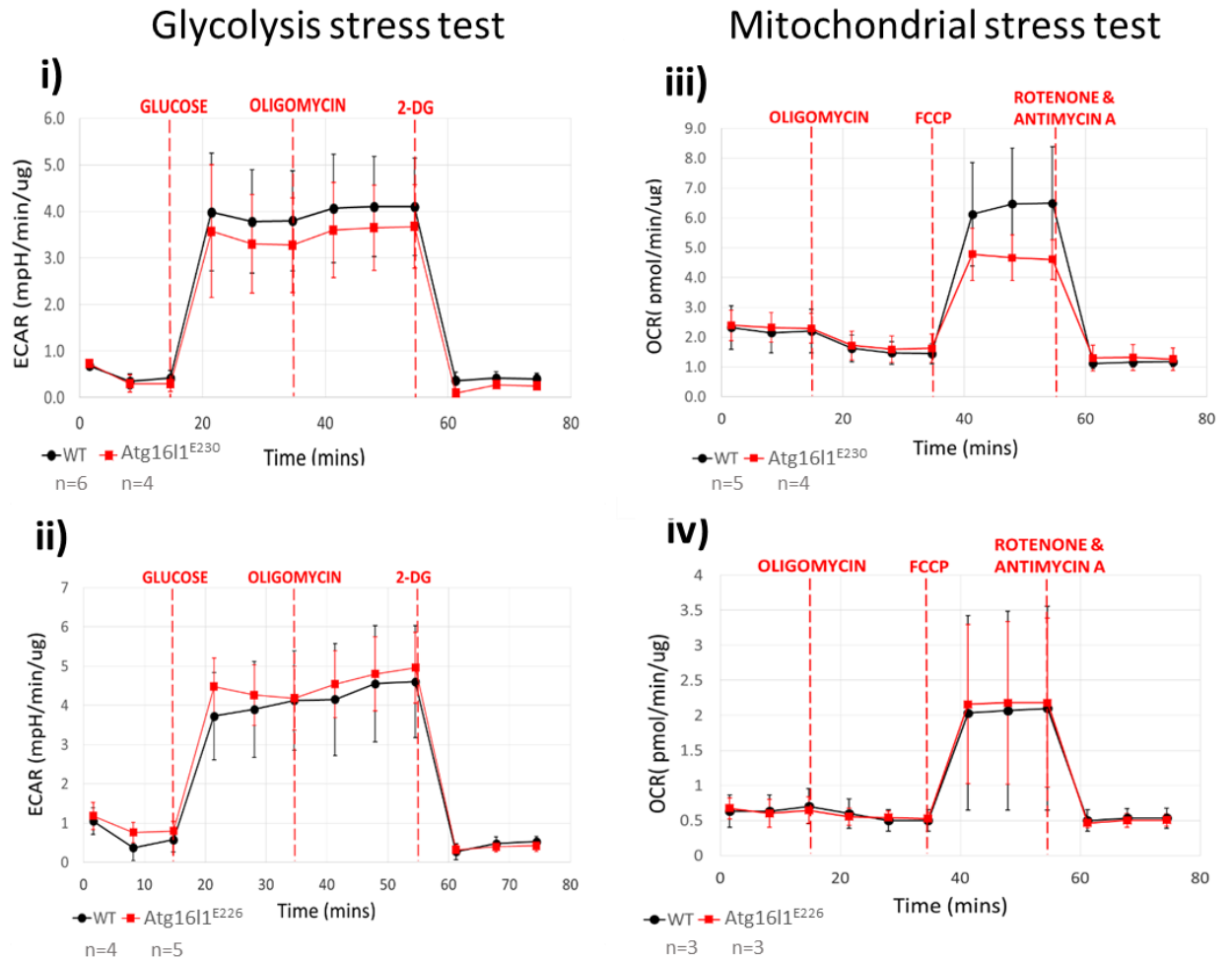
Figure 6.3: Glycolysis and Mitochondrial stress test average data for wild type (WT) versus Atg16L1^{E230} and Atg16L1^{E226} BMDMs. Pooled data showing extracellular acidification rate versus time (glycolysis stress test), **(i)** WT versus Atg16L1^{E230}, **(ii)** WT versus Atg16L1^{E226} mice, and oxygen consumption rates versus time (mitochondrial stress test), **(iii)** WT versus Atg16L1^{E230} and **(iv)** WT versus Atg16L1^{E226} mice. Numbers of separate mice used are indicated below each key. No significant differences were found between the mutant versus wild type phenotypes (Students t-test).

capacity (histogram figure 6.4ii, v) though no clear response to oligomycin was observed. The final injection of a saturating concentration of 2-DG competitively inhibited glucose hexokinase, the first enzyme in the glycolytic pathway (see Materials and Methods, figure 2.5) and confirmed the ECAR values measured were due to glycolysis. Glycolytic reserve (histogram Figure 6.4iii, vi) was calculated as the difference between glycolysis (i) and glycolytic capacity (ii) and argued all cells were functioning at near maximal glycolysis to generate ATP. No significant differences (Student's t-test) were found between any flux analysis undertaken.

6.3.ii Mitochondrial stress test

Figure 6.3iii-iv shows the oxygen consumption rate (OCR) for macrophage cells derived from wild type, Atg16L1^{E230} and Atg16L1^{E226} mice. Basal respiration was determined immediately prior to the injection of oligomycin (histogram figure 6.5i, iv) and excluded non-mitochondrial respiration. Thereafter, a small decrease in oxygen consumption was shown in response to oligomycin injection, an inhibitor of complex V (see Materials and Methods, figure 2.7), and directly indicated the proportion of basal respiration oxygen consumption that was related to ATP production (histogram figure 6.5iii-iv). A subsequent injection of the mitochondrial un-coupler FCCP that collapses the proton gradient and mimics a metabolic challenge resulted in maximum cellular oxygen consumption by complex IV. The final injection of rotenone, a complex I inhibitor, and antimycin-A, a complex III inhibitor, ceased all OXPHOS and identified any OCR that was unrelated to OXPHOS. This measure of nonOXPHOS OCR subtracted from OCR utilised for ATP production allowed the proton leak

(histogram figure 6.5ii, v) to be calculated and was an indication of mitochondrial damage. Overall no significant differences (Students t-test) were found between comparisons of these data between WT or mutant BMDMs irrespective of genotype.
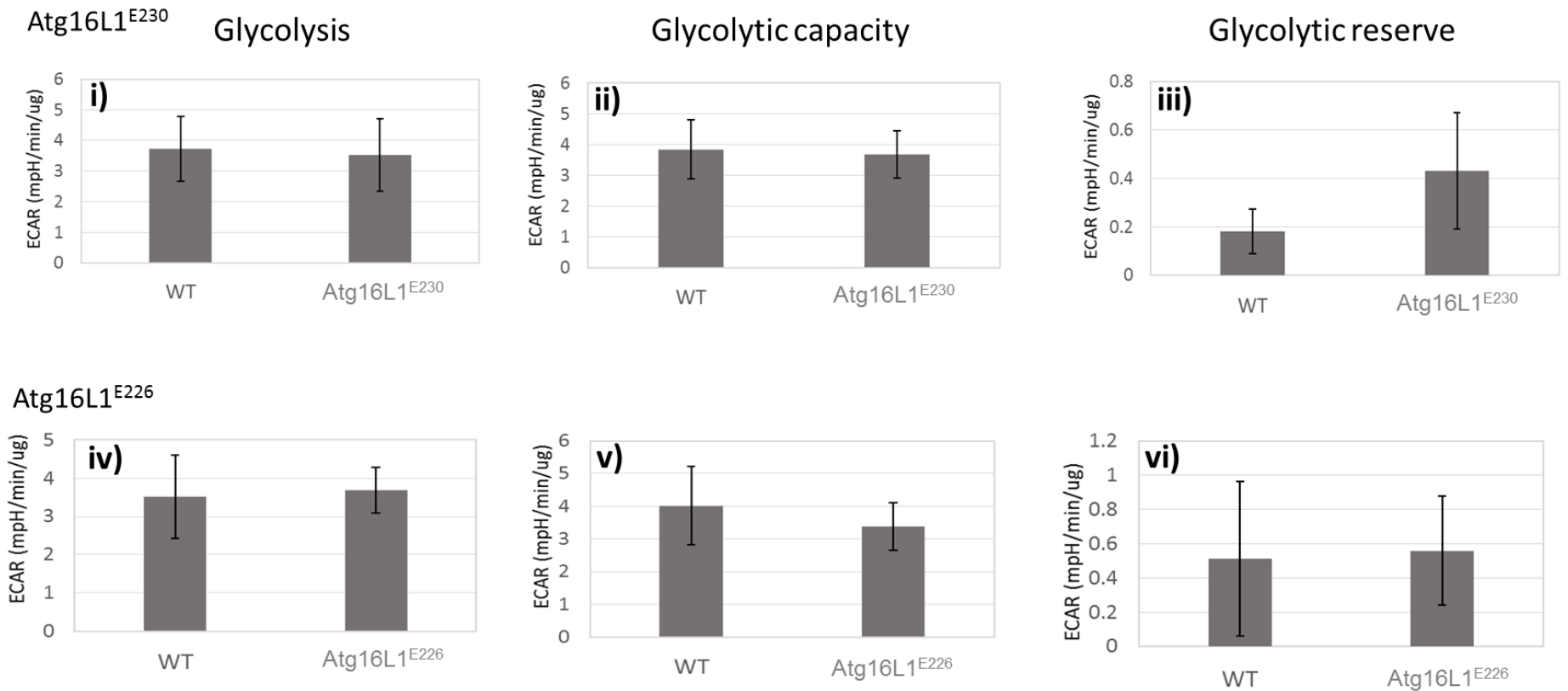
Figure 6.4: Histograms showing average data for respiratory parameters from a glycolysis stress test. Bar chart graphs from Atg16L1[E230] (n=4, **i-iii**) and Atg16L1[E226] (n=5, **iv-vi**) versus wild type mice (n=6&4, respectively) showing bone marrow-derived macrophage glycolytic metabolic function. Where glycolysis (**i,iv**), glycolytic capacity (**ii, v**) and glycolytic reserve (**iii, vi**) showed no significant differences between the mutant and wild type phenotypes (Student's t-test).
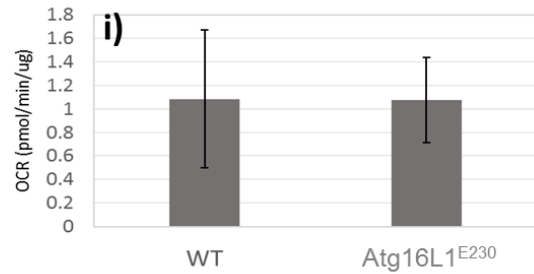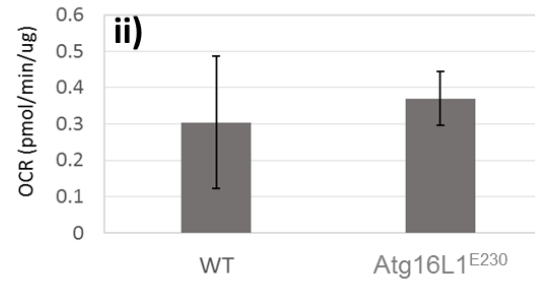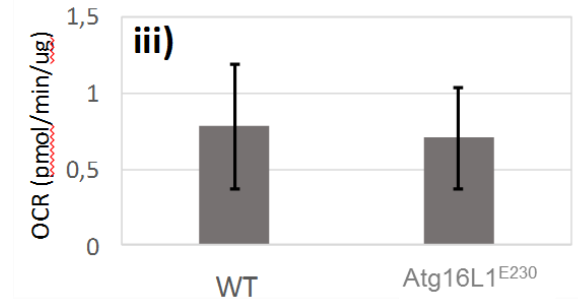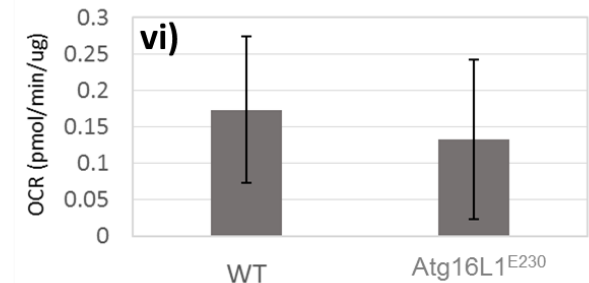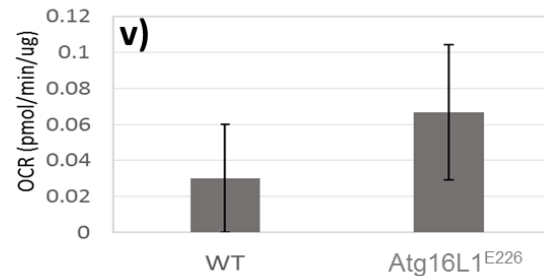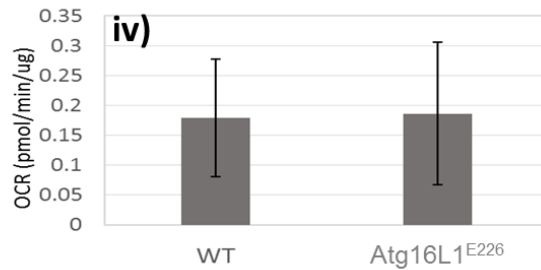
Figure 6.5: Histograms showing average data for respiratory parameters from a mitochondrial stress test. Bar chart graphs from Atg16L1^{E230} (n=4, **i-iii**) and Atg16L1^{E226} (n=3, **iv-vi**) versus wild type mice (n=5&3, respectively) showing bone marrow-derived macrophage OXPHOS metabolic function. Where basal respiration (**i, iv**), proton leak (**ii, v**) and ATP production (**iii, vi**) showed no significant differences between the mutant and wild type phenotypes (Student's t-test).

Chapter 7

Discussion

7.1 Atg16L1, LAP and inflammation

As described above, autophagy plays important roles in tissue homeostasis and development and provides a short-term supply of amino acids to sustain protein and energy production during starvation. Autophagy is also important in the immune system where it can suppress excessive inflammation during microbial infections and degrade pathogens in lysosomes to increase presentation of pathogen components to the immune system. The Atg16L1 protein is essential for autophagy and is composed of two main domains: the combined atg5-binding:CCD which is at the N-terminus of the protein, and a C-terminal WD repeat domain. This study has used mouse models to analyse the role played by these domains in suppressing inflammatory responses by macrophages.

The atg5-binding:CCD of Atg16L1 provides a binding site for PtdIns(3)P effector protein WIPI2b which ensures that the Atg12:5:16L1 complex can deliver lipidated LC3 (LC3-II) to the autophagosome membrane. Both mouse models lack the WD domainbut vary in their ability to bind WIPI2b. The CCD of the Atg16L1^{E226} mouse lacks the E230 residue required for binding to WIPI2b, and cells isolated from the mouse are negative for autophagy and autophagosome formation. The CCD of the Atg16L1^{E230} mouse retains the E230 residue necessary for WIPI2b binding and cells isolated from the mouse are positive for autophagy and autophagosome formation. Autophagy does not therefore require the WD domain of Atg16L1 and only requires an atg5-binding:CCD able to bind WIPI2b. Related experiments have been carried out by Saitoh *et al* (2008). In their experiment the Atg16L1 gene was modified so that the mouse expressed the WD domain but not the atg5-binding:CCD.

These mice were autophagy negative and died of post-natal starvation. The experiments showed that the CCD is required for autophagy but did not exclude the possibility that both the atg5-binding:CCD and the WD of Atg16L1 are required for autophagy in mice. The experiments in this thesis are the first to study mice expressing the atg5-binding:CCD but lacking the WD domain. The Atg16L1^{E230} mouse was autophagy positive and survived post-natal starvation, indicating that the mouse could maintain autophagy *in vivo* without the WD domain. This surprising result suggests that the scaffold generated by the 8 WD domains of the 800kD Atg5-12:16L1 hexamer, containing 56 beta propellers, are not involved in protein:protein interactions required for suppressing inflammation. Instead, evolution appears to have confined this important role to the N-terminal atg5-binding and CC domains conserved through to yeast. Further studies using macrophages cultured from Atg16L1^{E230} mouse bone marrow showed that the mice were defective in LAP. At the time of writing, this is the first evidence that the WD domain of Atg16L1 is required for LAP. This will prompt further work to understand how the 56 beta propellers of the Atg5-12:16L1 hexamer control the recruitment of LC3 to phagosomes containing pathogens as they enter cells.

The Atg16L1^{E226} and Atg16L1^{E230} mice provided a source of macrophages to study the roles played by autophagy and LAP in controlling IL-1beta secretion and M1/M2 polarisation. Taken together, the results showed that autophagy, rather than LAP, was important for controlling IL-1beta secretion in response to LPS-mediated TL4 signalling. Caspase-1 and caspase-8 activity as well as levels of A20 were also raised in the absence of autophagy, but again were not affected by loss of LAP. With

the time available, it was not possible to show that caspase-8 and A20 were cargoes for autophagy and degraded in lysosomes. Caspase-1 did not show co-localization with LC3, suggesting that proIL-1beta is segregated from caspase-1. Autophagy, rather than LAP, was also involved in pushing macrophage polarisation towards an M2, anti-inflammatory phenotype.

The effects of autophagy and LAP were also studied in the context of the signalling proteins that act upstream of IL-1beta processing. A20 is a signalling molecule that restricts inflammation by inhibiting NF-kB signalling. Polymorphisms and mutations in *Tnfaip3*, the gene encoding A20, have been linked to inflammatory, malignant and autoimmune diseases. Interestingly, our experiments showed a significant increase in A20 protein expression in the Atg16L1^{E226} macrophages compared to control and Atg16L1^{E230}. This finding suggests that A20 might be a substrate for autophagy. Moreover, previous studies have demonstrated that A20 co-localizes with p62, an autophagy adaptor protein, in tissue macrophages and is sequestered for degradation in the autophagosome (Kanayama, 2015). The observations do not easily explain increased levels of IL-1beta, based on the results obtained by Duong *et al* (2015), where *Tnfaip3-/-* BMDMs showed an increase in IL-1beta secretion compared to control wild type cells after LPS stimulation.

Therefore, increased A20 would be expected to decrease processing of IL-1beta by caspase-1. There is, however, an important difference between activation of proIL-1beta and levels of proIL-1beta protein. Our results show increased levels of IL-1beta in BMDMs from Atg16L1^{E226} mice, suggesting that proIL-1beta is degraded by autophagy. The

observation that A20 binds proIL-1beta, and is also a substrate for autophagy, raises the possibility that A20 may target IL-1beta for autophagy. This could be tested by silencing A20 which should raise IL-1beta levels. Moreover, A20 has been reported to be capable of targeting signalling molecules, such as TRAF2, to the lysosomes for degradation (Li *et al*, 2009).

7.2 Macrophage metabolism

It has long been known that macrophage functions and metabolism are tightly connected (Biswas&Mantovani, 2012). An increasing number of studies have emphasized the significance of investigating the link between the metabolic state and the phenotype of immune cells (Galvan-Pena&O'Neill, 2014). Moreover, defining the mechanisms of macrophage metabolic activity and regulation is crucial to pathology (Biswas&Mantovani, 2012). Here we show that unlike the autophagy-deficient Atg16L1^{E226} macrophages, the LAP-compromised Atg16L1^{E230} cells do not skew macrophage polarization into the pro-inflammatory M1 phenotype. Moreover, the Atg16L1^{E230} cells were not able to inhibit the anti-inflammatory M2 phenotype.

Autophagy is a process of general cellular housekeeping. It is predicted that where autophagy is absent, damaged proteins should start to accumulate. If this were to occur in the mitochondria, it might be expected that their ability to undergo OXPHOS might be compromised, similarly for the glycolytic pathway. We used the Mito stress test and glycolysis stress test to determine any differences in OXPHOS or glycolysis, respectively, between the different mouse genotypes. Analysis of OXPHOS showed no difference between the Atg16L1^{E226} and Atg16L1^{E230} macrophages versus wild type mice, nor were any

differences found for the glycolytic stress test. This argues the metabolic function of ATP generation using both OXPHOS or glycolysis is unaffected by autophagy or LAP, it further argues that if misfolded proteins or damaged organelles accumulate in Atg16L1^{E226} and Atg16L1^{E230} macrophages, they do not alter energy metabolism. It is also notable that the BMDMs predominantly use glycolysis at near maximal rates as no increase in ECAR was evident to oligomycin treatment that shuts down OXPHOS and should force the cells to use glycolysis only to make ATP. Furthermore, the glycolytic reserve is low as there was no increase in ECAR after oligomycin treatment and argues the ability of the cell to fill an energetic demand in response to a stress may not be fully satisfied by glycolysis. However, there is appreciable spare OXPHOS capacity that could supply additional ATP when demand is required. These observations are consistent with previous studies showing no mitochondrial alternations in Atg16L1-/- resting B-cells when compared to wild type (Martinez-Martin *et al*, 2017).

7.3 Atg16L1, Crohn's disease and LAP

The context of how the Atg12:5:16L1 complex is processed becomes important in relation to Crohn's disease where a mutation at T300A of Atg16L1 yields a caspase-3 sensitive site that can generate truncated Atg16L1 which only contains an intact CCD, but lacks the WD repeats. Several studies, mostly characterising the T300A mutation associated with Crohn's disease, suggest that the WD domain is important for controlling inflammation. One study suggests that the T300A mutation, located in the linker region of the protein, generates a caspase-3 cleavage site making Atg16L1 susceptible to cleavage when caspase-3 is activated during inflammation. Murthy *et al* (2014) show that this

148

results in diminished autophagy and increased cytokine production. Another study demonstrates that knock-out of rubicon in myeloid cells, a key protein in the LAP pathway, does not affect autophagy, but leads to an acute elevation of pro-inflammatory cytokine levels (Martinez *et al*, 2016). This thesis has demonstrated elevated proIL-1beta protein levels when autophagy is lost in the Atg16L1^{E226} macrophages but did not provide evidence for a significant increase for the Atg16L1^{E230} macrophages. These results are contrary to the conclusions of studies of the T300A mutation because they suggest that the atg5-binding:CCD of Atg16L1 is sufficient to suppress inflammation. Loss of the WD domain following caspase-3 cleavage would not be expected to increase pro-inflammatory cytokine production.

In this sense, Atg16L1^{E230} mouse model is not the same as the T300A Crohn's model contrary to the expectations. It is worth noting that the stop codon in the Atg16L1^{E230} mouse is located immediately after the CCD domain whereas in the T300A model, part of the linker region of Atg16L1 is preserved. Depending on the conformational status of the protein and in the absence of the WD domain, the linker in the T300A might be responsible for the pro-inflammatory response that is observed in this model. Another possibility that should be considered is based on the fact that in human T300A cells, inflammation activates caspase-3 which in turn cleaves Atg16L1 at T300A resulting in accumulation of free WD within the cell. This protein accumulation might be a signal which triggers an inflammatory response. In the case of Atg16L1^{E230}, however, such accumulation is not possible due to the lack of the WD domain. To investigate the possible reasons for the

observed results, future work should be aimed at investigating the role of the linker region in the Atg16L1 protein.

References

Agilent Technologies (2017) Seahorse XF Consumables [online] Available at: http://www.agilent.com/en-us/products/cell-analysis(seahorse)/seahorsexf-consumables [Accessed 28th September 2017]

Akira S, Uematsu S, Takeuchi O (2006) Pathogen recognition and innate immunity. *Cell* **124:** 783-801

Baeuerle PA, Henkel T (1994) Function and activation of NF-kappa B in the immune system. *Annu Rev Immunol* **12:** 141-179

Bajagic M, Archna A, Busing P, Scrima A (2017) Structure of the WD40-domain of human ATG16L1. *Protein Sci* **26:** 1828-1837

Biswas SK, Mantovani A (2012) Orchestration of metabolism by macrophages. *Cell Metab* **15:** 432-437

Boada-Romero E, Letek M, Fleischer A, Pallauf K, Ramon-Barros C, PimentelMuinos FX (2013) TMEM59 defines a novel ATG16L1-binding motif that promotes local activation of LC3. *EMBO J* **32:** 566-582

Boada-Romero E, Serramito-Gomez I, Sacristan MP, Boone DL, Xavier RJ, Pimentel-Muinos FX (2016) The T300A Crohn's disease risk polymorphism impairs function of the WD40 domain of ATG16L1. *Nat Commun* **7:** 11821

Cadwell K, Liu JY, Brown SL, Miyoshi H, Loh J, Lennerz JK, Kishi C, Kc W, Carrero JA, Hunt S, Stone CD, Brunt EM, Xavier RJ, Sleckman BP, Li E, Mizushima N, Stappenbeck TS, Virgin HWt (2008) A key role for autophagy and the autophagy gene Atg16l1 in mouse and human intestinal Paneth cells. *Nature* **456:** 259-263

Chen CZ, Ou CY, Wang RH, Lee CH, Lin CC, Chang HY, Hsiue TR (2015) Association of Egr-1 and autophagy-related gene polymorphism in men with chronic obstructive pulmonary disease. *J Formos Med Assoc* **114:** 750-755

Chi W, Li F, Chen H, Wang Y, Zhu Y, Yang X, Zhu J, Wu F, Ouyang H, Ge J, Weinreb RN, Zhang K, Zhuo Y (2014) Caspase-8 promotes NLRP1/NLRP3 inflammasome activation and IL-1beta production in acute glaucoma. *Proc Natl Acad Sci U S A* **111:** 11181-11186

Crotzer VL, Blum JS (2009) Autophagy and its role in MHC-mediated antigen presentation. *J Immunol* **182:** 3335-3341

Denes A, Lopez-Castejon G, Brough D (2012) Caspase-1: is IL-1 just the tip of the ICEberg? *Cell Death Dis* **3:** e338

Deretic V (2012) Autophagy: an emerging immunological paradigm. *J Immunol* **189:** 15-20

Dooley HC, Razi M, Polson HE, Girardin SE, Wilson MI, Tooze SA (2014) WIPI2 links LC3 conjugation with PI3P, autophagosome formation, and pathogen clearance by recruiting Atg12-5-16L1. *Mol Cell* **55:** 238-252

Duong BH, Onizawa M, Oses-Prieto JA, Advincula R, Burlingame A, Malynn BA, Ma A (2015) A20 restricts ubiquitination of pro-interleukin-1beta protein complexes and suppresses NLRP3 inflammasome activity. *Immunity* **42:** 55-67

Fejer G, Sharma S, Gyory I (2015) Self-renewing macrophages--a new line of enquiries in mononuclear phagocytes. *Immunobiology* **220:** 169-174

Florey O, Gammoh N, Kim SE, Jiang X, Overholtzer M (2015) V-ATPase and osmotic imbalances activate endolysosomal LC3 lipidation. *Autophagy* **11:** 8899

Franchi L, Eigenbrod T, Munoz-Planillo R, Nunez G (2009) The inflammasome: a caspase-1-activation platform that regulates immune responses and disease pathogenesis. *Nat Immunol* **10:** 241-247

Fujita N, Hayashi-Nishino M, Fukumoto H, Omori H, Yamamoto A, Noda T, Yoshimori T (2008) An Atg4B mutant hampers the lipidation of LC3 paralogues and causes defects in autophagosome closure. *Mol Biol Cell* **19:** 4651-4659

Gabrilovich DI, Nagaraj S (2009) Myeloid-derived suppressor cells as regulators of the immune system. *Nat Rev Immunol* **9:** 162-174

Gaidt MM, Hornung V (2017) Alternative inflammasome activation enables IL1beta release from living cells. *Curr Opin Immunol* **44:** 7-13

Galvan-Pena S, O'Neill LA (2014) Metabolic reprograming in macrophage polarization. *Front Immunol* **5:** 420

Gao P, Liu H, Huang H, Zhang Q, Strober W, Zhang F (2017) The Inflammatory Bowel Disease-Associated Autophagy Gene Atg16L1T300A Acts as a Dominant Negative Variant in Mice. *J Immunol* **198:** 2457-2467

Gordon S, Taylor PR (2005) Monocyte and macrophage heterogeneity. *Nat Rev Immunol* **5**: 953-964

Guo H, Callaway JB, Ting JP (2015) Inflammasomes: mechanism of action, role in disease, and therapeutics. *Nat Med* **21:** 677-687

Gurung P, Kanneganti TD (2015) Novel roles for caspase-8 in IL-1beta and inflammasome regulation. *Am J Pathol* **185:** 17-25

Hailey KL, Li S, Andersen MD, Roy M, Woods VL, Jr., Jennings PA (2009) Prointerleukin (IL)-1beta shares a core region of stability as compared with mature IL-1beta while maintaining a distinctly different configurational landscape: a comparative hydrogen/deuterium exchange mass spectrometry study. *J Biol Chem* **284:** 26137-26148

Hampe J, Franke A, Rosenstiel P, Till A, Teuber M, Huse K, Albrecht M, Mayr G, De La Vega FM, Briggs J, Gunther S, Prescott NJ, Onnie CM, Hasler R, Sipos B, Folsch UR, Lengauer T, Platzer M, Mathew CG, Krawczak M, Schreiber S (2007) A genome-wide association scan of nonsynonymous SNPs identifies a susceptibility variant for Crohn disease in ATG16L1. *Nat Genet* **39:** 207-211

Harris J, Lang T, Thomas JPW, Sukkar MB, Nabar NR, Kehrl JH (2017) Autophagy and inflammasomes. *Mol Immunol* **86:** 10-15

Harris J (2013) Autophagy and IL-1 Family Cytokines. *Front Immunol* **4:** 83

Harris J, Hartman M, Roche C, Zeng SG, O'Shea A, Sharp FA, Lambe EM, Creagh EM, Golenbock DT, Tschopp J, Kornfeld H, Fitzgerald KA, Lavelle EC (2011) Autophagy controls IL-1beta secretion by targeting pro-IL-1beta for degradation. *J Biol Chem* **286:** 9587-9597

Hunter CA, Jones SA (2015) IL-6 as a keystone cytokine in health and disease. *Nat Immunol* **16**: 448-457

Inomata M, Niida S, Shibata K, Into T (2012) Regulation of Toll-like receptor signaling by NDP52-mediated selective autophagy is normally inactivated by A20. *Cell Mol Life Sci* **69:** 963-979

Kanayama M, Inoue M, Danzaki K, Hammer G, He YW, Shinohara ML (2015) Autophagy enhances NFkappaB activity in specific tissue

macrophages by sequestering A20 to boost antifungal immunity. *Nat Commun* **6:** 5779

Kim J, Kundu M, Viollet B, Guan KL (2011) AMPK and mTOR regulate autophagy through direct phosphorylation of Ulk1. *Nat Cell Biol* **13:** 132-141

Kimura T, Jain A, Choi SW, Mandell MA, Schroder K, Johansen T, Deretic V (2015) TRIM-mediated precision autophagy targets cytoplasmic regulators of innate immunity. *J Cell Biol* **210:** 973-989

Komatsu M, Waguri S, Ueno T, Iwata J, Murata S, Tanida I, Ezaki J, Mizushima N, Ohsumi Y, Uchiyama Y, Kominami E, Tanaka K, Chiba T (2005) Impairment of starvation-induced and constitutive autophagy in Atg7-deficient mice. *J Cell Biol* **169:** 425-434

Kovacs JR, Li C, Yang Q, Li G, Garcia IG, Ju S, Roodman DG, Windle JJ, Zhang X, Lu B (2012) Autophagy promotes T-cell survival through degradation of proteins of the cell death machinery. *Cell Death Differ* **19:** 144-152

Kuma A, Hatano M, Matsui M, Yamamoto A, Nakaya H, Yoshimori T, Ohsumi Y, Tokuhisa T, Mizushima N (2004) The role of autophagy during the early neonatal starvation period. *Nature* **432:** 1032-1036

Lai SC, Devenish RJ (2012) LC3-Associated Phagocytosis (LAP): Connections with Host Autophagy. *Cells* **1:** 396-408

Lassen KG, Kuballa P, Conway KL, Patel KK, Becker CE, Peloquin JM, Villablanca EJ, Norman JM, Liu TC, Heath RJ, Becker ML, Fagbami L, Horn H, Mercer J, Yilmaz OH, Jaffe JD, Shamji AF, Bhan AK, Carr SA, Daly MJ, Virgin HW, Schreiber SL, Stappenbeck TS, Xavier RJ (2014) Atg16L1 T300A variant decreases selective autophagy resulting in altered cytokine signaling and decreased antibacterial defense. *Proc Natl Acad Sci U S A* **111:** 7741-7746

Lawrence T, Natoli G (2011) Transcriptional regulation of macrophage polarization: enabling diversity with identity. *Nat Rev Immunol* **11:** 750-761 Levine B, Mizushima N, Virgin HW (2011) Autophagy in immunity and inflammation. *Nature* **469:** 323-335

Li L, Soetandyo N, Wang Q, Ye Y (2009) The zinc finger protein A20 targets TRAF2 to the lysosomes for degradation. *Biochim Biophys Acta* **1793:** 346353

Liu K, Zhao E, Ilyas G, Lalazar G, Lin Y, Haseeb M, Tanaka KE, Czaja MJ (2015) Impaired macrophage autophagy increases the immune response in obese mice by promoting proinflammatory macrophage polarization. *Autophagy* **11:** 271-284

Lopez-Castejon G, Brough D (2011) Understanding the mechanism of IL-1beta secretion. *Cytokine Growth Factor Rev* **22:** 189-195

Lu Q, Yokoyama CC, Williams JW, Baldridge MT, Jin X, DesRochers B, Bricker T, Wilen CB, Bagaitkar J, Loginicheva E, Sergushichev A,

Kreamalmeyer D, Keller BC, Zhao Y, Kambal A, Green DR, Martinez J, Dinauer MC, Holtzman MJ, Crouch EC, Beatty W, Boon AC, Zhang H, Randolph GJ, Artyomov MN, Virgin HW (2016) Homeostatic Control of Innate Lung Inflammation by Vici Syndrome Gene Epg5 and Additional Autophagy Genes Promotes Influenza Pathogenesis. *Cell Host Microbe* **19:** 102-113

Malhotra R, Warne JP, Salas E, Xu AW, Debnath J (2015) Loss of Atg12, but not Atg5, in pro-opiomelanocortin neurons exacerbates diet-induced obesity. *Autophagy* **11**: 145-154

Man SM, Kanneganti TD (2016) Converging roles of caspases in inflammasome activation, cell death and innate immunity. *Nat Rev Immunol* **16:** 7-21

Mantovani A, Sozzani S, Locati M, Allavena P, Sica A (2002) Macrophage polarization: tumor-associated macrophages as a paradigm for polarized M2 mononuclear phagocytes. *Trends Immunol* **23:** 549-555

Martinez J, Cunha LD, Park S, Yang M, Lu Q, Orchard R, Li QZ, Yan M, Janke L, Guy C, Linkermann A, Virgin HW, Green DR (2016) Noncanonical autophagy inhibits the autoinflammatory, lupus-like response to dying cells. *Nature* **533:** 115-119

Martinez J, Malireddi RK, Lu Q, Cunha LD, Pelletier S, Gingras S, Orchard R, Guan JL, Tan H, Peng J, Kanneganti TD, Virgin HW, Green DR (2015) Molecular characterization of LC3-associated phagocytosis reveals

distinct roles for Rubicon, NOX2 and autophagy proteins. *Nat Cell Biol* **17:** 893-906

Martinez-Martin N, Maldonado P, Gasparrini F, Frederico B, Aggarwal S, Gaya M, Tsui C, Burbage M, Keppler SJ, Montaner B, Jefferies HB, Nair U, Zhao YG, Domart MC, Collinson L, Bruckbauer A, Tooze SA, Batista FD (2017) A switch from canonical to noncanonical autophagy shapes B cell responses. *Science* **355:** 641-647

Mizushima N, Kuma A, Kobayashi Y, Yamamoto A, Matsubae M, Takao T, Natsume T, Ohsumi Y, Yoshimori T (2003) Mouse Apg16L, a novel WD-repeat protein, targets to the autophagic isolation membrane with the Apg12-Apg5 conjugate. *J Cell Sci* **116:** 1679-1688

Morita I (2002) Distinct functions of COX-1 and COX-2. *Prostaglandins Other Lipid Mediat* **68-69:** 165-175

Mosser DM, Edwards JP (2008) Exploring the full spectrum of macrophage activation. *Nat Rev Immunol* **8:** 958-969

Murray PJ, Wynn TA (2011) Protective and pathogenic functions of macrophage subsets. *Nat Rev Immunol* **11:** 723-737

Murthy A, Li Y, Peng I, Reichelt M, Katakam AK, Noubade R, Roose-Girma M, DeVoss J, Diehl L, Graham RR, van Lookeren Campagne M (2014) A Crohn's disease variant in Atg16l1 enhances its degradation by caspase 3. *Nature* **506:** 456-462

Nakahira K, Haspel JA, Rathinam VA, Lee SJ, Dolinay T, Lam HC, Englert JA, Rabinovitch M, Cernadas M, Kim HP, Fitzgerald KA, Ryter SW, Choi AM (2011) Autophagy proteins regulate innate immune responses by inhibiting the release of mitochondrial DNA mediated by the NALP3 inflammasome. *Nat Immunol* **12:** 222-230

Ohashi W, Hattori K, Hattori Y (2015) Control of Macrophage Dynamics as a Potential Therapeutic Approach for Clinical Disorders Involving Chronic Inflammation. *J Pharmacol Exp Ther* **354:** 240-250

O'Neill LA, Golenbock D, Bowie AG (2013) The history of Toll-like receptors - redefining innate immunity. *Nat Rev Immunol* **13:** 453-460

Park S, Buck MD, Desai C, Zhang X, Loginicheva E, Martinez J, Freeman ML, Saitoh T, Akira S, Guan JL, He YW, Blackman MA, Handley SA, Levine B, Green DR, Reese TA, Artyomov MN, Virgin HW (2016) Autophagy Genes Enhance Murine Gammaherpesvirus 68 Reactivation from Latency by Preventing VirusInduced Systemic Inflammation. *Cell Host Microbe* **19:** 91-101

Qiao Y, Wang P, Qi J, Zhang L, Gao C (2012) TLR-induced NF-kappaB activation regulates NLRP3 expression in murine macrophages. *FEBS Lett* **586:** 1022-1026

Randow F, Munz C (2012) Autophagy in the regulation of pathogen replication and adaptive immunity. *Trends Immunol* **33:** 475-487

Roszer T (2015) Understanding the Mysterious M2 Macrophage through Activation Markers and Effector Mechanisms. *Mediators Inflamm* **2015:** 816460

Saitoh T, Fujita N, Jang MH, Uematsu S, Yang BG, Satoh T, Omori H, Noda T, Yamamoto N, Komatsu M, Tanaka K, Kawai T, Tsujimura T, Takeuchi O, Yoshimori T, Akira S (2008) Loss of the autophagy protein Atg16L1 enhances endotoxin-induced IL-1beta production. *Nature* **456:** 264-268

Shi CS, Shenderov K, Huang NN, Kabat J, Abu-Asab M, Fitzgerald KA, Sher A, Kehrl JH (2012) Activation of autophagy by inflammatory signals limits IL1beta production by targeting ubiquitinated inflammasomes for destruction. *Nat Immunol* **13**: 255-263

Shibutani ST, Saitoh T, Nowag H, Munz C, Yoshimori T (2015) Autophagy and autophagy-related proteins in the immune system. *Nat Immunol* **16:** 10141024

Sica A, Mantovani A (2012) Macrophage plasticity and polarization: in vivo veritas. *J Clin Invest* **122:** 787-795

Sollberger G, Strittmatter GE, Garstkiewicz M, Sand J, Beer HD (2014) Caspase1: the inflammasome and beyond. *Innate Immun* **20:** 115-125

Sou YS, Waguri S, Iwata J, Ueno T, Fujimura T, Hara T, Sawada N, Yamada A, Mizushima N, Uchiyama Y, Kominami E, Tanaka K, Komatsu M (2008)

The Atg8 conjugation system is indispensable for proper development of autophagic isolation membranes in mice. *Mol Biol Cell* **19:** 4762-4775

Sutterwala FS, Haasken S, Cassel SL (2014) Mechanism of NLRP3 inflammasome activation. *Ann N Y Acad Sci* **1319:** 82-95

Uniprot (2002-2017) UniProtKB - Q8C0J2 (A16L1_MOUSE) [online] Available at: http://www.uniprot.org/uniprot/Q8C0J2 [Accessed 21 September 2017]

Varin A, Gordon S (2009) Alternative activation of macrophages: immune function and cellular biology. *Immunobiology* **214:** 630-641

Vince JE, Wong WW, Gentle I, Lawlor KE, Allam R, O'Reilly L, Mason K, Gross O, Ma S, Guarda G, Anderton H, Castillo R, Hacker G, Silke J, Tschopp J (2012) Inhibitor of apoptosis proteins limit RIP3 kinase-dependent interleukin-1 activation. *Immunity* **36:** 215-227

Vural A, Kehrl JH (2014) Autophagy in macrophages: impacting inflammation and bacterial infection. *Scientifica (Cairo)* **2014:** 825463

Wang C, Yu X, Cao Q, Wang Y, Zheng G, Tan TK, Zhao H, Zhao Y, Wang Y, Harris D (2013) Characterization of murine macrophages from bone marrow, spleen and peritoneum. *BMC Immunol* **14:** 6

Yoshii SR, Kuma A, Akashi T, Hara T, Yamamoto A, Kurikawa Y, Itakura E,

Tsukamoto S, Shitara H, Eishi Y, Mizushima N (2016) Systemic Analysis of Atg5Null Mice Rescued from Neonatal Lethality by Transgenic ATG5 Expression in Neurons. *Dev Cell* **39:** 116-130

Zavodszky E, Vicinanza M, Rubinsztein DC (2013) Biology and trafficking of ATG9 and ATG16L1, two proteins that regulate autophagosome formation. *FEBS Lett* **587:** 1988-1996

Appendix

Below is an abstract summarizing the work done between October 2013 and May 2015 that had to be terminated upon the leaving of my supervisor Dr Nigel Belshaw.

Abstract

It has long been known that DNA methylation can influence gene expression and thus result in disease. Colorectal cancer is one example of a disorder which results from a progressive accumulation of genetic and epigenetic alterations. Polymorphisms in different genes have been associated with a higher risk or overall survival in cancer. Global DNA hypomethylation and gene-specific hypermethylation have both been linked to the process of tumour growth and progression. Autophagy, a lysosomal degradation pathway of cellular proteins and organelles, on the other hand, has a dual role in tumorigenesis. Genetic evidence has suggested that autophagy has tumour suppressive functions during the first initiation step. Various monoallelic deletions in genes involved in autophagy have been found in a high percentage of human cancers. However, there is also compelling evidence that autophagy promotes the survival of established tumours during progression and metastasis. It is believed that autophagy provides cancer cells with selective advantages to cope with stress conditions such as hypoxia, for example. However, little is known about the cancer-related genetic and epigenetic alterations of the genes involved in autophagy. To address this question, DNA methylation analysis was performed on *TFEB, TLR9, NOD2, Atg5, Atg12*, and *Atg16L1* in tumour, adjacent normal and healthy control

samples. Based on the variations observed, gene expression analysis was also carried out in tumour vs adjacent normal samples. However, the importance of the differences in gene expression in regard to autophagy activity in cancer remains to be established. Additional statistical analyses were carried out to investigate the relationships between DNA methylation and age, gender and tumour location. Significant associations were identified suggesting that age, gender and tumour location can influence the pattern of DNA methylation. Further work is required to understand the functional consequences of these observations for autophagy activity.